

DECIPHERING OKMOK VOLCANO'S RESTLESS YEARS (2002-2005)

By

Celso Guillermo Reyes


RECOMMENDED:




Dr. Jessica Larsen



Dr. Jeffrey Freymueller



Dr. Michael West
Advisory Committee Co-Chair




Dr. Stephen McNutt
Advisory Committee Co-Chair

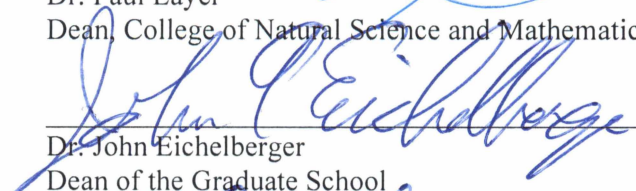


Dr. Sarah Fowell
Chair, Department of Geosciences

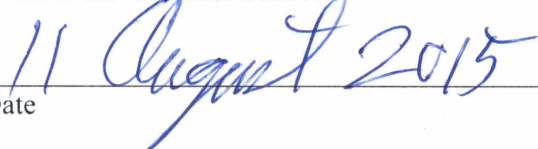
APPROVED:



Dr. Paul Layer
Dean, College of Natural Science and Mathematics



Dr. John Eichelberger
Dean of the Graduate School



Date

DECIPHERING OKMOK VOLCANO'S RESTLESS YEARS (2002-2005)

A

DISSERTATION

Presented to the Faculty
of the University of Alaska Fairbanks

in Partial Fulfillment of the Requirements

for the Degree of

DOCTOR OF PHILOSOPHY

By

Celso Guillermo Reyes, B.S.

Fairbanks, AK

August 2015

Abstract

Okmok Volcano is an active island-arc shield volcano located in the central Aleutian islands of Alaska. It is defined by a 10-km-diameter caldera that formed in two cataclysmic eruptions, the most recent being ~2050 years ago. Subsequent eruptions created several cinder cones within the caldera. The youngest of these, Cone A, was the active vent from 1815 through its 1997 eruption. On July 12 2008 Okmok erupted from new vents located northwest of Cone D. Between 2001 and 2004, geodetic measurements showed caldera inflation. These studies suggested that new magma might be entering the system. In 2002, a newly installed seismic network recorded quasi-periodic (“banded”) seismic tremor signals occurring at the rate of two or more episodes per hour. This tremor was a near-continuous signal from the day the seismic network was installed. Although the volcano was not erupting, it was clearly in a state of unrest. This unrest garnered considerable attention because the volcano had erupted just six years prior. The seismic tremor potentially held insight as to whether the unrest was a remnant of the 1997 eruption, or whether it signaled a possible rejuvenation of activity and the potential for eruption. To determine the root cause and implications of this remarkable seismic tremor sequence, I created a catalog of over ~17,000 tremor events recorded between 2003 and mid-2005. Tremor patterns evolved on the scale of days, but remained the dominant seismic signal.

In order to facilitate the analysis of several years of data I created a MATLAB toolbox, known as “The Waveform Suite”. This toolbox made it feasible for me to work with several years of digital data and forego my introductory analyses that were based on paper “helicopter” records. I first attempted to locate the tremor using the relative amplitudes of the seismograms to determine where the tremor was being created. Candidate tremor locations were constrained to a few locations along a corridor between Cone A and the caldera center. I then determined theoretical ratios between a reference station and stations nearby the candidate sources. Results suggested that the signal originated in the shallow portion of the corridor connecting the surface of Cone A to the top of the central magma chamber. This study also suggested that the source migrated along this corridor. I integrated the tremor patterns with other studies and proposed that heat and pressure from continued injections of magma were responsible for maintaining an open venting system at Cone A. The tremor resulted from the boiling of a shallow hydrothermal system in the vicinity of Cone A and volatiles potentially coming from the magma itself. The tremor catalog demonstrates that the seismic signal waned during the study period suggesting that fewer fresh volatiles entered the system, which may have allowed the pathways connecting the magma and volatiles to the surface to close up. By the time new magma entered the system in 2006, this network of pathways was closed, forcing the volatiles to seek a new exit. In hindsight, the 2003–2005 period of varied and

waning seismic tremor, and the inferred end of massive open venting, may have been a pivotal era at Okmok that eventually led to the 2008 eruption.

Table of Contents

	Page
Signature Page	i
Title Page	iii
Abstract	v
Table of Contents	vii
List of Figures	ix
List of Tables	xi
Acknowledgements	xiii
Chapter 1 Introduction	1
Chapter 2 The Waveform Suite	5
2.1 Introduction	5
2.2 Benefits inherent in using the Waveform Suite's classes	7
2.3 Description of the Waveform Suite's core classes	9
2.3.1 Waveform	9
2.3.2 Scnobject	11
2.3.3 Datasource	11
2.3.4 Companion classes	14
2.4 Concluding remarks	14
2.5 Where to get the Waveform Suite	14
2.6 Requirements	14
2.7 Acknowledgements	15
Chapter 3 Using relative amplitudes to evaluate potential tremor sources at Okmok Volcano	17
3.1 Introduction	17
3.1.1 Background	17
3.1.2 Locating a signal based on attenuation	21
3.1.3 Revised goal: differentiating between candidate tremor sources	22
3.2 Methods	24
3.2.1 Technique overview	24
3.2.2 Determining the RMS magnitudes	25
3.2.3 Choosing a reference station	26

	Page
3.2.4 Determination of the model parameters.....	27
3.3 Tremor comparisons between stations.....	31
3.3.1 Reading the comparison plots.....	31
3.3.2 Interpreting the tremor amplitude ratios.....	32
3.3.3 Interpretations.....	36
3.4 Discussion.....	38
3.5 Conclusion.....	42
Chapter 4 Tremor evolution in context at Okmok Volcano, 2003–2005.....	43
4.1 Introduction.....	43
4.2 Data.....	49
4.3 Methods.....	52
4.3.1 Measuring amplitudes.....	52
4.3.2 A Catalog of tremor start and end times.....	53
4.3.2.1 Automating tremor detection.....	53
4.3.2.2 Manually reviewing tremor picks.....	55
4.3.3 Determining tremor strength.....	55
4.3.4 Determining frequency content.....	56
4.4 Two years of unrest at Okmok: 2003–2005.....	59
4.4.1 Evolution and occurrence of tremor.....	59
4.4.1.1 Tremor amplitude.....	59
4.4.1.2 Distribution.....	61
4.4.2 Spectrograms.....	67
4.4.3 Earthquakes.....	68
4.4.4 Remote sensing.....	69
4.5 Interpretations.....	69
4.6 Conclusion.....	73
Chapter 5 Conclusions.....	75
References.....	77

List of Figures

	Page
2.1 Plotting example	9
2.2 Using datasource to access data from ad-hoc file systems	13
3.1 Location of Umnak Island.....	17
3.2 Close-up map of Okmok caldera	18
3.3 Seismogram traces of two stations for June 6 2003.....	19
3.4 Seismogram traces for February 24 2004 at station OKCF	20
3.5 Seismogram traces for September 15 2004 at station OKCF	20
3.6 Model of subsurface Okmok.....	24
3.7 Comparison of RMS amplitude relationships.....	26
3.8 Distance between each station and three sources with depth.....	28
3.9 Relative amplitude locations for active tremor on June 6 2003.....	29
3.10 Expected amplitudes for possible tremor sources.....	30
3.11 Expected ratios relative to station OKTU for selected locations and depths.....	30
3.12 Interpretation guide for the ratio comparison plots.....	32
3.13a Ratio comparisons for June 6 2003	33
3.13b Ratio comparisons for September 26 2003	34
3.13c Ratio comparisons for February 24 2004.....	34
3.13d Ratio comparisons for September 15 2004.....	35
3.13e Ratio comparisons for January 5 2005	35
3.14 Tremor ratio time series	37
3.15 Time series showing tremor migration from September 11–24 2004	38
3.16 Tremor location model.....	40
3.17 Tremor vs. inflation estimated from geodesy	41
4.1 Location of Umnak Island, Alaska	43
4.2 Okmok caldera detail	44

	Page
4.3 Okmok seismic network.....	46
4.4 Model of subsurface Okmok.....	48
4.5 Cumulative inflation at Okmok.....	49
4.6 Locally recorded earthquakes through 2006.....	51
4.7 Comparison of calculated 10-second RMS values to filtered raw data.....	53
4.8 Manual picking program.....	56
4.9 Catalog of active tremor at Okmok.....	57
4.10 Overview of Okmok unrest: 2003–2005.....	58
4.11 Inflation during 2003.....	59
4.12 Start of 2004 inflation.....	60
4.13 Inflation during 2004.....	61
4.14 Deflationary period, 2004–2005.....	62
4.15 Example of bimodal tremor.....	63
4.16 Tremor durations for February 23–25 2004.....	63
4.17 Generalized tremor styles, as recorded at OKCF.....	64
4.18 Example of tremor initiated by a strong signal.....	65
4.19 Example of tremor from September 15 2004 at station OKCF.....	66
4.20 Gliding tremor at OKCF.....	67
4.21 Example of tremor being disrupted by an earthquake.....	68
5.1 Summary of Okmok activity from 1997 to 2008.....	75

List of Tables

	Page
2.1 Selected waveform class methods, with return type	10
3.1 Possible tremor source locations at Okmok Volcano	22
4.1 Recent geodetic studies	46
4.2 Multiplet earthquakes occurring underneath Cone A	50
4.3 Okmok local seismic stations	50
4.4 Dike model parameters	72

Acknowledgements

Although I didn't realize it at the time, my Ph.D. experience started in the summer of 2002. I was on my way back to school in Flagstaff, Arizona from geology field camp in Idaho when I stopped in to stay with a friend who lived about halfway in between. As I walked in her door, she tossed a University of Alaska Fairbanks (UAF) catalog to me and basically said, "See ya! I'm off to Alaska to study seismology. I think you'll love it there, too."

Over the next few months of phone conversations, I heard about the uniqueness of Fairbanks, Alaska. I heard about cold and volcanoes and the Denali Fault earthquake that rattled interior Alaska in December 2002. Meanwhile, I was looking into possibilities for graduate school. I kept coming back to UAF, where I would have the opportunity to work with the Alaska Volcano Observatory, and (hopefully) handle actual eruptions. In the spring of 2003, I arrived in Fairbanks to start work on my volcano seismology degree.

When I first embarked upon this project, my available tools included some hand-me-down BASH shell scripts that allowed me to plot data from our in-house Antelope database, and MATLAB. Over the course of my graduate career, I was able to create a MATLAB framework, the Waveform Suite, which allowed me to easily write programs that analyzed and plotted the continuous data. I had no idea when I started that my chosen problem in 2003 that the data I would be analyzing would encompass over two years. I was also unaware that it would take the 2008 eruption of Okmok, and several subsequent analyses, to put my observations into perspective.

Over the course of my extended Ph.D., I've had the fortune to interact with many people who've influenced either my work or my life. First of all, I have to thank my committee co-chairs, Dr. Stephen McNutt and Dr. Michael West. It is through your continued commitment that the research presented here will finally be translated into the literature. Thank you, Steve, for taking me on as your graduate student way back when. Thanks for supporting my research for many years, showing me the volcanological community ropes, and providing me with such a meaty project. And, thank you of course, for the fantastic fieldwork opportunities.

Thank you, Mike, for the **amazing** support throughout my academic career, especially during my writing process both in Seattle and in Fairbanks. Without the many meetings, and revision help, this may not have happened. And thank you also for allowing me to bounce MATLAB ideas off you that tended to keep you up at nights programming. These conversations influenced the direction of the Waveform Suite in countless ways.

Thank you to my committee members, Dr. Douglas Christensen, Dr. Jessica Larsen, and Dr. Jeffrey Freymueller for guidance through the years, and for the patience that allowed my photo finish.

Thanks go to Jackie Caplan-Auerbach for being my first influence at UAF, for fascinating lunchtime conversations, unbounded scientific enthusiasm, and for inspiring the core of the Waveform Suite with her workflow. Thanks to Guy Tytgat, Ed Clark, John Paskievitch, and Cyrus Read for field experiences worthy of song. I would like to thank all the good people of the Alaska Earthquake Center and the Alaska Volcano Observatory, especially Tina Neal, who provided me with an excellent internship opportunity during the Redoubt 2009 eruption.

Thank you to the users of the Waveform Suite, for your feedback and encouragement. It's both thrilling and a little daunting to continually run into people I've never met that depend on the code I've written to make their research easier.

Thank you to my Fairbanks friends, too numerous to mention, that have affected my experience here. A few key players in my Fairbanks experience include my ice carving partners, Katie H., Katie J., Tim, Jill, Chloe, and Summer; my original housemates: Kelly (who is the reason I even knew UAF was a thing), Tom; my fellow Belfarians: Lars, Sharon, Evan and Matt; my many paddling partners, including those who did so at their peril; Dr. Helena Buurman; the glaciers group; the many baristas who've fed my caffeine habit; the World Ice Art Championships and the Red Green Regatta for providing critical creative outlets; and so many more.

Thank you to my family, both old and new, who have all shown me the best support, and seem to be under contract to put up with me no matter what I'm up to.

Finally, thank you, Barbara, for showing me unconditional patience and love and supporting my final bid for academic freedom. This would not have happened without your support.

Chapter 1 Introduction

Much has changed since I first stepped foot inside the Geophysical Institute, to the hum of the rotating “helicorder” drums and scratch-scratch-click of the pens as they scrawled out their watch over the volcanoes on paper records. In 2003, tracking the activity of the over twenty seismically monitored volcanoes in the remote Aleutians consisted of counting scratches on a piece of paper. The data archive consisted of stacks and stacks of large brown boxes stored in the basement of an adjacent building. Each box contained the hundreds of papers that represented one year of data from a seismometer buried in a shallow hole somewhere in the middle of nowhere.

Most of the electronic data being used were tied directly to earthquakes. “Continuous data”, sampled 100 times per second, took up too much room and was difficult to manipulate on the underpowered computers of the time. Continuous data could only be accessed by downloading them from special tape drives. The process was extremely slow. Painfully slow.

That isn’t to say we didn’t use electronic data, but it was fleeting. Spectrograms were updated every 10 minutes that allowed us to examine the frequency content of each channel of seismic data received from the volcanoes. However, after a few days the spectrograms were no longer available, and would have had to be manually regenerated in MATLAB.

Improvements to the amount of available electronic storage soon allowed continuous data to be available for analysis. However, grabbing data from a station, then getting it into MATLAB, then poking at it until something meaningful dropped out still remained a challenge.

The second chapter of this dissertation is a product of that environment. The Waveform Suite was born from the frustration of having to chase separate variables around my MATLAB workspace. Each variable described something important about the pieces of data that lived somewhere else in one of my programs. I’m thrilled to say that I had something to do with bringing that era to an end, not just for myself, but for the seismology group at the Geophysical Institute (and, the glaciology group) and, surprisingly, graduate students around the world. The Waveform Suite has made it easier for people to work with their seismic analyses.

But that was just the start. Programs such as the Seismic Wave Analysis and Realtime Monitor (SWARM) came along representing a new way to interact with continuous digital data, and the world opened up. Displays were updated every few seconds, and one could look at frequency content on a whim. Seismology had moved away from scratching pens and onto computer monitors.

The ability for seismologists to access and manipulate data has leapt forward in the last ten years. Now with only an Internet connection, one can access a vast library of seismological data from the Incorporated Research Institutions for Seismology. The MATLAB Waveform Suite allows direct access to this library. The resulting paper, which is presented as chapter two, was coauthored with Michael West (Reyes and West, 2011).

In 2003, very little volcanic activity was happening in the Aleutian island chain. However, somewhere in the Aleutians exists a volcano, named Mount Okmok, which had been instrumented the previous two summers. Now that we were starting to record its seismicity, a curious pattern of tremor could be seen. Data from Okmok, however, were not being printed out on the drum seismographs. Instead, the data were pre-filtered to remove the ubiquitous ocean and wind noise, and then printed out. These printed plots were called “pseudohelicorder records”.

Had we been using the old drums, this tremor would be known as banded tremor, since it appeared as bands on the seismograph. However, I always just called it quasi-periodic tremor, based on its apparent regularity.

Semantics has always played an important role in volcano monitoring. This is a discipline where multiple labels get applied to the same signal but have different connotations. McNutt (1992) offers a treatment of various volcanic tremor types. Tremor can be described by appearance (banded, quasi-periodic, continuous), by circumstance (eruptive, non-eruptive), by frequency content (harmonic, broad-band, gliding), or by location (volcanic, non-volcanic).

It seems that any time a volcano exhibits any behavior there is inevitably a discussion on how to label it. Labels, applied to a phenomenon, influence the way people think about the phenomenon. This, in turn, affects the interpretations. The discussion of semantics regularly recurs at meetings. “LIME GREEN” is one such label. The volcanoes that the Alaska Volcano Observatory (AVO) monitors are assigned an aviation color code that describes their state of unrest. A change to the color code changes the way the volcano is handled, and also activates different emergency-management plans. This change, therefore, is not undertaken lightly. When a volcano is quiet (GREEN), but starts to show signs of activity, such as tremor, many earthquakes, or some other behavioral change, the color might be elevated to (YELLOW). The question has often been, “What are the criteria for reducing a color code?” In several instances (Red to Orange, Orange to Yellow), the criteria are clear-cut. However, volcanoes are ever changing in their behavior, and at some point “elevated activity” can become the new background level. For these, “LIME-GREEN” has often half-jokingly been suggested.

Okmok volcano, from 2003–2005, probably fits into this lime-green category. Background levels were defined by this quasi-periodic, broadband, banded, non-eruptive tremor that sometimes exhibited gliding harmonics. Active tremor suggests an active volcano, so something was happening, but what?

Chapters three and four attempt to answer that question.

As I write this, there are seismometers that I have personally set on their watch on the remote islands of Semisopochnoi and Little Sitkin. Surprisingly, they continue to send signals after ten years without maintenance. They continue to transmit their stories to this day, even though the batteries that they depend upon exceeded their life expectancy several years ago.

It is not quite the same story with the instruments stationed at Okmok Volcano. The support electronics for one instrument were struck by lightning, in the process scattering electronics across the hut that provides a safe-haven against the elements. Winds tear up the large metal pipe constructions, called “swing sets”, that were cemented into the ground and are used to hold additional solar panels required to feed power to the hungry electronics. Solar panels tend to get smashed over the winter. Huts fill with windblown ash. It is a tough environment.

Oh, and then there’s the eruptions.

Okmok does not look like the stereotypical volcano. It isn’t a tall, majestic steaming cone. Okmok is a large shield volcano and looks from the outside like nothing more than a very long ridge. This ridge marks the edge of the 10 km-diameter caldera that defines Okmok. Inside the caldera are the remains of tephra cones, each of which has at some time been the source of one or more eruptions.

“Cone A” is the name of a tephra cone that stands in the southwest of the caldera (Chapter 3, Figure 3.1 below). It has been the source of all the eruptions from 1815 on. It last erupted in 1997, six years before I came to Alaska. A blocky lava flow extends from Cone A across the caldera floor to the foot of Cone D, which stands in the eastern quadrant of the caldera.

One seismic station, OKCD existed on the flank of cone D when I first visited Okmok in 2004 (Chapter 3, Figure 3.2). It is no longer there, because it was either blown away or buried when Okmok erupted in 2008 from new vents in the vicinity.

Maybe the tremor signal already warned us that activity had moved to a new part of the caldera and contained clues as to why the activity changed. In chapter three, I attempt to locate the tremor using the

signal amplitudes recorded at the few seismic stations that were both functioning and close enough to record it.

Seismometers are not the only instruments used to decipher volcanic behaviors. At Okmok, we also have GPS stations that report how the volcano changes shape. Satellites have been employed to measure the deformation of volcanoes, through the use of radar images. Other satellite images report the temperatures of the land and clouds, providing the first level of confirmation that an eruption has occurred.

In chapter four, I combine the tremor observations with a variety of other observations to explain what was happening at Okmok in between these two eruptions. It is possible that the tremor seen in 2003–2005 meant that the system was in equilibrium, and the subsequent disappearance of tremor reflected changing conditions that set the stage for the eventual 2008 eruption from a new vent.

Chapter 2 The Waveform Suite

2.1 Introduction

The Waveform Suite, developed at the University of Alaska Geophysical Institute, is an open-source collection of MATLAB classes that provide a means to import, manipulate, display, and share waveform data while ensuring the integrity of the data and providing stability for programs that build upon them.

Many seismic investigations begin by extracting data from a database or archive in order to carry out some type of advanced processing on segments containing the relevant signal(s). This extraction process might include requesting data from the IRIS Data Management Center, a regional seismic network, or an in-house project database. Locally the extracted data may be stored in numerous well-established data formats or databases including SAC (Tapley and Tull, 1992), SeisAn (Havskov and Ottemöller, 1999), AH, SEG Y (Barry *et al.*, 1975), Winston (Cervelli *et al.*, 2004) and Antelope (BRTT, 2010; Lindquist, 2009). MATLAB has proven to be a popular environment in which to work with the extracted data in part because of the ready access to powerful platform-independent routines for signal processing and plotting. Once in MATLAB, however, the original data format is often replaced with a variety of ad-hoc formats as each user employs a variety of structures, arrays, and cells to manage the data. The independent nature of these homegrown formats can make it difficult to transfer data from one system (or project) to another without spending time on single-use conversion routines.

The ease of programming in MATLAB makes it particularly vulnerable to impromptu or disposable coding with the consequence being that many of the resulting scripts are transient affairs that serve an immediate need. Many scripts are then discarded, while others enjoy a more celebrated existence; bolstered by quick success, users (including the authors) often decide to build out these routines into standalone packages, only to realize that the vast majority of this effort is consumed by bookkeeping, exception handling, documentation, and error checking. Though thankless, these tasks make the difference between robust reusable codes and thesis appendices.

We introduce here the Waveform Suite, a MATLAB-based format for handling waveform data. The Waveform Suite consists of three MATLAB classes that have been designed from scratch to provide a robust foundation for manipulating waveforms. For users seeking the ability to import, manipulate, and display seismic data, the Waveform Suite provides this functionality directly. The supplied interface allows users to both import several standard formats and write import routines for their own formats. The suite's full benefits will be gained by users looking to build more advanced packages such as for receiver functions, shear wave splitting, wavefield migration, phase picking, cross correlation, synthetics or source

inversion. By replacing ad-hoc systems with a common framework, the Waveform Suite can provide an architecture upon which more complex programs may be created and shared.

The Waveform Suite is not tailored for any particular type of analysis (e.g. earthquakes, ambient noise, volcanic tremor, synthetics, etc.) but attempts to provide generic tools specific to seismology programming. This is somewhat different than similar efforts such as the CORAL toolbox (Creager, 1997) and MATLAB's built-in time series toolbox. The suite minimizes the need for considering the sometimes grotesque details required for error checking or manipulating large numbers of waveforms. Both the error handling ability and the improved code readability help programs built upon the Waveform Suite to be more robust, with fewer crashes and logical errors (McConnell, 2004).

The Waveform Suite relieves the user of routine bookkeeping chores by automating the tedious aspects of data manipulation and by keeping related information together. Tasks managed through the suite include automatically updating attributes as required by various data manipulations (such as integrating, resampling, stacking, etc.), ensuring that arrays are of proper dimensions, determining the times of samples, keeping track of station-channel combinations, automatically labeling graphs, and more. A core feature of the Waveform Suite is its ability to handle multiple waveforms simultaneously, dispensing with the frequent need to loop through each individual trace. The suite is extensible, providing the user with the ability to write import routines for their own formats. Databases or file systems may be queried for vast numbers of waveforms that can then be manipulated en masse. The suite allows the user to make changes to waveforms using standard mathematical operators (+, -, .*, etc.) and provides the ability to perform common manipulations such as filtering, subsetting or demeaning. Some basic statistics are supported as are more complex operations such as integration and Hilbert transforms. See Table 2.1 for a representative sample of functions.

The Waveform Suite consists of three primary MATLAB classes:

- *Waveform* – This class provides easy data manipulation and display of evenly-sampled (e.g. seismic) data.
- *Datasource* – This class provides the interface between programs and stored data.
- *Scnobject* – This class handles each trace's station-channel-network-location information.

In most applications, *datasource* and *scnobject* are used to set up the importation of data as in this example:

```
>> ds = datasource('Antelope','/iwrn/op/db/archive_2010_02_27');
```

```
>> scn1 = scnlobject('SPBG', 'BHZ', 'AV', '--');  
>> w = waveform(ds, scn1, startTime, endTime);
```

where `startTime` and `endTime` happen to be NxM matrices of trace start and end times. The result is an NxM waveform object, `w`. This particular example draws data from an Antelope database. This could be pointed to a different type of input data by just changing the first line. As will be the case for all scripting examples, the user-typed commands are shown after the MATLAB prompt “>>”, while computer-generated output is represented in italics.

The terms *class* and *object* appear repeatedly throughout this paper and deserve brief mention. An *object* is essentially a variable and is treated as such, but is special in ways that are discussed throughout the next section. A *class* refers to the template that explicitly lays out the types of data within an object, as well as the functions (called *methods*) that are allowed to operate on those data. In fact, the standard MATLAB data types ('double', 'char', and 'cell') are classes.

2.2 Benefits inherent in using the Waveform Suite's classes

The Waveform Suite's classes provide a sturdy and flexible framework that frees the user from bookkeeping details, allowing the user to concentrate instead upon getting results. The functions and the data upon which they operate are treated as a unit, providing the user with a simple, seamless interface upon which more complex programs can be easily created. Additional benefits include reducing the need for variable juggling, providing familiar ways to work with data, and insulating the program from bad data while protecting data from bad input, all of which results in speedier and more effective program development and facilitates reproducible results.

Classes provide a way to unify data, reducing the number of variables that must be tracked separately. Working with seismic data typically requires tracking amplitudes, times, stations, frequencies, units, etc. The Waveform Suite's classes allow the user to merely track a single all-encompassing object of the class waveform. This variable may be N-dimensional, representing multiple seismic traces (building on the prior example):

```
>> w(3,4)  
  
ans =  
    station:   SPBG           network:  --  
    channel:   BHZ           location:  --  
    start: 2010-03-15 03:08:01.000  
    duration(00:00:15.000)
```



```
data: 1500 samples
freq: 100.0000 Hz
units: nm / sec
history: [4 items], last modification: 15-Mar-2010 12:35:01
With misc fields...
CALIB: 1.0583
```

Input routines have been designed for each of the Waveform Suite's classes. These are capable of pre-screening values to avoid the assignment of erroneous values that would cause a program to misbehave. Values that have been assigned to an object are protected from unsupervised modification and instead are accessed through functions tailored to work with the data. Each of the suite's functions provide targeted access to the underlying structure in order to prevent accidental or nonsensical data modification. According to MATLAB convention, the assignment function is called set and the retrieval function is called get. Through set, data types and formats can be strictly enforced, and it can be ensured that data lie within proper ranges and have appropriate dimensions and units. This last point is important because matrix operations treat $1 \times N$ arrays differently than $N \times 1$ arrays. Through these routines, the user may access derived or interpreted properties as well as native properties. A simple example of this behavior is a request for a date: while the date is internally represented in a waveform as a MATLAB serial date number, the user may opt to retrieve the date as a text string or an epoch. To an external program, actual or derived data are indistinguishable.

```
>> get(w, 'START_STR')

ans =
    2010-03-15 03:06:01.000
    2010-03-15 03:21:01.000
    2010-03-15 03:19:01.000
    ...
```

Since MATLAB determines which version of a function to use based upon the data type (class) passed to it, defining waveforms as a distinct MATLAB class permits the reuse of standard function names such as plot() and min() as well as existing symbols for standard mathematical manipulations including “+” and “.*”.

The ability to use existing operators and create routines that replace multiple lines of code with a simple intuitive command improves the understandability of routines, which helps reduce errors. Compact legible code is illustrated by this example, which plots the normalized traces of three of the waveforms stored in w from the previous examples. The output can be seen in Figure 2.1.

```

>> w = w(1:3)
>> peak2peak = max(w) - min(w);
>> normalized_traces = w ./ peak2peak;
>> plot(normalized_traces);
>> legend(w);

```

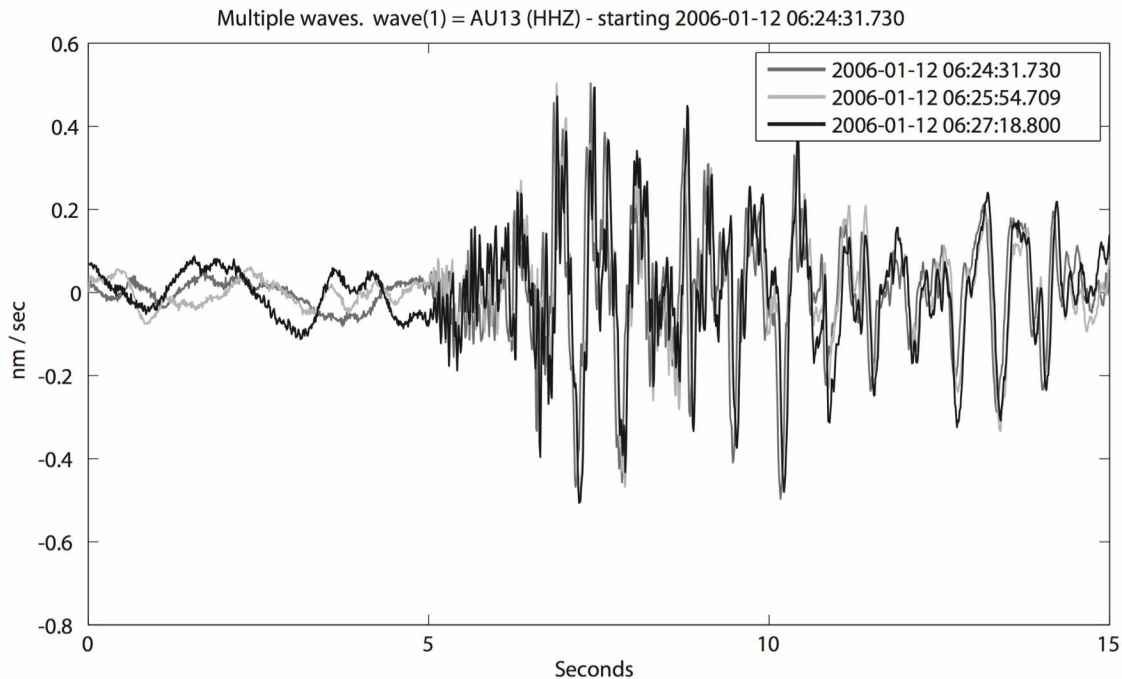


Figure 2.1 Plotting example. Example of output generated by the waveform's plot command. These data are from repeating earthquakes at Augustine Volcano near the beginning of the 2006 eruption. Traces have been normalized (see text).

Every attempt has been made in the Waveform Suite to provide thorough and meaningful error messages to expedite the debugging process. For cases where the cause is outside the user's control (as in erroneous values within a data stream, data gaps, etc.), the classes within Waveform Suite may be able to recover intelligently, rather than crash. Ideally, no application using these classes should retrieve nonsensical data since errors within the data are reported or corrected at the time of assignment.

2.3 Description of the Waveform Suite's core classes

2.3.1 Waveform

The waveform class is the suite's workhorse, providing a way to manipulate evenly-sampled data (e.g., seismic data) within MATLAB. Waveform tracks data relating to frequency, start time, trace identification, measured amplitudes, and history, along with user-defined fields. A selected list of waveform functions is included in Table 2.1.

Table 2.1 Selected waveform class methods, with return type.

Function Name	Function Description	Return Type
ABS	Absolute value of a waveform's data	Waveform
ADDFIELD	Add user-defined fields to waveform object(s)	Waveform
ADDHISTORY	Add an event to the history to a waveform	Waveform
ALIGN	Resample a waveform at over every specified interval	Waveform
CLEARHISTORY	Reset the history of a waveform	Waveform
CLIP	Clip a waveform's data at a particular max/min value range	Waveform
COMBINE	Merges waveforms based on start/end times and SCNL info	Waveform
DELFIELD	Removes user-defined fields from waveform object(s)	Waveform
DEMEAN	Remove offset voltage from signal	Waveform
DETREND	Remove linear trend from a waveform's data	Waveform
DIFF	Differentiate waveform	Waveform
DISP (or DISPLAY)	Display the contents of a waveform	N / A
DOUBLE	Returns a waveform's data as a double type	Double
EXTRACT	Creates a waveform with a subset of another's data	Waveform
FILLGAPS	Fill missing data with values of your choice	Waveform
FIX_DATA_LENGTH	Adjust length of waveform data to allow batch processing	Waveform
GET	Get waveform properties	Waveform
GETPEAKS	Return mask for peak values for a waveform	Logical
HILBERT	Discrete-time analytic Hilbert transform	Waveform
HISTORY	Retrieve the history of a waveform object	Cell, Double
INTEGRATE	Integrates a waveform signal	Waveform
ISEMPTY	Returns TRUE if waveform contains no data	Logical
ISFIELD	Returns TRUE if the a field exists within the waveform	Logical
ISMEMBER	Returns TRUE if waveform info matches scnobjects	Logical, Double
MAX	Largest value of a waveform's data	Double
MEAN	Average or mean value of a waveform's data	Double
MEDIAN	Middlemost value of waveform's sorted data	Double
MIN	Smallest value of a waveform.	Double
MINUS (-)	Overloaded waveform subtraction (w - q)	Waveform
MRDIVIDE (/)	Slash or right matrix divide (w / q)	Waveform
PLOT	Plots a waveform object	Handle
PLUS (+)	Waveform addition (w + q)	Waveform
POWER (.^)	element-by-element power (w .^ q)	Waveform
RDIVIDE (./)	Right array divide (w ./ B)	Waveform
RESAMPLE	Resample a waveform at over every specified interval	Waveform
RMS	Root mean square of a waveform's data	Double
SAVESAC	Creates a SAC file from a waveform	N / A
SET	Change properties for waveform object(s)	Waveform
SIGN	Returns a waveform consisting of the signums of the data	Waveform
SMOOTH	Overloaded smooth function for waveform	Waveform
STACK	Stacks data from array of waveforms	Waveform
STD	Standard deviation of a waveform's data	Double
SUBTIME	Grab time-indexed snippets of waveform data	Waveform
TAPER	Applies a cosine taper to the ends of a waveform	Waveform
TIMES (.*)	Waveform Array multiply (w .* q)	Waveform
UMINUS (-)	Unary minus (-w)	Waveform
VAR	Variance of a waveform's data	Double
WAVEFORM	Waveform Class constructor	Waveform

Modifications to waveform objects are recorded in the history of each waveform. The history is capable of recording text blurbs as well as other types of information, such as other objects used to modify the waveform (e.g. details of an applied filter). Detailed history may later be retrieved to determine how the data was modified or, more importantly, how to reproduce results.

User-defined fields expand the capabilities of waveform by allowing users to include additional information relevant to each trace. In practice these user-defined fields serve as extensible header fields. These fields are created automatically in some instances; when a SAC file is imported, header information is transferred into user-defined fields. Though this information can be stored in adjacent matrices, incorporating it directly into the waveform object allows it to pass automatically into existing routines. Because these fields can be of any type it is possible to store not only simple information (e.g. an event location), but also more complex information such as an instrument response or the frequency spectrum of the trace. While there is some danger in infinitely extensible header information, in our experience thus far, this capability has given considerably more power than anticipated to the Waveform Suite. Access to the data within user-defined fields is through the same get and set methods that are used to access the rest of waveform's details.

```
>> w = addfield(w, 'SENSOR_SN', 'T3529');
>> w = addfield(w, 'SPECTRALPEAKS', [1.6 3.2 6.4]);
>> get(w, 'SPECTRALPEAKS')
ans =
    1.6000    3.2000    6.4000
```

2.3.2 Scnobject

The `scnobject` class was created to simplify handling station, channel, network, and location information. Though not required in all situations, the four parameter SEED naming convention is now nearly ubiquitous in earthquake seismology. Each `scnobject` represents a single `sta_chan_net_loc` combination. (Ahern *et al.*, 2009). Encapsulating these descriptors into a dedicated object improves the management of large numbers of traces by facilitating single-command subsets, concatenations and queries against waveform objects. Commonly accessed `scnobjects` can be stored for automatic retrieval, so that they are not required to be created manually each time. `Scnobjects` understand ‘*’ wildcards, further improving the ability to sift through large numbers of traces for desired information.

2.3.3 Datasource

The `datasource` class provides the connection between waveforms (or other classes) and their databases or stored files. The `datasource` class has proven to be a valuable way to insulate the waveform

class from the (often changing) data streams. Together, the datasource and waveform classes have built-in interpreters for several database and file formats including:

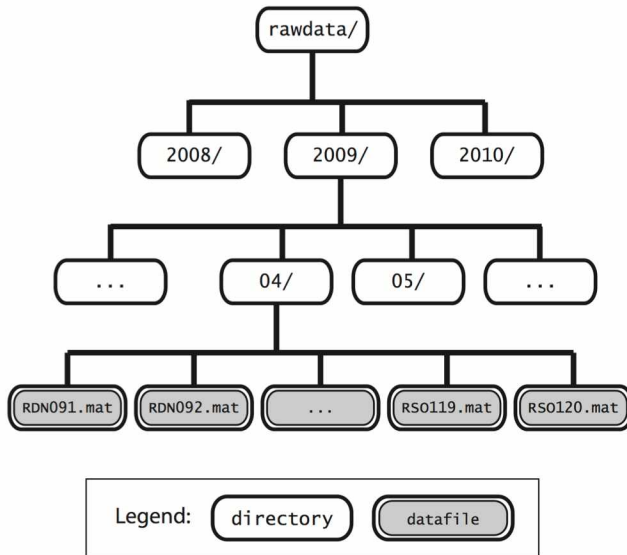
- *Antelope* – The Waveform Suite wraps the required elements from the Antelope toolbox for MATLAB (Lindquist, 2009), providing the ability to access Antelope databases. This is included in the standard Antelope distribution from Boulder Real Time Technologies.
- *Winston* – the Waveform Suite reaches directly into Winston using the java library distributed with SWARM (Cervelli *et al.*, 2004).
- *SAC* – SAC (Seismic Analysis Code) files (Tapley and Tull, 1992) may be imported without additional codes. Additional header fields are translated into similarly named user-defined fields.
- *SeisAn* – No additional utilities are required to import files from the SEISmic ANalysis system (Havskov and Ottemöller, 1999). However, due to SeisAn's file naming conventions, datasource may not be able to automatically determine which file is desired. In this case, the datasource should be created using specific filenames.
- *.mat file* – Datasource is capable of looking within .mat files for all variables of a desired type. This allows it to parse data from files which contain previously generated waveform objects.
- *User-defined* – The datasource/waveform object combination makes it straightforward to translate a file of any type into an array of one or more waveform objects. A short wrapper function should be all that is necessary to make an existing import routine compatible with the Waveform Suite. Notably, this does not require an understanding of the datasource/waveform codebase beyond the set function.

Most users are well acquainted with reading data on a per file basis. This is straightforward in the Waveform Suite. In addition, complex directory structures and file naming schemes can be traversed thanks to the datasource's ability to interpret fprintf() style formatting statements which may describe a file's time and/or station/channel/network/location information (see Figure 2.2). The following example shows how a datasource might be created that can access SAC files stored in the current directory.

```
>> ds_sac = datasource('sac', '%04d%02d%02d_%s_%s_%s__.sac',...
    'year', 'month', 'day', 'network', 'station', 'channel');
>> getfilename(ds_sac, scnl, {'5/3/2009', '2010 03 15', now})
ans =
    '20090503_AV_SPBG_BHZ__.sac'
    '20100315_AV_SPBG_BHZ__.sac'
```

'20100325_AV_SPBG_BHZ__ .sac'

A. Example ad-hoc file system



B. Another typical ad-hoc file system



Figure 2.2 Using datasource to access data from ad-hoc file systems. Both A and B represent typical data storage systems. File system *A* consists of waveforms saved within .mat files in date-dependent directories, while system *B* consists of a series of SAC files scattered within a single directory. Datasources may be created that are capable of navigating these systems:

```
>> system_A = datasource('file', 'rawdata/%4d/%02d/%s%03d.mat',...  
    'year', 'month', 'station', 'jday');  
>> system_B = datasource('sac', 'data/%4d%02d%02d_%s_%s_%s_%s.sac',...  
    'year', 'month', 'day', 'network', 'station', 'channel', 'location');
```

Essentially the combination of the waveform, scnobject and datasource objects allow a user's homegrown data organization structure to be queried as a simple relational database. Datasource facilitates this by providing separation between data requests and the explicit data storage structure. Though not required, this approach is in our opinion generally preferable to hardwiring code to specific file names.

Additionally, the datasource is able to return information that crosses file or database boundaries. Data that is retrieved from individual files or databases can be combined into a continuous object. In the case of a waveform object, this is done automatically. By accessing files through their generalized formats, instead of individually, issues such as the “11:59 PM earthquake problem” can be avoided.

While the datasource class works in concert with the waveform class to retrieve information, it is not dependent upon waveform, and may be used to access data of any type. Many users choose to save

commonly used datasource objects in a .mat data file or an .m script file where they can be loaded automatically, such as from the startup.m file.

2.3.4 Companion classes

Additional companion classes are included with the Waveform Suite to assist common tasks. The filterobject class provides a method of filtering waveform data with a Butterworth filter. Using this class, multiple waveforms can be filtered with minimal coding. The spectralobject class was designed to simplify the creation and display of spectrogram (or periodogram) data. Uispecgram is an included application that provides a graphical interface for creating custom spectrograms.

2.4 Concluding remarks

Though importing data into MATLAB is not necessarily difficult, choices about how to store and work with the data have a tremendous influence on a project's success. A project underpinned by the Waveform Suite's object-oriented framework has access to tools able to retrieve data from a variety of sources, manipulate and display the same data in an intuitive manner, and develop robust applications that are easy to maintain. Each class's internal structure remains invisible to dependent applications, allowing the suite to change as it matures without breaking the programs that implement it. However, users should not expect the suite to grow into an all-encompassing singularly defined seismic format. Several people have used the Waveform Suite as the foundation for their own processing packages, using this common, flexible framework to reduce development time and making it easy to share waveform data with other MATLAB users.

2.5 Where to get the Waveform Suite

The Waveform Suite is available as a self-contained distribution from the MATLAB file exchange: <http://www.mathworks.com/MATLABcentral/fileexchange/23809>

This distribution is regularly updated as new stable releases are produced.

The Waveform Suite codebase is maintained as an open source project together with several associated seismic tools in the GISMO toolbox at:

<https://github.com/giseislab/gismotools/>

2.6 Requirements

The Waveform Suite requires MATLAB. The current release of the Waveform Suite has been successfully tested against MATLAB 7.1 (R14SP3); however, MATLAB's object handling has changed

considerably in recent years, so current development is occurring only in MATLAB version R2009b and later. The Waveform Suite does not depend upon any additional toolboxes from The MathWorks, Inc. Additional libraries are required to read data from Antelope or Winston databases.

2.7 Acknowledgements

Thanks to all those who have helped the Waveform Suite evolve to its current state. We would like to recognize J. Amundson (a great debugger and source of additional functionality), M. Thorne (whose SAC routines were thoroughly cannibalized), G. Thompson and S. DeAngelis (as testers and for SeisAn help), M. Robinson and L. Valcic (for network and computer support), and S. McNutt (one author's advisor, who let him develop these codes when, just perhaps, he should have been concentrating on interpreting the wiggles themselves). Also, the authors would like to thank K. Creager for his thoughtful review. This work was partially supported by the Alaska Volcano Observatory and the U.S. Geological Survey as part of their Volcano Hazard and Geothermal studies, and by additional funds from the State of Alaska.

3.1 Introduction

3.1.1 Background

Okmok Volcano is an active basaltic andesite island-arc shield volcano, located on Umnak Island in the Aleutian chain (Figure 3.1). It is defined by a 10-km-diameter nested caldera that was formed by two cataclysmic eruptions, Okmok I and Okmok II. The most recent of these occurred approximately 2050 years ago (Kienle and Nye, 1990; Begét *et al.*, 2005; Larsen *et al.*, 2007). Subsequent eruptions have created several cinder cones within the caldera, with the most recent activity centered at Cone A, located in the southwest of the caldera. Cone A is known to have erupted eight times since 1943 (Miller *et al.*, 1998) and last erupted in 1997, emplacing a lava flow along the caldera floor (McGimsey and Wallace, 1999). On July 12 2008 Okmok erupted from multiple new vents located northwest of Cone D (Neal *et al.*, 2009). This shift in activity presents an opportunity to elucidate how a spatial change in activity might be reflected in the seismic data.

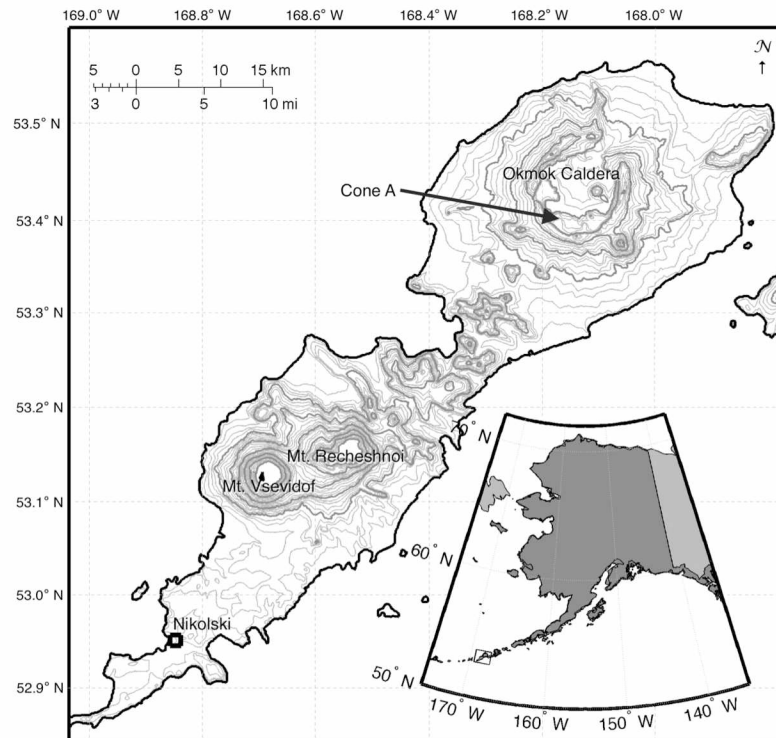


Figure 3.1 Location of Umnak Island. Okmok Volcano occupies the northeast half of the island.

No seismic network existed during the 1997 eruption, but geodetic measurements using GPS and Interferometric Synthetic Aperture Radar (InSAR) have revealed co- and post- eruptive deflation and subsequent inflation, located beneath the center of the caldera (e.g. Mann *et al.*, 2002; Miyagi *et al.*, 2004; Lu *et al.*, 2005; Fournier *et al.*, 2009; Lu *et al.*, 2010; Biggs *et al.*, 2010). A seismic network was installed for monitoring purposes between 2002 and 2004, consisting of short-period (1-Hz) L-4c seismometers (Figure 3.2). During installation, flyovers of Cone A showed vigorous fumarolic activity and incandescence within the conduit (J. Larsen, pers comm; C. Neal, pers comm.). In early 2003, continuous seismic data started to be received from the Okmok network.

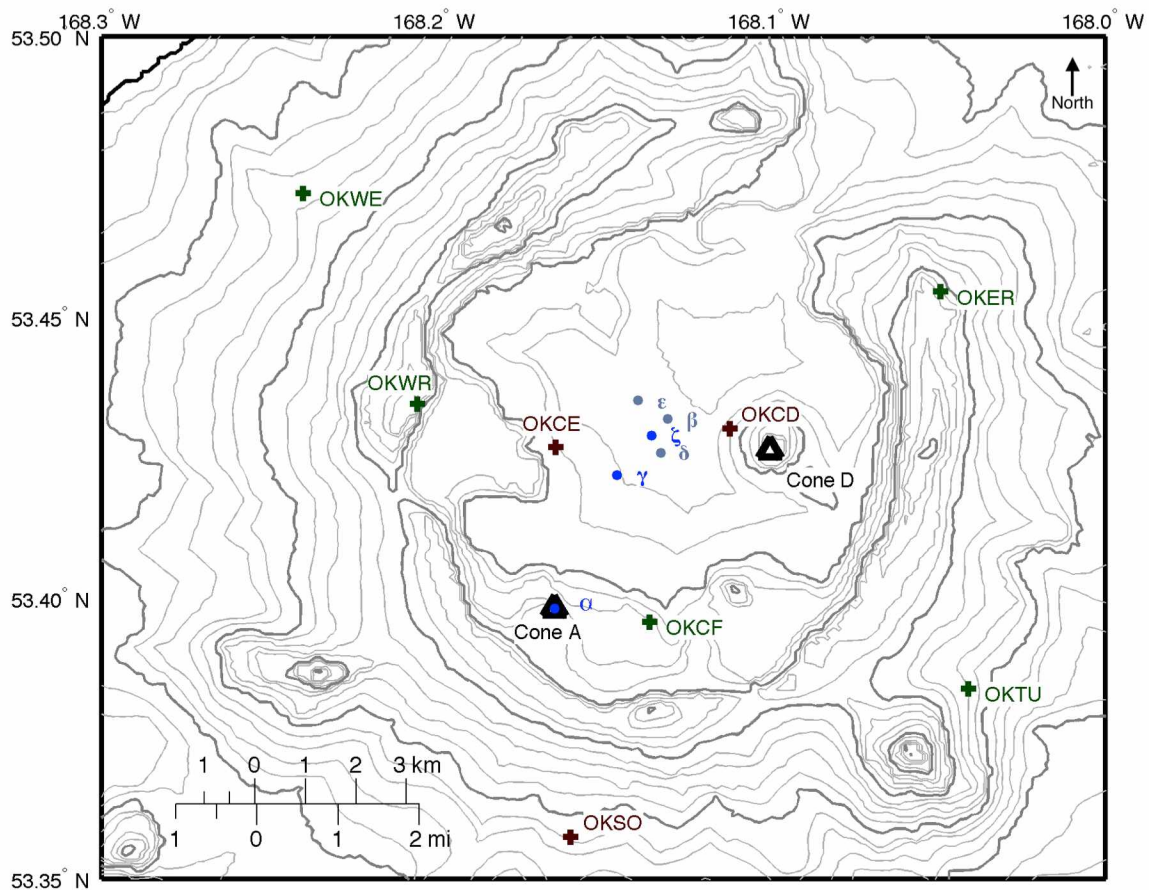


Figure 3.2 Close-up map of Okmok caldera. Suggested source locations listed in Table 3.1 are shown as small circles: blue circles are the locations examined in this study, grey circles show the other possible source locations. Broadband seismic stations are shown as red plus symbols; short-period seismic stations are green plusses.

From the outset, the seismicity was characterized by patterns of tremor (defined below), as shown in Figures 3.3 through 3.5. These figures show seismograms for several stations during three days of active tremor. Although tremor was apparent as early as February 20 2003 at stations OKWR and OKWE, data

coverage was extremely spotty throughout the winter and into the spring of 2003. This can be the case when radio signals are disrupted because a station is buried deep in wet snow or loses power due to the lack of available solar recharge energy during the winter. The network started to stabilize by late May 2003, after which tremor dominated the seismic data. Tremor continued off-and-on throughout much of the following two years until September 2005, at which point tremor was no longer readily apparent. Knowing where the tremor was located may provide insight into where magma degassing or other processes were occurring, where and when magma moved, and perhaps may help to define possible magma or gas pathways. In turn, this may tell us something about how activity at Cone A and the center of inflation (COI) may be related.

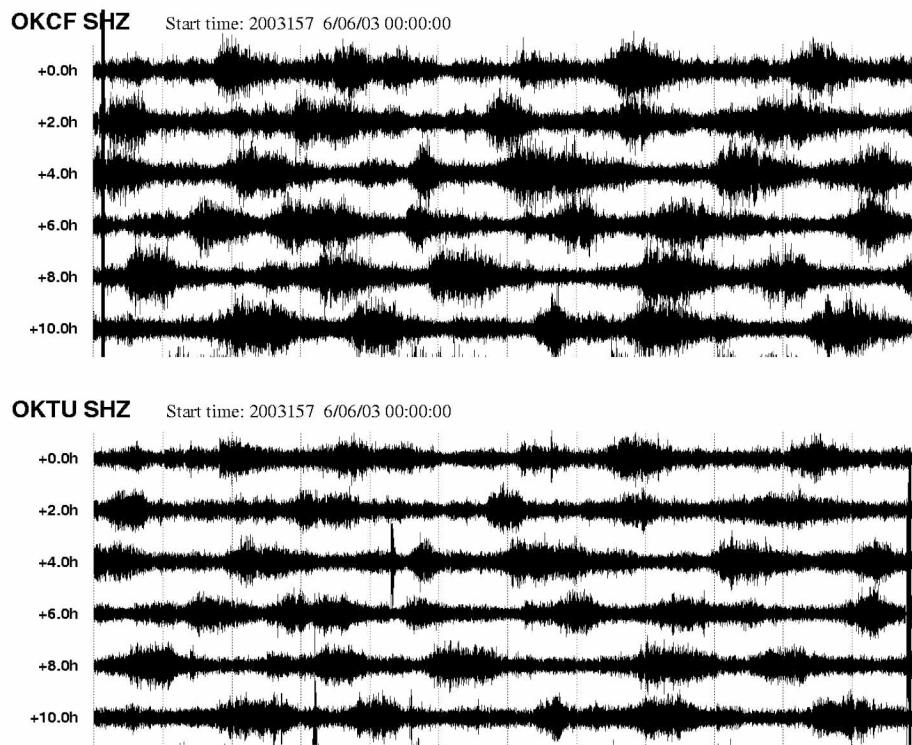


Figure 3.3 Seismogram traces of two stations for June 6 2003. Each plots shows twelve hours of filtered [0.8–5 Hz] data, presented in rows that are each two hours long.

Volcanic tremor appears on seismograms as a long-duration (minutes to years) signal at frequencies that usually range from 1–10 Hz (McNutt and Nishimura, 2008). Tremor is commonly dominated by Rayleigh waves (McNutt, 1989). Volcanic tremor often indicates fluid movement or pressurization (e.g. Aki *et al.*, 1977; Aki and Koyanagi, 1981; Chouet, 1985, 1996; Chouet *et al.*, 1987; McNutt 1992; Julian 1994), and is a common signal at active and erupting volcanoes (e.g. Koyanagi *et al.*, 1987; Dean *et al.*, 2002; Thompson *et al.*, 2002).

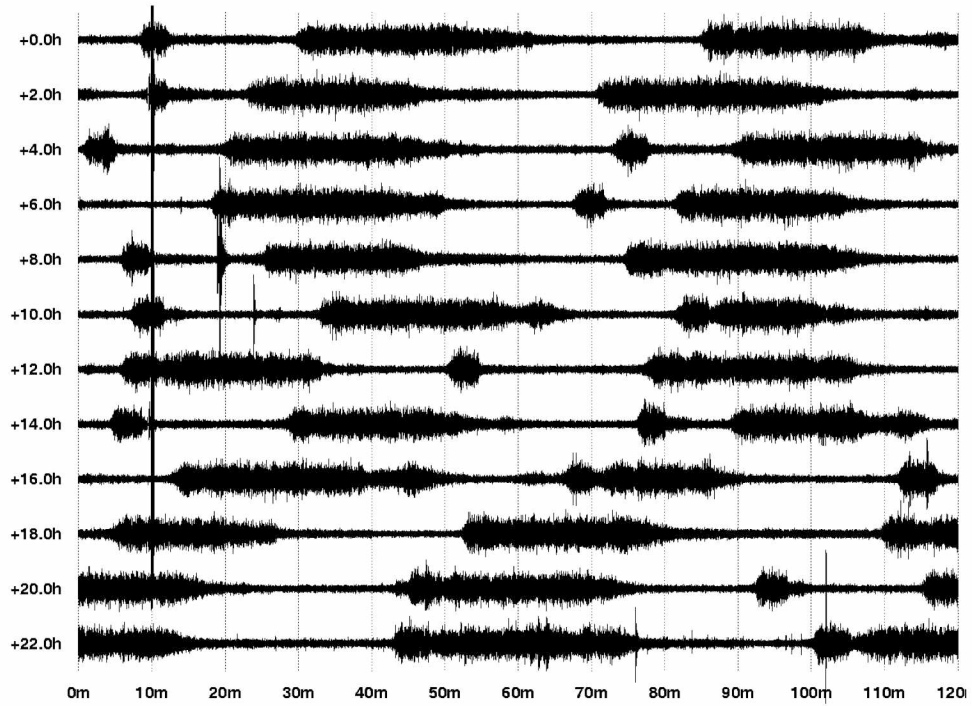


Figure 3.4 Seismogram traces for February 24 2004 at station OKCF.

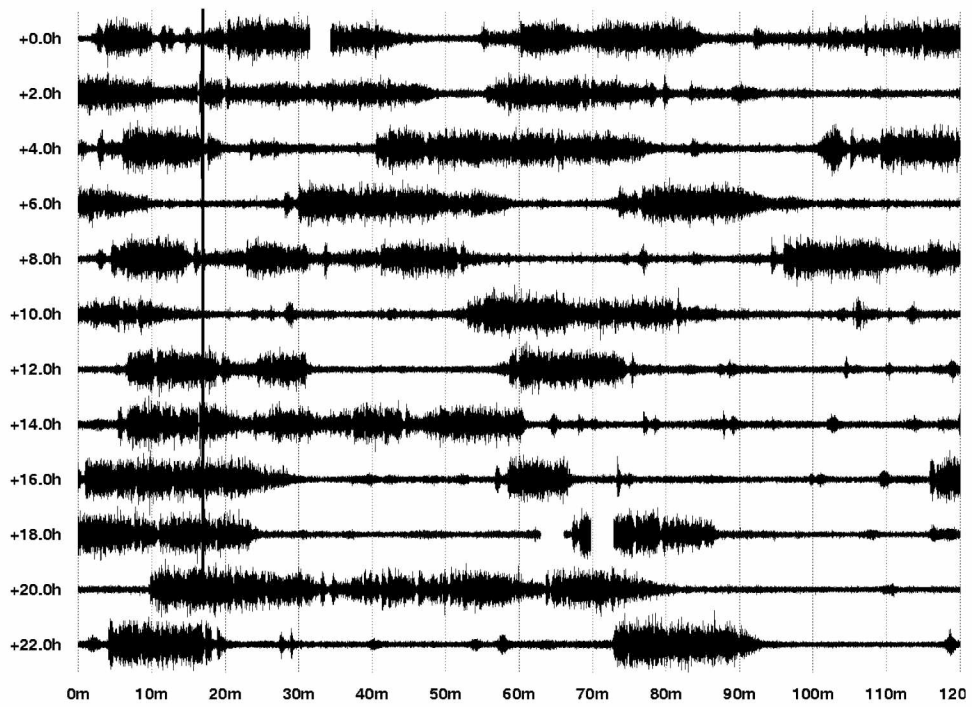


Figure 3.5 Seismogram traces for September 15 2004 at station OKCF.

The phaseless character of tremor renders ineffective the traditional methods of location, which rely on distinct arrival times of P and S waves. To address this, several authors have demonstrated alternate methods of locating tremor (Benoit and McNutt, 1997; Battaglia and Aki, 2003; Takagi *et al.*, 2006; Haney, 2010).

3.1.2 Locating a signal based on attenuation

Battaglia and Aki (2003) presented one method for locating seismic signals, based on the decay of a signal's amplitude with distance. The attenuation of a signal A_0 with distance is governed by geometric decay of the signal, as well as by energy loss due to the fact that the earth is not a perfectly elastic medium. Geometrically, surface waves decay as the square root of distance because the energy is confined to the 2-dimensional surface interface. The energy from body waves, which travels throughout the medium, dissipates in three dimensions, resulting in a decay that scales directly with distance. Energy loss through the medium is frequency sensitive, with the higher frequencies attenuating faster. The equation governing the observed amplitude A_r at distance r for the decay of body waves travelling within the earth is

$$A_r = A_0 \frac{e^{-Br}}{r}, \text{ with } B = \frac{\pi f}{Q\beta} \quad (3.1)$$

while that for surface-wave decay is

$$A_r = A_0 \frac{e^{-Br}}{\sqrt{r}} \quad (3.2)$$

where A_0 is the source amplitude, f is the signal frequency, and Q is the quality factor describing anelastic attenuation, which varies inversely with attenuation (Aki and Richards, 2002). β is the propagation velocity (Battaglia and Aki, 2003).

Battaglia and Aki (2003) created a misfit function that allowed them to score the correctness of fit at each point in a search volume. Locations with the lowest misfit were the places where the signal likely originated. Using this method they were able to use the network of seismic stations around Piton De la Fournaise Volcano, located on the French island of La Réunion, to locate rockfalls, long-period events, and eruptive tremor.

The seismic network at Piton de la Fournaise was relatively dense compared to that at Okmok. Eight stations were located within 5 km of the summit and 8 more stations within 15 km of the summit, with

good azimuthal coverage. Rockfalls were constrained to the surface, and eruptive fissure tremor was visible on much of their network.

At Okmok the network is much sparser, with a total of eight short-period seismic stations that range from 1.9–24.7 km from Cone A. Only two stations are located within 5 km of Cone A, and a total of five stations are within 10 km. In addition, the two closest stations were often plagued by communication issues that resulted in the loss of data. On a day with low background noise and strong tremor, only these five closest stations typically recorded a tremor signal. Three additional 3-component broadband stations existed within 10 km of Cone A but were not operational during much of this study.

Nonetheless, I originally attempted to implement a methodology similar to that of Battaglia and Aki (2003). The resulting tremor locations were highly sensitive to station coverage, causing the location solutions to either lock in one position that depended more upon the station geometry than on the signal strength or locate tremor in a corner of the search grid at great depths when the distribution of seismic amplitudes clearly suggests that the signal originates from the caldera. In the end, using Battaglia and Aki’s grid-search method proved to be infeasible.

3.1.3 Revised goal: differentiating between candidate tremor sources

Instead, we have adapted the attenuation-with-distance concept from Battaglia and Aki’s (2003) grid search method to a simple algorithm that attempts to discern between a few a priori source locations. I chose candidate tremor sources based upon geodetic studies and previous activity. These candidate source locations include Cone A, which was the source of the 1997 eruption, and various COIs, which are modeled locations where magma may be accumulating after intruding from depth (Table 3.1 and Figure 3.2).

Table 3.1 Possible tremor source locations at Okmok Volcano.

Source Name	GPS	InSAR	Lat	Lon	Depth (km)	Map Designation
Cone A			53.3983	-168.1646		α
COI 1997–1998 ^a		×	53.4320	-168.1310	3.5–4.1	β
COI 2000–2001 ^a		×	53.4220	-168.1460	1.9	γ
COI 2001–2002 ^a		×	53.4260	-168.1330	3.1	δ
COI Fournier ^b	×		53.4353	-168.1397	3.5	ϵ
COI Biggs ^c	×	×	53.4290	-168.1357	3	ζ

COI – Center of Inflation

^aMann *et al.*, 2002

^bFournier *et al.*, 2009

^cBiggs *et al.*, 2010

At a minimum, this methodology should be able to differentiate between signals originating within the center of the caldera and signals originating at Cone A. Signals from near the caldera center could be associated with inflation observed in both GPS and InSAR data sets due to magma injection and associated degassing. Signals occurring near Cone A may be indicative of the hydrothermal system, or of active degassing from the magma reservoir. This degassing could come directly up from the reservoir, or it could travel laterally along cracks and fissures.

At Okmok, we assume that the tremor source is between the surface and 5 km depth. This corresponds to the center of inflation modeled previously via both InSAR and GPS data (Mann *et al.*, 2002; Fournier *et al.*, 2009; Biggs *et al.*, 2010; Masterlark *et al.*, 2010). The petrologic indicators, such as olivine crystals and H₂O concentrations within melt inclusions, were consistent with a basaltic magma that migrated upward from a 3–5 km deep storage region (Larsen *et al.*, 2013) before rising to the surface in the 1997 eruption at Cone A.

Using InSAR and GPS data, Mann *et al.* (2002) modeled Okmok inflation as a change in pressure and volume in the magma reservoir located near the center of the caldera at a depth of 1.9– 4.1 km. They offered a structural model for Okmok Volcano that showed the magma transported from the COI to erupt at Cone A. Masterlark *et al.* (2010) used Finite Element Modeling in conjunction with InSAR and Ambient Noise Tomography to determine a velocity structure below the caldera and constrain the magma storage under the volcano. Their study revealed significantly lower shear velocities within the top 2 km and a magma reservoir deeper than 4 km. They also suggested that a structure may exist connecting the observed COIs with Cone A (Figure 3.6). In the present work, tremor locations will be interpreted assuming the same basic elements and geometry.

Several assumptions and simplifications are built into this algorithm. First, I assume that the signal at any particular moment in time is a point source. This source may migrate over time, but is expected to be in a relatively stable location. A further simplification concerns the components of the seismic signal. When comparing amplitude ratios for tremor episodes occurring during the course of each day, I assume that the path and station effects do not change. This assumption is backed by observations that the tremor has a consistent frequency content during the active episodes on any particular day, that events repeat, and that the range of amplitude ratios is fairly constant.

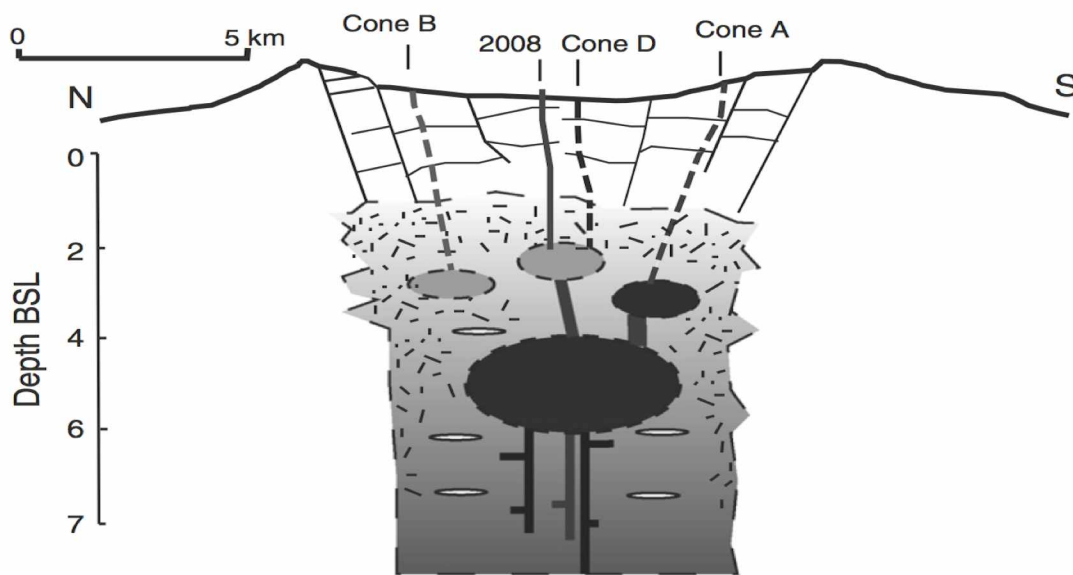


Figure 3.6 Model of subsurface Okmok. A large magma reservoir is postulated to exist between 4 and 6 km depth. Pods of differentiated magma exist between 2 and 3 km below sea level. As magma recharges the central reservoir, fluids may migrate up through existing weaknesses and exit the system at one of several cones. (from Larsen et al., 2013)

Secondly, there is no treatment within the algorithm for the directivity of seismic energy. When earthquakes occur, seismic energy is radiated in a pattern dependent upon the fault plane and direction of rupture, creating areas of compression, dilatation, and neutrality of varying amplitudes that depend upon the location of the receiving station with respect to the source. Tremor modeled as oscillations within a dike or sill would also exhibit directivity (Chouet, 1981, 1988), whereas tremor within a cylindrical conduit or spherical body would be more likely to radiate symmetrically (Chouet, 1985; Crosson and Bame, 1985). Here, I assume a symmetrical source so that recorded amplitudes are unaffected by the azimuth to the tremor source.

3.2 Methods

3.2.1 Technique overview

Since locating the tremor seems an unachievable goal with so few stations, I attempted to discern between candidate tremor locations along a linear feature that extends from Cone A through the center of the caldera. I also constrained the lateral extent or migration of the source. First, distances from each station to possible source locations were determined. Using this information, I used the amplitude decay over distance (equation 3.2) to create expected tremor amplitude profiles for each station. Next, I

compared the amplitudes as a ratio between each station and a station more or less equidistant from the candidate sources. I refer to the latter as the reference station.

By using amplitude ratios I can effectively remove the source amplitude from the equation, which simplifies the problem and makes it friendlier to a sparse network. Although changes in the strength of a stationary source will affect the amplitudes at each station, the *relative* amplitude ratios at each station are unaffected. Using amplitude ratios allows me to treat changes in location separately from changes in amplitude. I then interpret results by comparing them to calculated ratios for each candidate source.

It is doubtful with such a sparse network that this technique will be able to differentiate between the various geographically close sources (Table 3.1). Instead, this study concentrates on the variability at Cone A and two of the COIs, the 2001–2002 COI, and the Biggs joint inversion result.

3.2.2 Determining the RMS magnitudes

I decided to use the root-mean-square (RMS) amplitude of the signal, gathered in 10-second samples (N=1000 at a 100 Hz sampling rate), as my yardstick for tracking the seismic activity. This resolution smooths over the short-scale variations in signal strength. First, the appropriate gain was applied to each channel of data in order to convert from counts to nm s^{-1} . Then, I filtered the data with a bi-directional Butterworth filter, band passed between 0.8 and 6.0 Hz. This is a slightly wider spectrum than the original filtered seismic data that triggered this investigation, but it encompasses most of the seismic energy, which appeared on spectrograms in the range between 1.5 and 6 Hz.

The RMS for each data segment was calculated using

$$A_{rms} = \sqrt{\frac{\sum_{i=1}^N s_i^2}{(N-1)}} \quad (3.3)$$

where N is the number of samples and s_i is the amplitude of the i^{th} sample. These filtered RMS values served as the signal envelope that became the basis of all the subsequent analysis.

To understand the possible effect of travel-time between stations OKCF (nearer) and OKTU (farther), I shifted the data by one sample (ten seconds). The effect was negligible for the two sample dates I used: June 6 2003 and February 24 2004. Therefore, the RMS data were not shifted in time to account for travel time.

3.2.3 Choosing a reference station

All ratios are taken in relation to a reference station. The reference station must be functioning on most days during our investigation. Ideally, it will also be quasi-equidistant from the candidate locations, making the results more intuitive and easier to interpret. It must be far enough away so that the amplitude is still stable with depth, yet close enough to record the tremor signal. Station OKTU (Figure 3.2) met these requirements, and was therefore our reference station.

A linear relationship between RMS values at stations is demonstrated in the scatter plot (Figure 3.7) for data from 24 February 2004. In this figure, the RMS values for all functioning stations are plotted on the vertical axis against the RMS values at station OKTU. Amplitudes at all stations scale approximately linearly with the amplitude observed at OKTU. The only station within the caldera, OKCF, is more sensitive to the tremor signal than is OKTU. Distant stations OKID and OKSP are less sensitive, and the

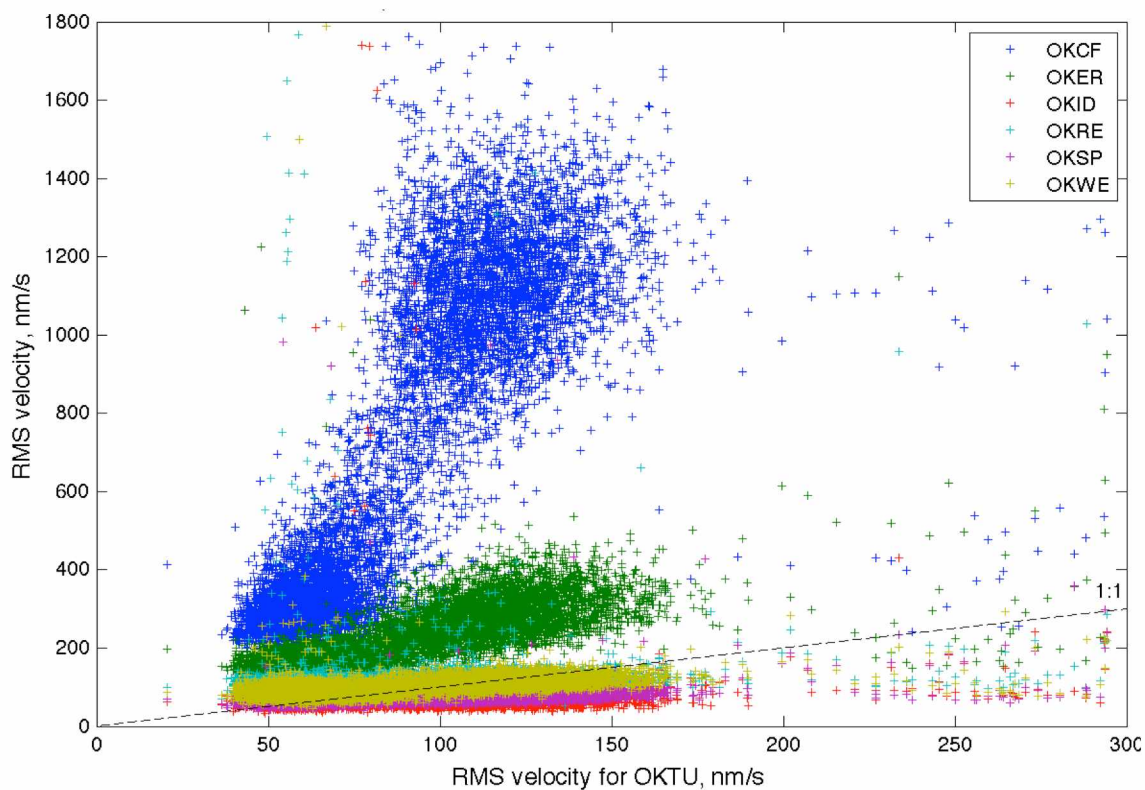


Figure 3.7 Comparison of RMS amplitude relationships. Comparison between station OKTU and all other stations at all short-period stations for 24 February 2004. This plot shows the linear relationship between the stations' amplitudes. Station OKID (red) is farthest from the center of the caldera, while station OKCF (blue) is closest. The dashed line represents a ratio of 1:1, where RMS values from station OKTU would plot against themselves.

slope of their signals is nearly flat. During periods of active tremor, station OKTU recorded a signal with filtered RMS amplitudes of between 100–150 nm s⁻¹. One can infer from this graph the sensitivity of each station to this tremor source.

Two other, three-component broadband stations (OKCE and OKCD) existed within the caldera but were not functioning prior to September 2004, so they were not used. Information from these stations would have helped to distinguish between tremor occurring at Cone A, or at the COI, or on the pathway in between.

I chose to compare observations on five initial dates that span much of the active tremor period: June 6 2003, September 26 2003, February 24 2004, September 15 2004, and January 5 2005. These dates were chosen because on each date there was a clear tremor signal that was recorded at multiple stations, and because there was a clear signal at the reference station, OKTU.

3.2.4 Determination of the model parameters

To use equation 3.1, I determined values for attenuation Q , velocity β , and frequency f empirically. Tremor at Okmok is composed of a broad spectrum of frequencies; peak frequency varies between 1.5 Hz and 6 Hz, with a nearly constant peak between 2–3 Hz at station OKTU. Based on this observation, a frequency of 2.5 Hz is used here for the attenuation calculations.

Three stations were located at roughly equal epicentral distances between the candidate sources (Figure 3.8): OKTU (8.0–8.3 km), OKWR (4.5–5.0 km), and to a lesser extent OKWE (8.5–9.5 km). Because tremor originating at any of our candidate locations would exhibit a relatively similar amplitude signature, I could use these stations to refine the values of Q and β . Correct values of Q and β allow the decay equation to correctly describe the amplitudes at these stations, regardless of the source location. As Q increases, so does the range of amplitude ratios that can describe each depth. Changing β affects the expected amplitude for any given point source. I varied the attenuation and velocity until the ratios between station OKTU and stations OKWE and OKWR provided answers that matched well for all candidate tremor sources. This provided some assurance that these parameter choices were reasonable.

The resulting values of $Q=40$, $\beta=0.7$ km s⁻¹, and $f=2.5$ Hz compare favorably with observations by previous authors. Although $Q=50$ is common at volcanoes, $Q_r=45$ has been observed at Pavlof at 1.5 Hz (McNutt, 1986), and lower Q values have been observed at other volcanoes (McNutt, 1986; Del Pezzo *et al.*, 1989). Figure 3.9 demonstrates the fit of these values on real data at Okmok.

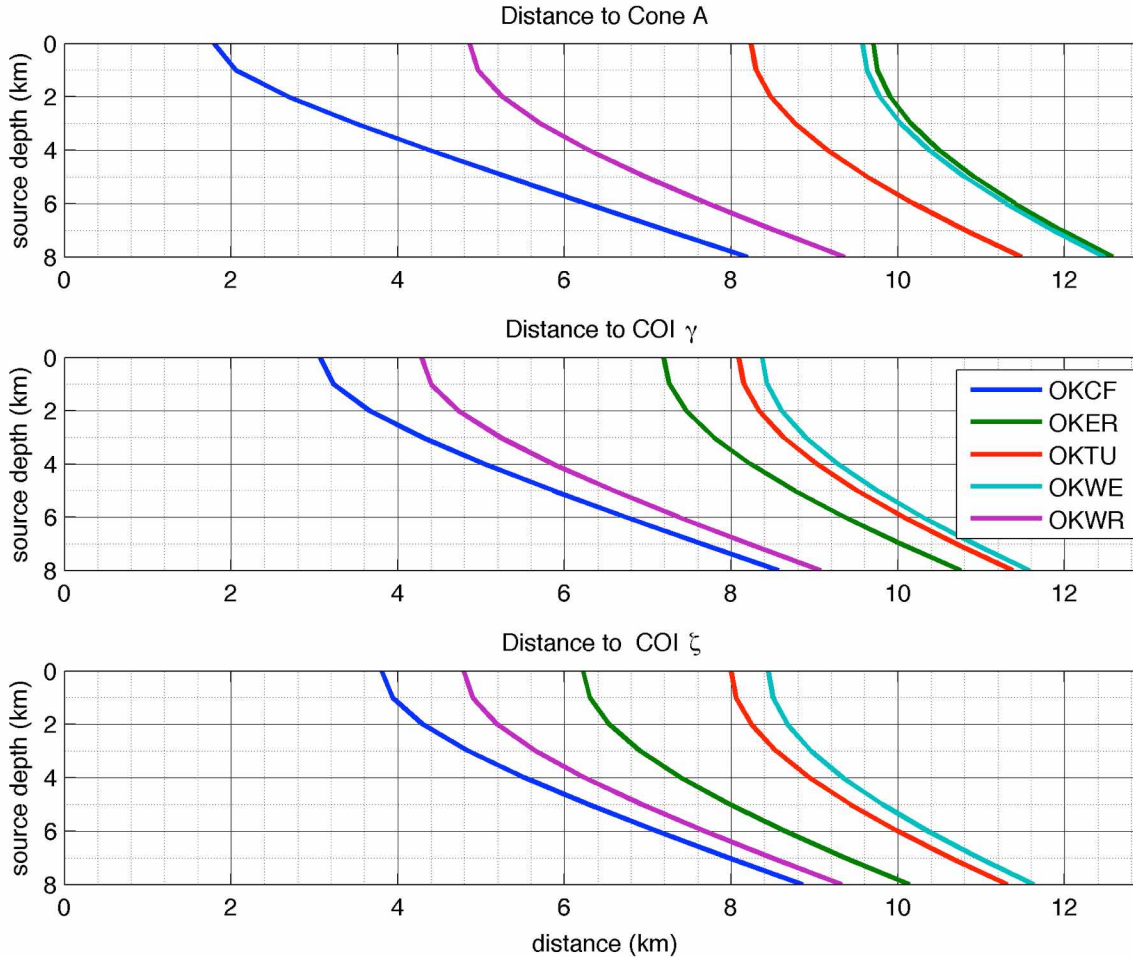


Figure 3.8 Distance between each station and three sources with depth. Stations OKCD (Cone D) and OKCE (Cone E), while well positioned within the caldera, were not operational during much of this study, and were therefore not used. Locations are listed in Table 3.1 and shown in Figure 3.2.

Battaglia and Aki (2003) used a group propagation velocity of 1.0 km s^{-1} for their study of Piton de la Fournaise. Masterlark *et al.* (2010) determined that the top two kilometers at Okmok have group velocities between 1.5 and 1.8 km s^{-1} , as measured at $0.2\text{--}0.4 \text{ Hz}$. Saccorotti *et al.* (2003) determined that phase velocities underneath and around Kilauea Volcano could be as slow as 300 km s^{-1} . Thus a group velocity of $0.5\text{--}1.0 \text{ km s}^{-1}$ for a 2.5 Hz signal seems plausible.

Using these values in equation 3.2, I determined the amplitudes at each station for a source with the arbitrary amplitude $A_{\text{rms}}=100$ in each of the three candidate locations. The resulting Figure 3.10 demonstrates that only station OKCF is well positioned to differentiate between source locations, especially within the first 2–3 kilometers of the surface. Although amplitudes at both OKCF and OKWR change quickly with depth, OKWR provides consistent depth profiles for all sources, making it the

lynchpin for depth determination. Station OKER is also relatively well positioned to distinguish between candidate locations. Distal stations (OKRE, OKWE, and OKTU) are poorly suited to localizing a tremor source, because there is little variation in amplitude with either source depth or lateral source variability. OKTU is especially indifferent to the position of a source within 3 kilometers of the surface. Figure 3.10 also illustrates that the ability to determine the location of tremor diminishes rapidly as tremor moves deeper, since all amplitudes rapidly converge. This fact is further illustrated in Figure 3.11, in which all values have been normalized by station OKTU. Here we see the amplitude ratio expected at each station for tremor originating at each candidate location (fig 3.2).

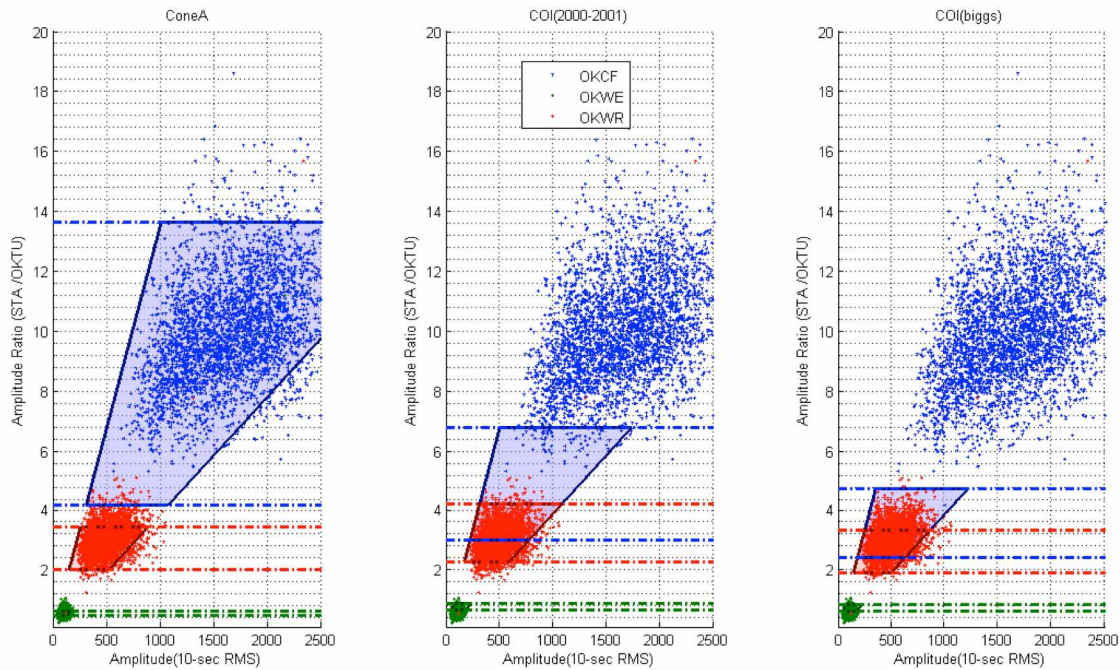


Figure 3.9 Relative amplitude locations for active tremor on June 6 2003. These plots allow one to visualize how well the data fit the possible tremor locations, given the parameters $Q=40$, $\beta=0.7 \text{ km s}^{-1}$, and $f=2.5 \text{ Hz}$. Ten-second RMS amplitude values at each station are plotted along the horizontal axis. The vertical axis shows the amplitude relative to station OKTU. For a stationary, point-source tremor of varying strength, the relative amplitudes should remain constant, resulting in a horizontal spread. Systematic vertical deviations indicate a source that migrates or extends in a direction perpendicular to the reference station.

Polygons in each panel show the predicted tremor amplitudes for a given location. The reference station's amplitude range and calculated tremor depth (0–3 km) define the shape. The two populations that appear on this figure include both tremor and background values. Dashed lines are visual extensions of the depth boundaries.

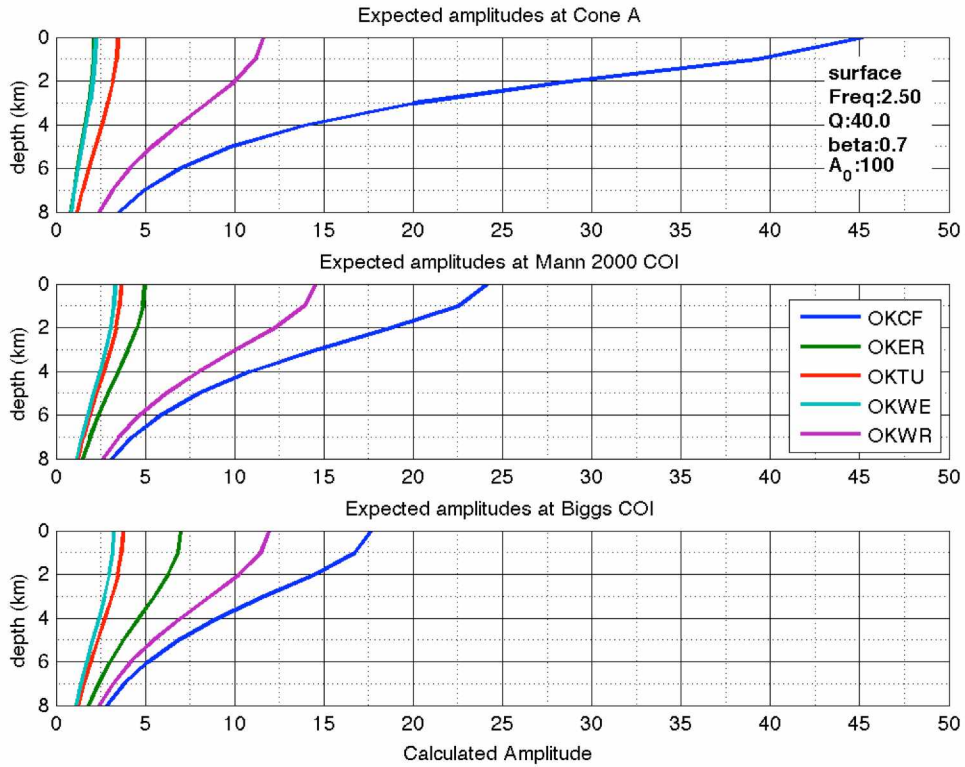


Figure 3.10 Expected amplitudes for possible tremor sources. Values were based on a source of $A_0=100$, at a range of depths. Values were determined via the amplitude decay equation 3.2, using $Q=40$, $\beta=0.7 \text{ km s}^{-1}$, and $f=2.5 \text{ Hz}$.

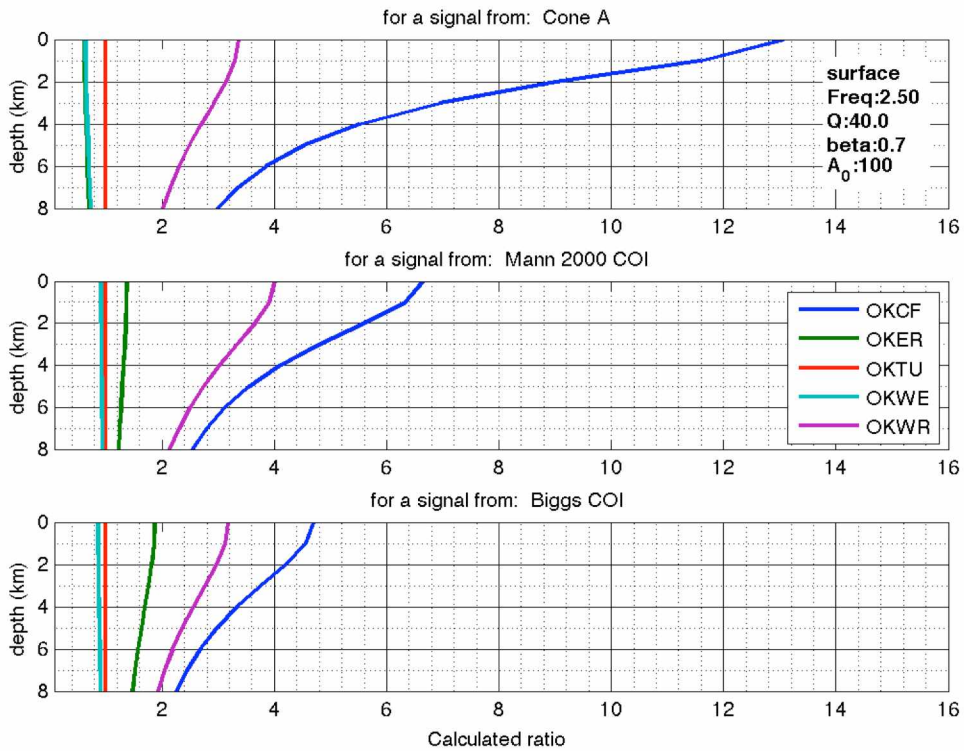


Figure 3.11 Expected ratios relative to station OKTU for selected locations and depths.

3.3 Tremor comparisons between stations

3.3.1 Reading the comparison plots

Figure 3.12 serves as a guide for the amplitude relationships, which are plotted in Figures 3.13a-e. Each figure illustrates the seismicity for one day and is comprised of three density-plot panels plus the associated RMS time series for stations OKCF, OKWR, OKER, and OKTU. The color range (MATLAB's default "hot" color scale) varies for clarity and depends upon the number of measurements. Black represents the fewest measurements, grading through red and orange, with the most measurements in pale yellow.

Each value in the density-plot panel represents the number of observations that match a particular combination of amplitude-ratio and amplitude. Bin sizes are selected based on readability. Although bins differ for each station to account for different amplitude ranges, they remain consistent across days. The amplitude of a signal at a station is plotted along the horizontal axis, while the same value scaled by the value at OKTU is plotted along the vertical axis.

For example, assume a station X records a signal at time i with amplitude RMS_X , while reference station OKTU records a signal with amplitude RMS_R . This observation would plot at $(RMS_X, RMS_X/RMS_R)$. Equation 3.2 shows that the observed amplitude scales linearly with the source amplitude. This implies that each location has a signature ratio, which is independent of the source strength. Therefore when the strength of the source intensifies, the observation migrates rightward on the plot, with no vertical translation. The vertical axis is only sensitive to source location. When a higher ratio is observed it reflects a migration toward the observing station relative to the reference station.

Background seismic levels appear on the comparison plots as a concentration with low RMS and relatively spread-out ratio values. This behavior is not seen in the plots from 2003 (Figures 3.13a-b), since that entire time period is dominated by various tremor intensities. However, background levels feature prominently at stations OKER and OKWR for the remaining plots (3.13c-d).

If the tremor source region has an areal extent instead of being a point source, then the RMS at each station may be dominated by signals generated from different locations. For example, if tremor is generated by the vibration of a crack that extends from the center of the caldera to Cone A, that source may appear to be near stations OKCF and OKER simultaneously.

Ratio comparison guide

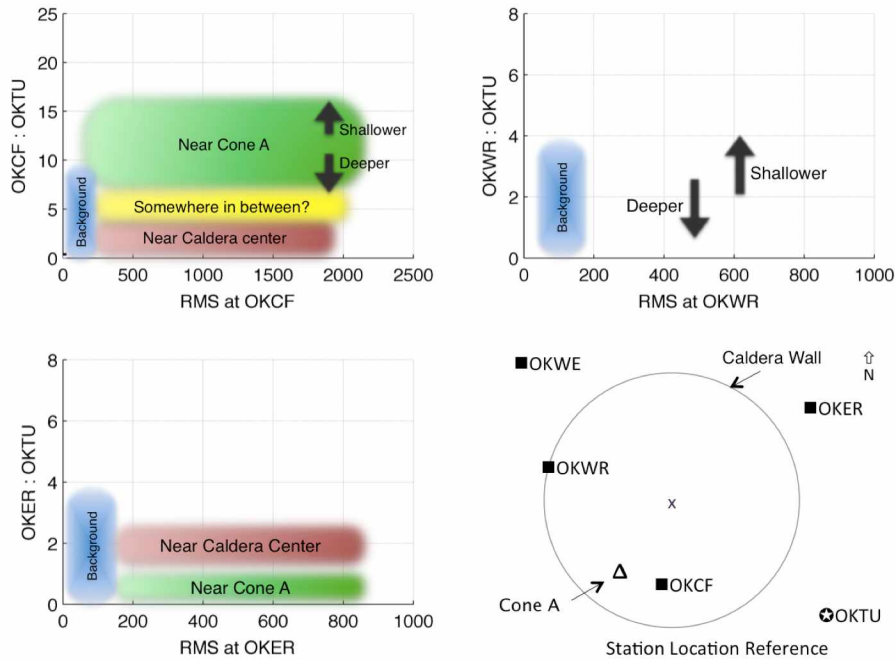


Figure 3.12 Interpretation guide for the ratio comparison plots. This is the key to interpreting the ratio comparison plots (Figures 3.13a-e). Suggested locations are based on expected ratios for each station (Figure 3.11). The ratio at OKCF is most sensitive to depth at Cone A. The ratio at OKWR is mainly governed by depth to source, since there is little variation among the sources. Station OKER is on the opposite side of the caldera from OKCF, so activity here should track opposite that seen at OKCF. However, the ratio at OKER is unaffected by source depth. When no tremor is present, then values are expected to fall in the “Background” area, with low amplitudes and variable ratios

3.3.2 Interpreting the tremor amplitude ratios

Using Figure 3.11 as a guide, we can hypothesize about the amplitude ratio behavior for a number of scenarios (Figure 3.12). First, we see that the amplitude ratios between OKCF and OKTU are particularly sensitive to depth. As the source becomes shallower, the expected amplitude ratio increases. We also see that if tremor originates in the vicinity of Cone A, we expect an OKCF:OKTU ratio of at least seven. When the same ratio drops below five, then Cone A becomes a less likely candidate.

The ratio between OKER and OKTU appears to be relatively insensitive to depth. A change in this value likely reflects a lateral tremor migration. Tremor that emanates from the COI has higher amplitude than tremor originating near Cone A.

The relative amplitudes between OKWR and OKTU vary little among the candidate sources. For this station pair, amplitude ratios of approximately four are expected for a shallow source in between the COIs and Cone A. This value decreases as tremor migrates either towards Cone A or towards the center of the caldera.

When no tremor is present, then stations are recording “background” noise. This should appear as observations at low amplitudes, while the ratio between any pair of stations will be spread across relatively low ratios.

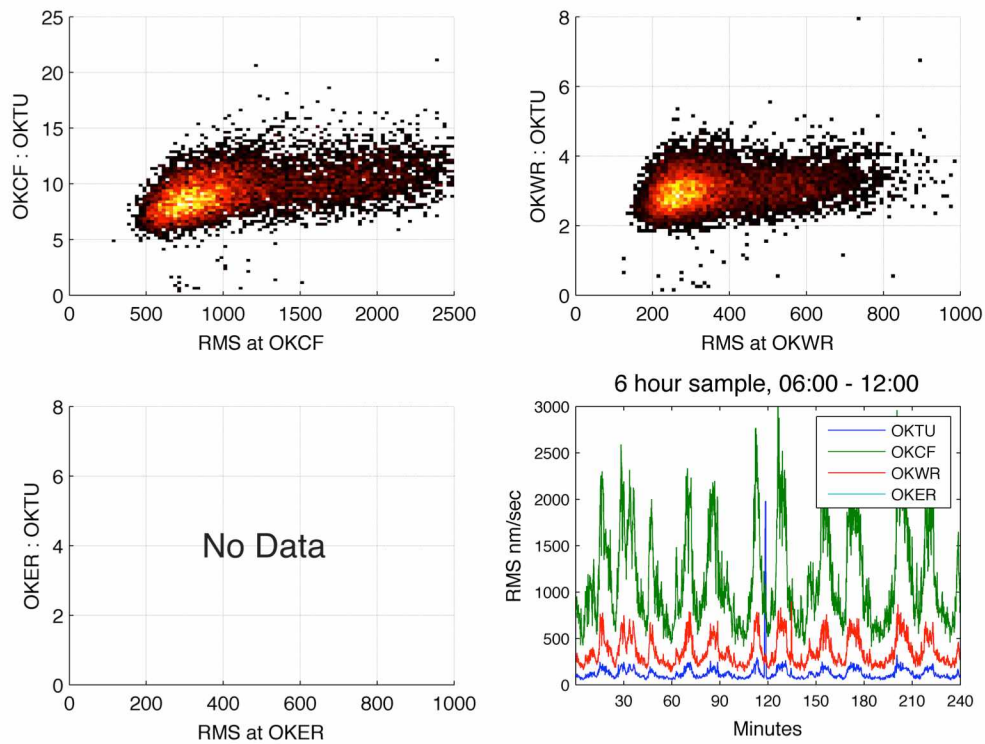


Figure 3.13a Ratio comparisons for June 6 2003. Each panel represents the day's observations at a different station. The vertical axis (amplitude ratio) is a proxy for distance from each station. The horizontal axis charts the signal intensity at each station (filtered RMS amplitudes). Each colored point represents the number of observations made at that particular ratio-amplitude combination. Each observation spans 10 seconds, for a total of 8640 data points per day. In the lower-right quadrant I have plotted a six-hour RMS amplitude time series. The color scale itself varies based on the maximum number of measurements at any particular RMS – Ratio bin.

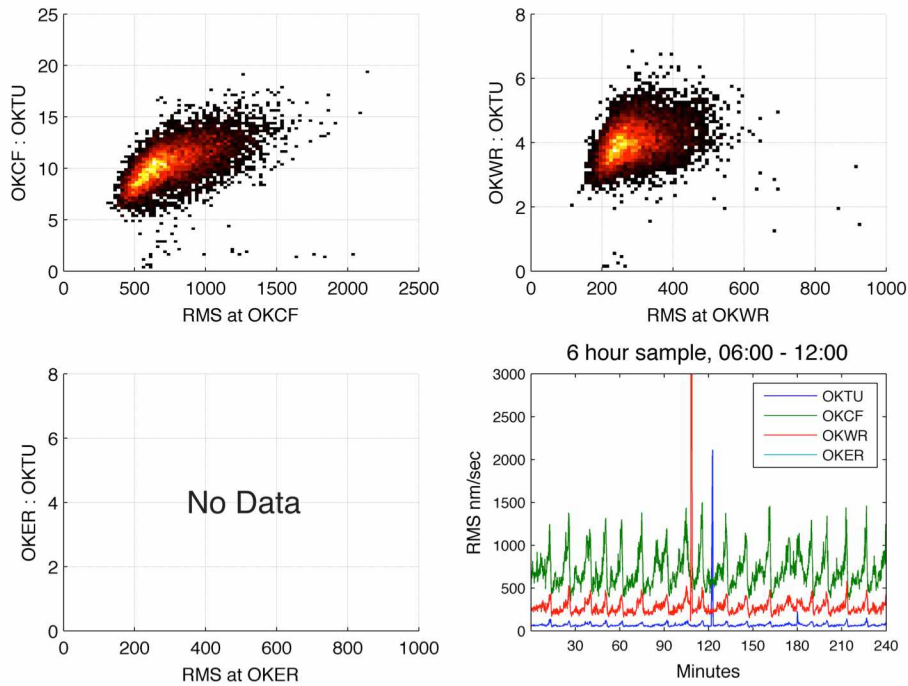


Figure 3.13b Ratio comparisons for September 26 2003. See Figure 3.13a for explanation.

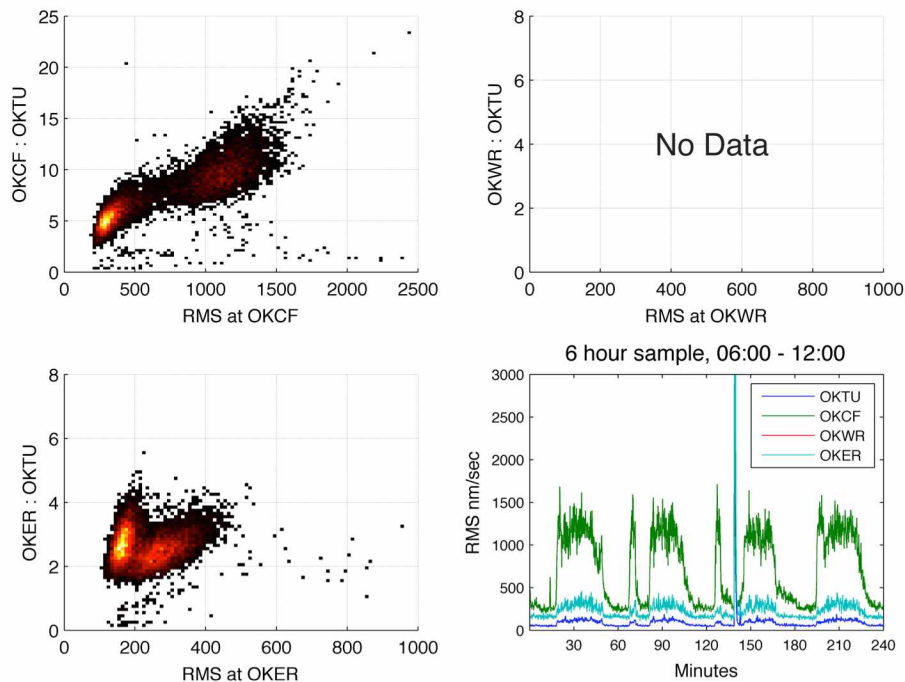


Figure 3.13c Ratio comparisons for February 24 2004. See Figure 3.13a for explanation.

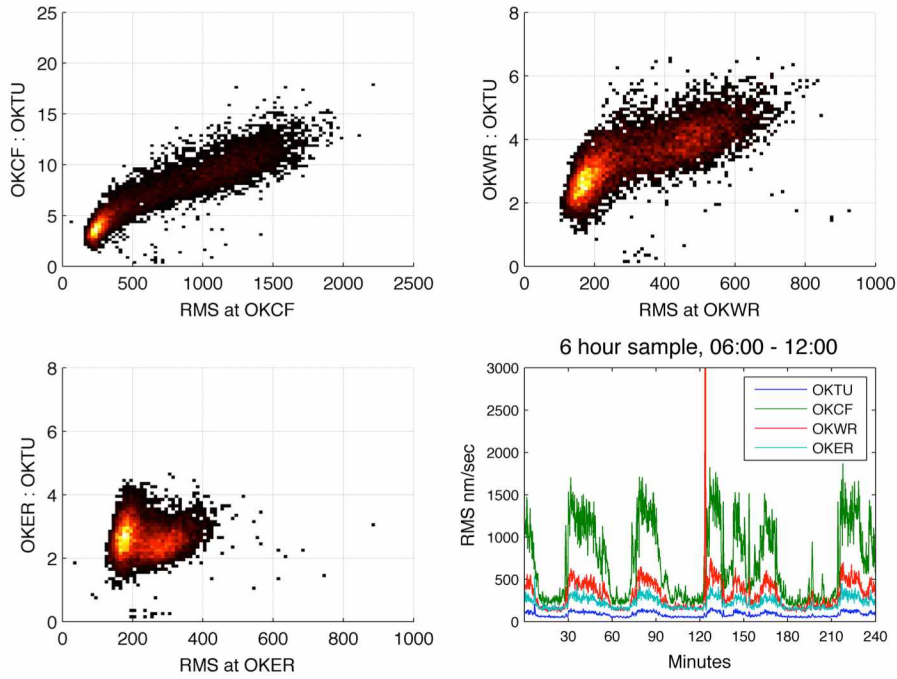


Figure 3.13d Ratio comparisons for September 15 2004. See Figure 3.13a for explanation.

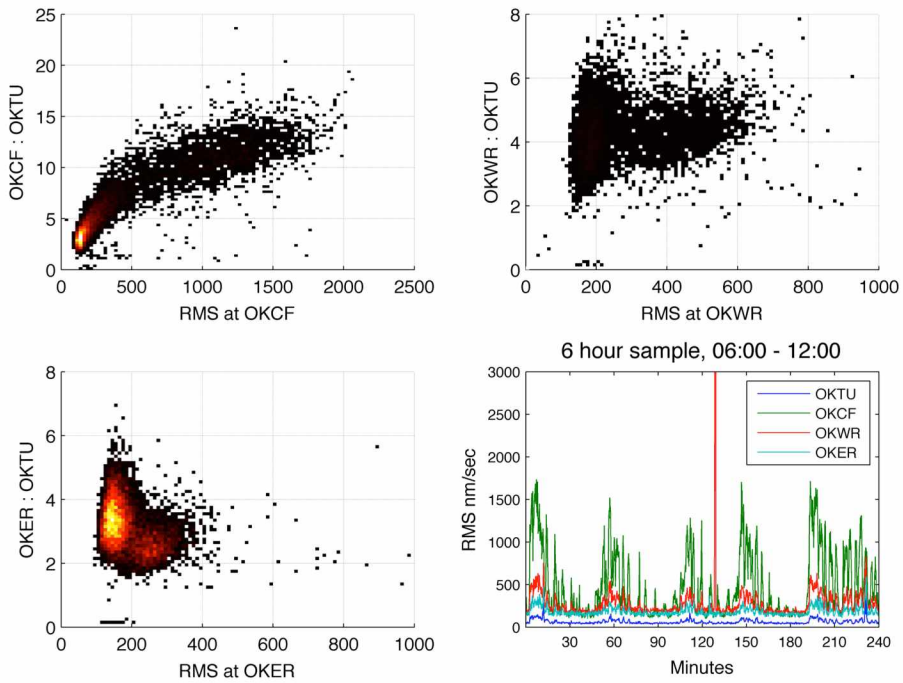


Figure 3.13e Ratio comparisons for January 5 2005. See Figure 3.13a for explanation.

3.3.3 Interpretations

Tremor episodes on **June 6 2003** (Figure 3.13a) lasted roughly 15 minutes and occurred without pause. Throughout the day ratio values remained stable, independent of the amplitude, suggesting that the signal came from a single location. Compared to the later dates, the amplitude ratios at station OKCF were low, suggesting that either this particular source is deeper or is located NW of Cone A. Data were not received from station OKER on this date.

On **September 26 2003** (Figure 3.13b) the tremor was weaker, but the occurrence interval was roughly the same as before. The ratios at OKCF were also similar to those observed in June, albeit compressed into a smaller range of amplitudes. However, the higher values at OKWR suggest that perhaps the source was shallower than in June.

On **February 24 2004** (Figure 3.13c) the character of the tremor changed. Short ~5 min bursts of tremor occurred alongside longer episodes, lasting ~33 minutes (Figure 3.4). In between bursts, periods of relative quiet occurred. The ratios show a bimodal distribution; the background levels plot in a tight cluster of low-amplitude observations at both OKCF and OKER. The tremor signal ratios are more spread out at OKCF, with little apparent differentiation between short and long episodes. OKCF ratio values range from 7 to over 15, continuing to suggest that the signal remained in the vicinity of Cone A. This observation was confirmed because the ratios at OKER noticeably dip with higher signal amplitude. This dip supports the idea that the active signal originated farther away than the OKER location.

Short strong shallow pulses appear to occur at Cone A, as evidenced by the large ratio at OKCF. These seem independent of the longer pulses which appear to occur somewhere between the COIs and Cone A. Three hours of tremor activity are examined in detail in Figure 3.14. The rapid increase and decrease of high-amplitude ratios can be described by a vertical movement of the source below/near Cone A or by the source migrating along some pathway that originates deeper within the caldera and ascends towards Cone A. The fact that OKER amplitudes change little in relation to OKTU suggests that the two stations were at roughly the same distance from the source. At times the ratio at OKER moves opposite to that at OKCF; at other times the ratios track each other. This suggests a lateral migration of the source. The systematic change in ratios occurs even while OKTU appears to be at background levels, suggesting that some underlying process continues, but is only recorded at closer stations.

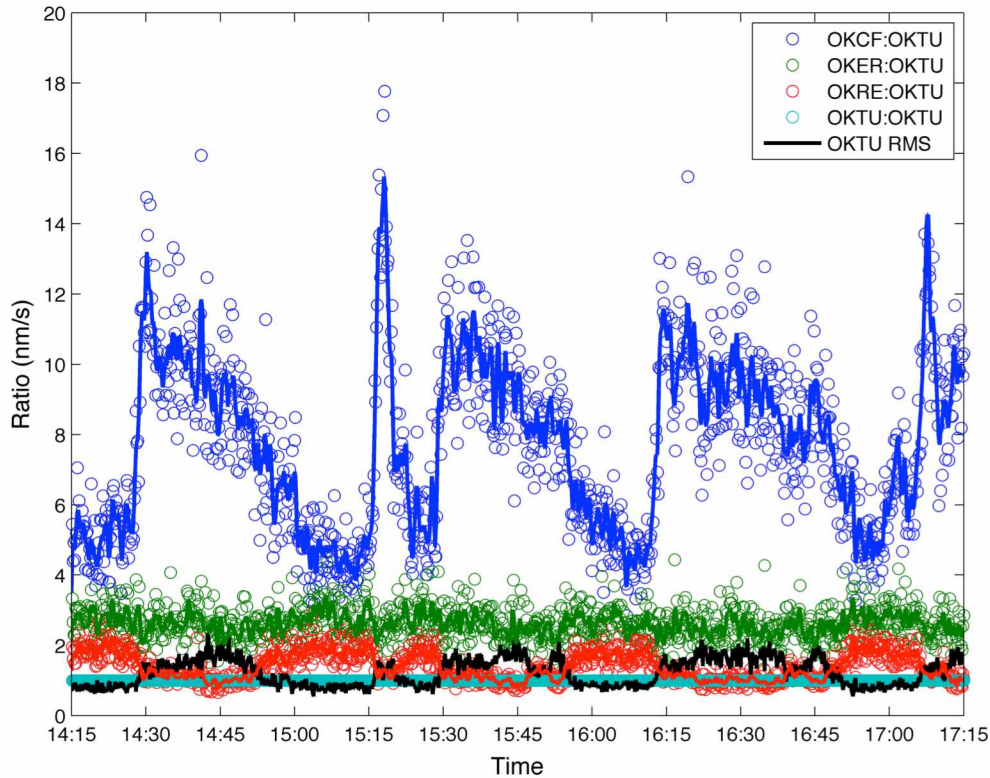


Figure 3.14 Tremor ratio time series. This plot highlights 3 hours of amplitude ratios, with respect to OKTU, for tremor occurring on February 24 2004. The solid colored lines are the running 7-point averages. For reference, the tremor amplitudes (arbitrary units) from OKTU are shown in black.

On **September 15 2004** (Figure 3.13d) the tremor was expressed once again as a combination of short and long pulses (Figure 3.5). The longer pulses were as strong as they were in February, and this time they were picked up at all four stations. Meanwhile, the short pulses were briefer, often only lasting one minute, and did not reach the amplitudes that would have been required to show up at OKTU or OKER above the background noise level. There was more variability in tremor durations, which lasted from 10–70 minutes. The longer events seemed to be composed of sequential pulses. According to values at OKCF, the ratios range from 5–15, meaning that the tremor could have been located at a range of depths under Cone A, or could have occurred between Cone A and the COI. The ratios at OKER continue to suggest that the source was located farther away. Meanwhile, ratios at OKWR could mean that the tremor occurred at a range of depths.

Figure 3.15 shows activity over the course of two weeks, from September 11 through September 24 2004. During this series, a signal appeared to originate with low OKCF ratios, and then repeatedly migrated into a higher range of ratios. This would be consistent with a signal that originated deeper and further toward the COIs, and then repeatedly migrated upward and southward towards Cone A.

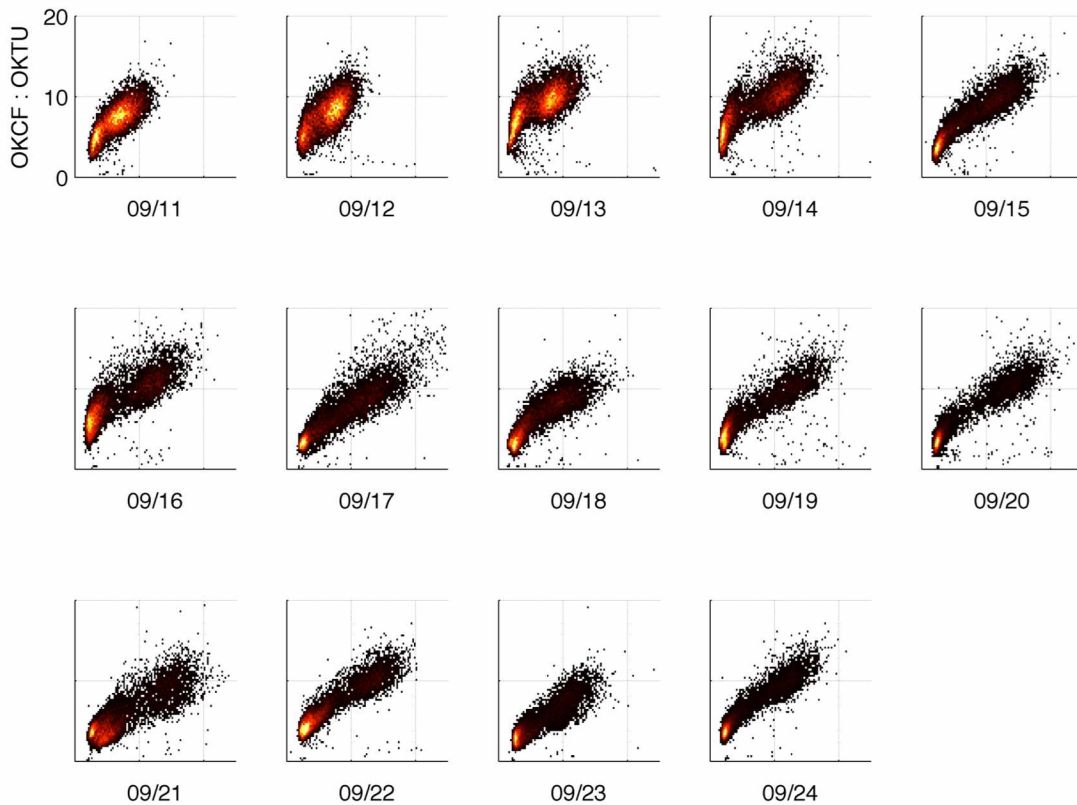


Figure 3.15 Time series showing tremor migration from September 11–24 2004. Each blob represents the number of observations occurring at a particular amplitude-ratio vs. amplitude combination for each day at OKCF. Higher values plot from red to yellow. Additional detail for September 15 is provided in Figure 3.13d. The general trends from lower left to upper right indicate that stronger signals occur closer to (and/or shallower than) OKCF, and by extension Cone A. This series reveals a signal that originated near the COI and repeatedly migrated upward and/or toward Cone A.

On **January 5 2005** (Figure 3.13e) the ratio plots appear similar to the previous days, but observations at OKWR have a relatively wide spread, which could imply a source that ranges in depth. Ratios at station OKER show that higher-amplitude signals were still relatively distant. Station OKCF still showed ratios in the 7–13 range, which suggests a nearby source.

3.4 Discussion

Surface observations confirm that Cone A was active during this study. Field crews at Okmok have witnessed active steaming at Cone A that occurred in cycles on roughly the same time scale as the tremor (C. Nye, pers. communication). Although no quantitative measurements of gas emission have been made at Okmok, a bluish plume (suggesting SO_2) was photographed in early August 2003 (J. Freymueller, pers. communication). This gas could have been coming off a magma source. Incandescence was also reported

within the small hole at the Cone A summit crater in September 2004 (T. Neal, S. McNutt, J. Larsen, pers. comm.), which also points to a shallow heat source.

These observations agree with the scenario suggested by the consistently high ratios visible at OKCF. Tremor appears to originate at a relatively shallow source associated with Cone A. When viewed on the scale of minutes, there is a ratio change that is at times systematic, as exemplified in Figure 3.14. On that day, each tremor episode initiated with a steep rise in both the amplitude at OKTU and the amplitude ratio at OKCF. Over the course of the following half hour, the ratios dropped from 12 to 5 before the next tremor episode started with another steep climb. This pattern appears decoupled from the amplitudes recorded at OKTU, suggesting that a migration of the source is real.

This leaves us with the explanation that the surface, or near surface, of Cone A lies at one end of the observed tremor source region, and that tremor occurs along some pathway that either extends deeper or has lateral extent. Given the geometry illustrated previously in Figure 3.6, it is quite reasonable to expect a combination of both. Let us investigate a few possibilities that fit the geometry presented in Figure 3.6 and end at Cone A.

First, I discount the idea that a shallow dike or sill emplacement would provide this signal. If the tremor were from magma movement in a dike or sill being emplaced at shallow depth, then it is reasonable to expect the InSAR or campaign GPS studies to have caught it. The geodetic studies all point toward inflation in the center of the caldera, not at Cone A.

If signals originate in a simple conduit underneath Cone A, then the changes in relative amplitude could be explained by a vibration starting high in the column, and migrating downward. Such might be the case with a hydrothermal system where boiling of a superheated system releases the pressure, allowing superheated water to flash to steam at progressively greater depths. Incandescence visible at the surface confirms that we have a heat source that is at least 530 °C and more likely at least 630 °C (Sostman and Metz, 1995). Another explanation, using the same geometry, is that the entire column could be reverberating with gas, and is then progressively stilled from the top down. The spread in amplitude values suggests that this process is occurring within the top kilometer or two.

A conduit scenario raises this question: While the relative magnitude between signals decreases, then how would the signals maintain a constant magnitude at a nearby station? This, if true, would suggest that the source grows stronger as it goes deeper. Were that the case, OKER and OKTU would have recorded coincident increases in amplitude. This does not obviously appear to be so.

Let us consider tremor occurring in a crack with a purely lateral extent, stretching from Cone A in the direction of the Caldera center. Any signal within the kilometer closest to Cone A could be considered equidistant to station OKCF. A signal migrating along this crack should not strongly affect the ratio at OKCF until it has travelled more than a kilometer. This seems unrealistic, given that the estimated depth to the heat (magma) source is 3–6 km.

Masterlark *et al.* (2010) suggest a crack could have propagated upward from the edge of the magma reservoir in the direction of Cone A. This scenario, the activation of a shallow crack that extends from a shallow magmatic source up to Cone A, provides a reasonably good explanation for the observed data (Figure 3.16). Tremor appears to be associated with periods of inflation at the volcano. Heat from the magmatic body could provide energy for hydrothermal boiling to generate tremor. Additionally, superheated gases escaping from the equilibrating magma could be driving the tremor.

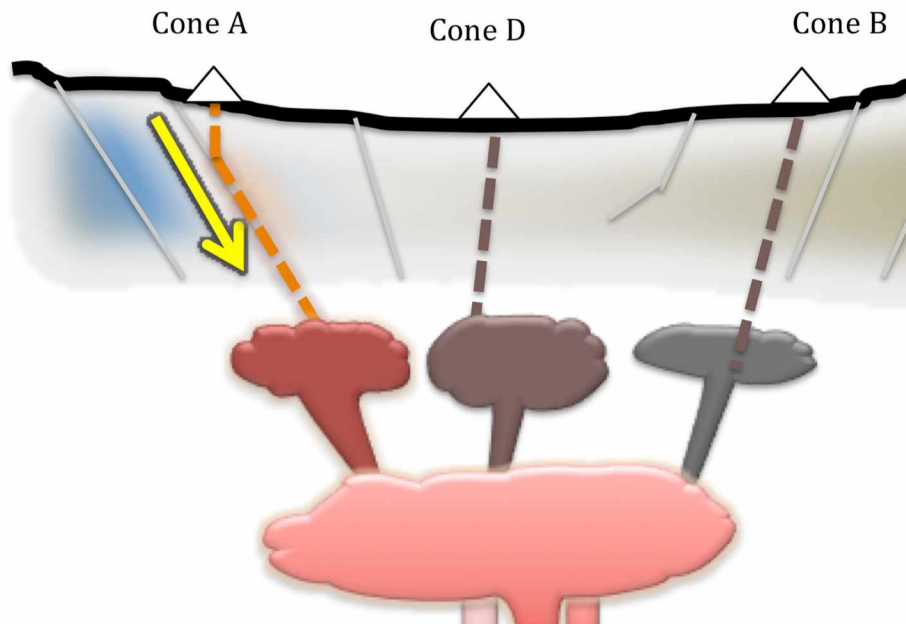


Figure 3.16 Tremor location model. Tremor occurs near the surface, and sometimes migrates downward toward the caldera center.

Short pulses, observed most strongly at OKCF, could be minor degassing events or boiling that occurs at a very shallow depth, but does not activate the entire system. Longer events appear at times to be triggered by a shorter event, to the point where some days nearly every tremor event is initiated by a brief, but strong signal. This gives the appearance of nails marching across the seismograph, with their points to the right.

There is a persistent, quasi-periodic signal emanating from the COI, visible at OKCF once the tremor subsides at Cone A. Over the course of a few days, additional tremor activity migrates away from the COI in the direction of Cone A (Figure 3.15). The pathway between the two is active during this time, and then either becomes inactive or is drowned out by the tremor occurring at shallower depths beneath Cone A. Eventually this activity calms down, and the only signal occurs near the caldera center again. These pulses of activity coincide well with periods when geodetic observations model a rapidly increasing source strength (Figure 3.17) suggesting that as magma is injected into the system, it degasses via a pathway that connects Cone A to the magmatic body.

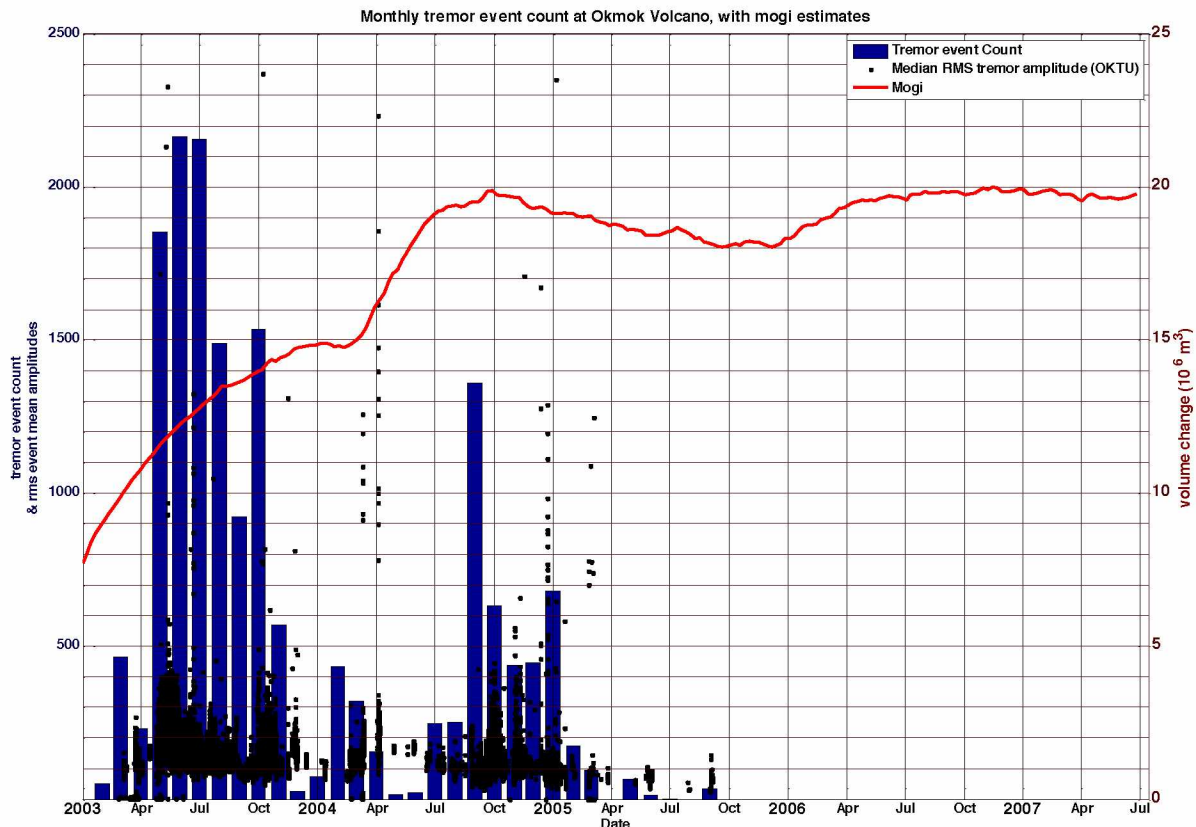


Figure 3.17 Tremor vs. inflation estimated from geodesy. The number of tremor episodes per month are shown as blue bars, median tremor amplitude at station OKTU are black dots, and the volume change modeled as a Mogi source (modified from Fournier 2009).

The system requires from ten minutes to an hour to reset, which suggests a relatively rapid recharge. Heat from the magma system interacting with groundwater could provide the sustained activity over the timescales expected (Fujita, 2008; Kedar, 1998). There is already evidence of a wet system. Cone A has been seen to be vigorously steaming during visits to the volcano. Masterlark *et al.* (2010) suggest that the top 2 km of the caldera are wet fill based on seismic tomography. Also, the phreatomagmatic nature of the

2008 eruption means that magma had interacted with water. The flashing of water to steam and upward migration of gas spurred by heat entering the system from a magmatic body could provide the resonating energy required at these time scales. The heat throughput and long-term nature of the signal imply that Okmok was maintaining some sort of equilibrium at this time.

3.5 Conclusion

The sparse network within Okmok caldera has necessitated the development of a new method of qualifying the movement of tremor that can be used with as few as two vertical short-period stations. By leveraging the likely geometry at Okmok, (Figure 3.6), I was able to use the relative tremor amplitude between nearby stations to show tremor appears consistently in similar locations. The relative ratios suggest the tremor is activated along the pathway or channels between Cone A and the top of a shallow pod of magma in the vicinity. At times, there are systematic changes in amplitude ratios that suggest a source that migrates from Cone A downward and in the direction of the caldera center (Figure 3.16). This migration of tremor could be indicative of the changing front of a two-phase oscillation between water and steam (Fujita, 2008) driven by the movement of volatiles and heat from a shallow magma source.

4.1 Introduction

Okmok volcano is an active basaltic andesite island-arc shield volcano that occupies the northeast half of Umnak Island, in the central Aleutian chain (Figure 4.1). It is defined by a 10-km-diameter caldera that was formed in the second of two cataclysmic eruptions, approximately 2050 years ago (Kienle and Nye, 1990; Begét *et al.*, 2005; Larsen *et al.*, 2007). Subsequent eruptions have created a series of scoria and tuff cones within the caldera (Figure 4.2). These cones are labeled in order of recent activity from Cone A through Cone H (Byers, 1959). Cone A, located in the southwest quadrant of the caldera, is the most recent of these and has been the source of at least eight known eruptions since 1943 (Miller *et al.*, 1998). Ash from Okmok occasionally reaches over ~9,000 m (30,000 ft) above sea level, as occurred in both 1997 and 2008. Ash at these altitudes poses a hazard to commercial aircraft flying great circle routes between the US and Asia.

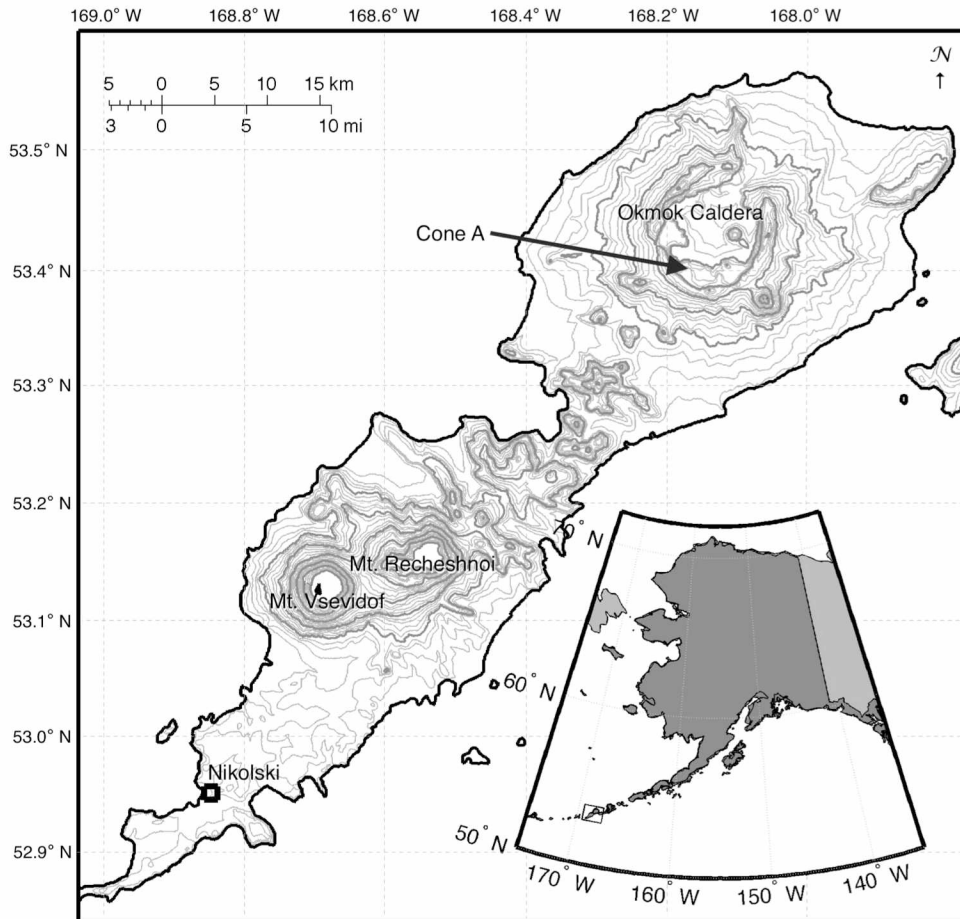


Figure 4.1 Location of Umnak Island, Alaska. Okmok Volcano occupies the northeast half of the island.

In November 1996, a pilot noticed a steam plume rising from Cone A. This was the first observed activity from the cone in several years, and was the precursor to what would culminate with an eruption in 1997 (McGimsey and Wallace, 1999). At the time, no seismic network existed on Umnak Island, though it was not unmonitored. Staff from the Alaska Volcano Observatory (AVO) routinely examined satellite images of Aleutian volcanoes, looking for thermal anomalies or signs of ash emissions. Thermal anomalies are often referred to as “hot spots” and show up in images taken in the infrared spectrum (Dehn *et al.*, 2000). On the morning of February 13, 1997 a hot spot was seen in a satellite image of Okmok. Shortly afterward, local ranchers called to report a dark ash plume rising up to ~1,500 m. Over the next six weeks, Cone A continued to erupt with strombolian lava fountaining and plumes of ash. It emplaced lava flows onto the caldera floor. Activity had significantly declined by March 27 1997 (McGimsey and Wallace, 1999).

The lava flow and associated deformation were studied primarily through satellite images. Patrick *et al.* (2004, 2005) used thermal images to understand how the lava cooled. Lu *et al.* (2003) determined the lava flow’s volume using interferometric synthetic aperture radar (InSAR). This technique estimates topography from line-of-sight radar distance measurements, taken from multiple satellite passes. Mann *et al.* (2002), also using InSAR techniques to measure deformation over time, inferred that the caldera deflated up to 140 cm during the eruption. Further, by modeling the inflation as a point source volume change (Mogi, 1958) they estimated that the center of this deflation was located in the center of the caldera. From pre-eruption deformation patterns, they inferred that magma may have migrated laterally toward Cone A two to three years prior to the 1997 eruption (Mann *et al.*, 2002).

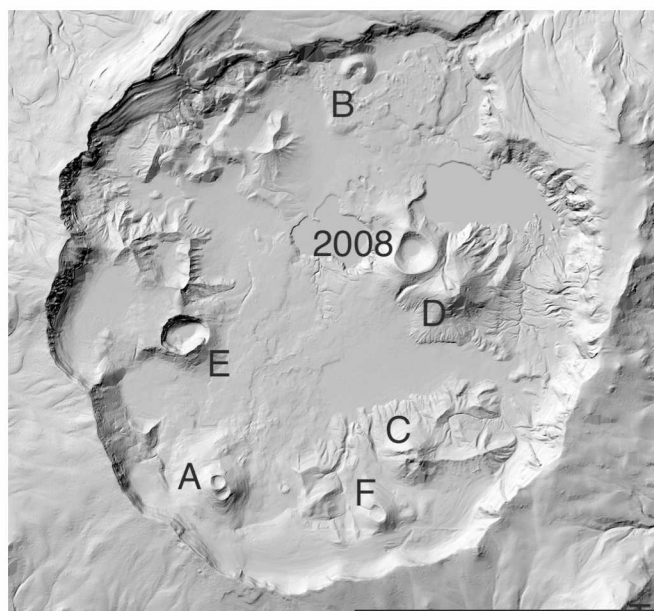


Figure 4.2: Okmok caldera detail. This image shows Okmok Caldera after the 2008 eruption. Each major tephra cone is labeled. (adapted from Schaefer *et al.*, 2011).

In June 2001 field crews deployed a temporary seismic array at Okmok and recorded a continuous ~2 Hz tremor signal associated with Cone A (Caplan-Auerbach *et al.*, 2004). This was a particularly

interesting observation since tremor is a long-duration seismic signal that is often associated with volcanic eruptions and the lead up to eruptions (Koyanagi *et al.*, 1987; McNutt, 1996; Thompson *et al.*, 2002).

In an attempt to determine the source of the tremor, the field team deployed seismometers along a transect between Cone D and Cone A. Each deployment was recorded for 10–20 minutes at sites that were 200–300 m apart. The tremor RMS amplitude increased roughly linearly as they approached Cone A. However, because not all seismometers were able to get a good signal, they could not definitively state that tremor came from Cone A and not the center of the caldera (Caplan-Auerbach *et al.*, 2004).

There are several models that seek to explain the origin of volcanic tremor. The character of seismic tremor likely depends on the fluid (magma and/or gas), the medium through which it flows, and the geometry of any pathways or oscillator (e.g., Julian, 1994; Chouet, 2003). Proposed tremor sources include fluid flowing within a sphere or crack (e.g., Chouet, 1983, 1985, 1988), and bubbles collapsing in a conduit (Kedar *et al.*, 1998; Leet, 1988). Tremor appears on seismograms as a long signal with a duration of minutes to years, with frequencies that usually range from 1–10 Hz (McNutt and Nishimura, 2008).

From 2002–2004, a geophysical network of seismic stations and GPS receivers was installed at Umnak to monitor the volcano (Figure 4.3). The addition of continuous GPS stations meant that deformation could be measured by the relative movements of the GPS receivers at finer timescales than with InSAR. The continuous GPS stations were augmented by campaign GPS measurements, where known surface points, or benchmarks, were located each summer.

During the next few years, InSAR and GPS indicated re-inflation of the volcano (Fournier *et al.*, 2009; Lu *et al.*, 2010; Lu and Dzursin, 2010). Okmok experienced over 0.5 m of uplift between 2000 and 2007. Most of the uplift occurred between January 2003 and July 2004. (Fournier *et al.*, 2009). These studies, summarized in Table 4.1, modeled the observed inflation with a volume change of a stationary source located roughly in the center of the caldera. These studies infer three pulses of magma into the system, with a major pulse in 2003 and again during the first half of 2004; this was followed by a period of deflation in 2005, with a final smaller pulse in 2006.

From 2003 through 2005, tremor remained the dominant seismic signal at Okmok. It appeared as pulses of increased seismic activity that occurred in patterns that remained remarkably consistent on the scale of days but changed in intensity and duration over the course of days to months. By the end of 2005 the tremor had faded in intensity and no longer appeared on most of the seismic network.

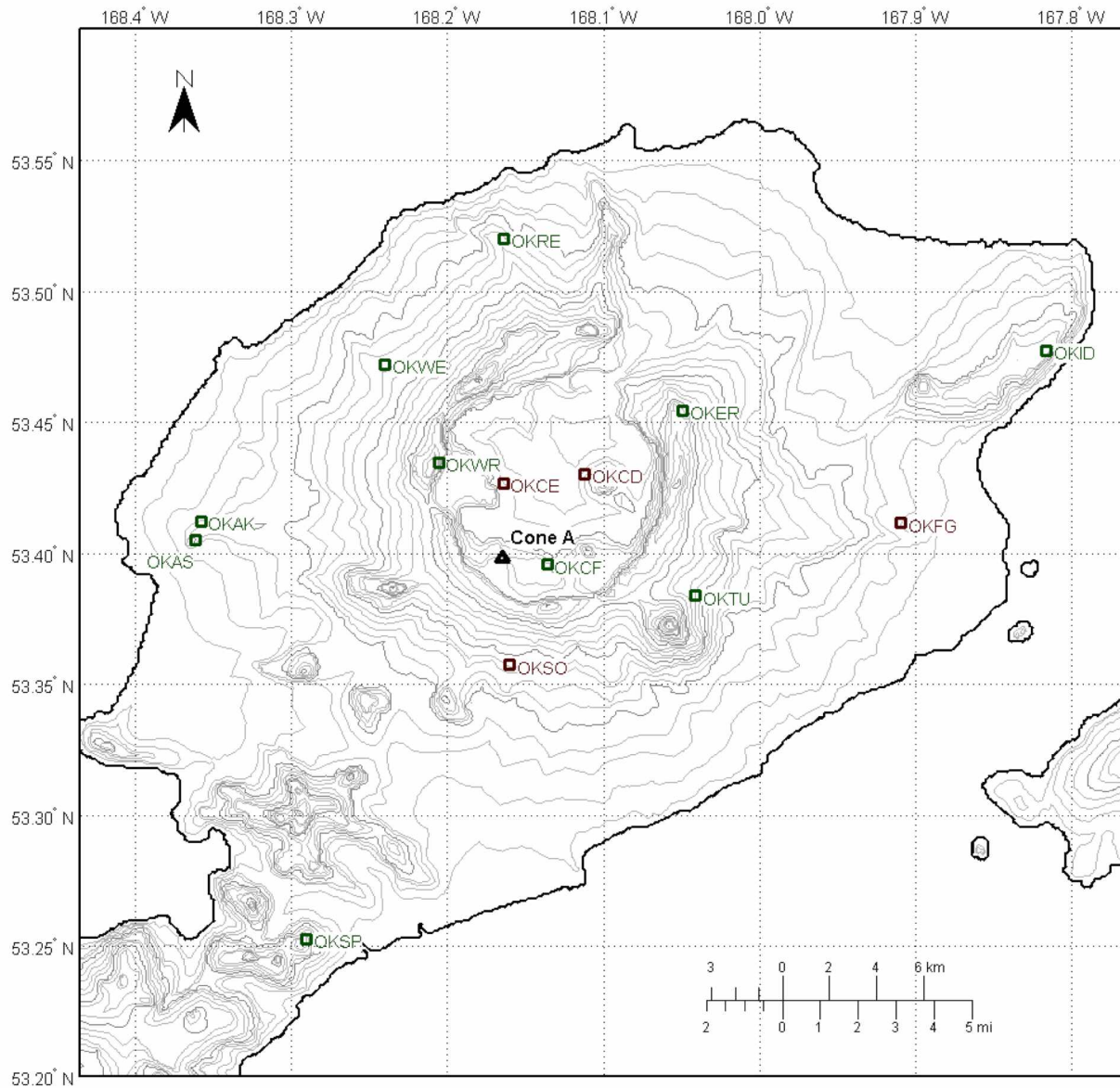


Figure 4.3 Okmok seismic network. Broadband seismic stations are shown as red squares; short-period seismic stations are shown as green squares.

Table 4.1 Recent geodetic studies. Modified from Ohlendorf *et al.* 2014.

Study	Time Period	GPS	InSAR	Lat	Lon	Depth (km)
Mann et al.(2002)	1992-1998		✓	53.3983	-168.1646	2.1-4.7
Miyagi et al. (2004)	2000-2002	✓				2.7
Lu et al. (2005)	1992-2003		✓			3.2
Fournier et al. (2009)	2000-2007	✓		53.4353	-168.1397	2.5
Lu et al. (2010)	1997-2008		✓			3.1
Lu and Dzurisin (2010)	2007-2008		✓			2-3
Biggs et al. (2010)	1992-2007	✓	✓	53.4290	-168.1357	3

Okmok remained relatively quiet, seismically, until July 12 2008, when it erupted with little precursory unrest from new vents located to the northwest of Cone D (Larsen *et al.*, 2009). This was the first eruption since 1817 to originate from somewhere other than Cone A. This eruption lasted five weeks, and was primarily phreatomagmatic—that is, it resulted primarily from the interaction of magma and water.

Haney (2010, 2014) used two methods to locate tremor during the 2008 eruption. Haney (2010) used inter-station arrival times of a very long period (VLP) signal, occurring between 0.2–0.4 Hz, to constrain the tremor to approximately 2 km below sea level. This source was inferred to be above the magma chamber and below the surface. Haney (2014) used back-projection to attempt to locate volcanic tremor during the 2008 eruptive event. This study was able to tease a location out of the network that inferred tremor migrating toward the intracaldera lake prior to the eruption. These studies leveraged data from three-component broadband seismic stations that were not available during most of the 2003–2005 period.

Geodetic studies (Table 4.1) generally agree that the deformation associated with the 2008 eruption of Okmok can be explained by a pressure source located under the geographic center of the caldera (Fournier *et al.*, 2009; Biggs *et al.*, 2010; Freymueller and Kaufman, 2010; Lu *et al.*, 2010). The proposed locations and depths vary, though there is general consensus that the source lay roughly 3 km below sea level. I refer to this location as the center of inflation (COI) throughout the rest of this study.

Masterlark *et al.* (2010) used ambient noise tomography to image the subsurface of Okmok. They found two zones of anomalously low seismic velocity, where seismic waves propagated more slowly than in other areas. They interpreted the top zone, extending from the surface down to 2 km, to be made up of structurally weak materials that were saturated, perhaps by groundwater. They interpreted the deeper zone, below 4 km, to indicate a region of magma storage. (Figure 4.4)

Ohlendorf *et al.* (2014) also mapped the substructure, this time using earthquakes that occurred around the time of eruption. They came to essentially the same conclusion:

The distribution of events preceding the 2008 eruption suggests that a combination of overpressure in the zone surrounding the magma chamber and the introduction of new material from below were jointly responsible for the explosive eruption. Magma escaping from the top of the main magma chamber likely reacted with both a smaller shallow pod of magma and groundwater on its way up below the Cone D area (Ohlendorf *et al.*, 2014)

Larsen *et al.* (2013) examined the products erupted in 2008 to determine the conditions under which they formed. The petrologic indicators, such as olivine crystals and H₂O concentrations within melt inclusions, were consistent with a basaltic magma that migrated upward from a 3–5 km deep storage region, where it intersected a more evolved magma body underneath Cone D, at a depth of approximately 2 km. This provides further evidence that the observed inflation was caused by new magma intruding from a deeper crustal or mantle source.

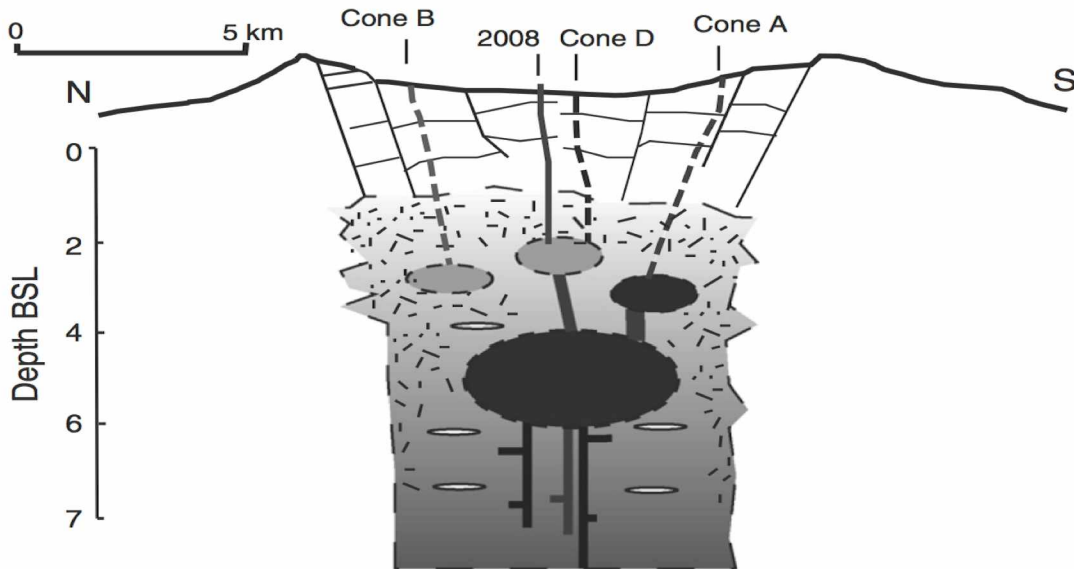


Figure 4.4 Model of subsurface Okmok. A large magma reservoir is postulated to exist between 4 and 6 km depth. Pods of differentiated magma exist between 2 and 3 km below sea level. As magma recharges the central reservoir, fluids may migrate up through existing weaknesses and exit the system at one of several cones. (from Larsen *et al.*, 2013)

Magma compositions from the 2008 eruption were significantly different from the 1997 eruption, indicating that the two eruptions did not originate from a single homogeneous and laterally continuous reservoir. Larsen *et al.* (2013) combined the geodetic findings with petrologic data to arrive at a model that contains a main magma reservoir at 4–6 km depth underlying the caldera, with local reservoirs underneath specific features, such as Cone A and the 2008 eruptive vents. (Figure 4.4)

To summarize, magma erupted from Okmok in 1997 that appeared to have previously migrated laterally from a magma reservoir located underneath the center of the volcano. Afterward, and until 2006, the volcano reinflated, with the inferred cause being magma entering the central reservoir from below. This period of reflation was marked by complex, systematic patterns of strong seismic tremor. Following this period, Okmok volcano was relatively quiet geophysically until 2008, when it erupted with

just a few hours of precursory warning. The inferred trigger for eruption was the intersection of magma with a smaller, shallower pod of magma and groundwater.

4.2 Data

This investigation combines data from the studies mentioned in the previous section with seismic data from the seismic network on Umnak Island. GPS data that describe the inflation of Okmok come from Fournier *et al.* (2009). They measured the relative movement of the volcano from 2001 to 2008 (Figure 4.5). A list of earthquakes that recur underneath Cone A comes from Johnson *et al.* (2010) and is provided in Table 4.2. Additional repeating earthquakes occurred after this study period, and continued up until the 2008 eruption.

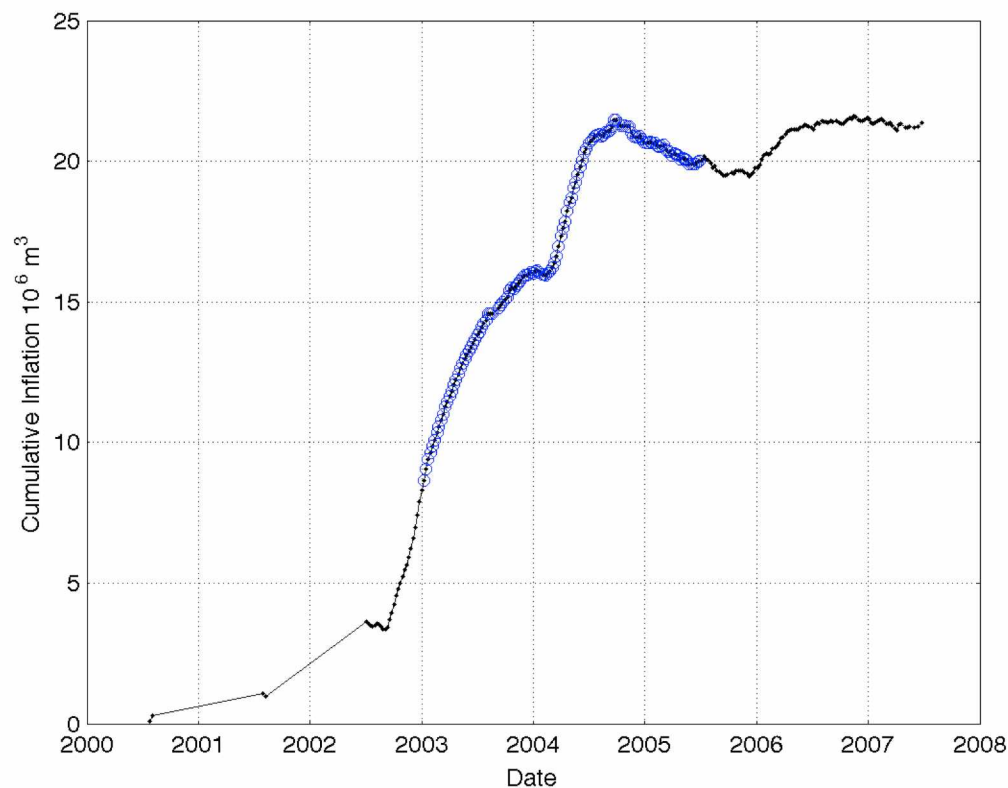


Figure 4.5 Cumulative inflation at Okmok. This figure shows the inflation at Okmok Volcano, from Fournier *et al.* (2009). Blue circles show inflation detailed in this study.

The Okmok seismic network was installed over the course of three summers, from 2002 to 2004 (Table 4.3) At the time of this study, the network comprised eight Mark Products L4 (1 sec period) vertical component seismometers at distances of 1.8–24 km from Cone A.

Analog data from each station were relayed over radio to Dutch Harbor where the signals were multiplexed and sent via phone lines to AVO at the Geophysical Institute in Fairbanks. Then, the individual channels were separated, digitized, and stored in an Antelope database. I then converted the raw digitized data into the MATLAB Waveform Suite format and stored them locally for further processing.

Table 4.2 Multiplet earthquakes occurring underneath Cone A. Only events from 2003-2005 are displayed here. Later events are not included here (Modified from Johnson *et al.*, 2010):

Date	Time	Latitude	Longitude	Depth (km)	Magnitude
2004-02-13	00:31:37.74	53.391	-168.221	-2.5	1.1
2004-11-12	16:57:30.82	53.442	-168.240	14.0	2.3
2005-02-14	10:41:28.76	53.374	-168.236	-0.1	0.7
2005-04-21	12:32:28.60	53.398	-168.236	1.5	1.2
2005-06-16	13:36:46.95	53.399	-168.185	8.2	1.1
2005-08-22	13:08:28.75	53.402	-168.188	5.0	0.7
2005-11-13	04:59:48.51	53.427	-168.175	3.9	1.1

Table 4.3 Okmok local seismic stations (Dixon *et al.*, 2006)

Station	Latitude	Longitude	Elevation (m)	Type	Start date
OKAK	53.4123	-168.3578	165	SP	2005-07-11
OKCD	53.4303	-168.1123	459	BB	2003-01-09
OKCE	53.4270	-168.1643	515	BB	2003-01-09
OKCF	53.3948	-168.1383	685	SP	2003-01-09
OKER	53.4537	-168.0512	956	SP	2003-01-09
OKFG	53.4107	-167.9115	201	BB	2003-01-09
OKID	53.4774	-167.8162	437	SP	2003-01-09
OKRE	53.5194	-168.1661	420	SP	2003-01-09
OKSO	53.3575	-168.1599	460	BB	2004-09-01
OKSP	53.2526	-168.2905	608	SP	2003-01-09
OKTU	53.3839	-168.0411	646	SP	2003-01-09
OKWE	53.4721	-168.2398	445	SP	2003-01-09
OKWR	53.4347	-168.2055	1017	SP	2003-01-09

SP, L4 short period seismometer (T=1); BB, Guralp CMG-6TD broad-band (T=30).

Additional broadband seismometers were installed but were not functioning during the majority of this study. Seasonal station outages were relatively common and strongly affected the ability to track tremor. This was especially so in the late winter and spring, when snow was deep, ice coated antennas, or power was low due to the lack of solar recharge during the long, dark winter. Stations within the caldera

are particularly susceptible to outages because the signal is relayed through multiple repeaters before reaching the Dutch Harbor acquisition site. A failure at any intermediate repeater results in lost data.

Earthquakes were retrieved from the AVO online earthquake catalog. Similar information can be retrieved in Dixon *et al.* (2004, 2005, 2006). Regional earthquake information was retrieved from the Alaska Earthquake Center catalog (http://www.aeic.alaska.edu/html_docs/db2catalog.html). Figure 4.6 shows the locations of earthquakes in the vicinity of Okmok from February 2003 through December 2006. In general, events occur in three clusters. There is a cluster of earthquakes in an area known as Geysers Bight, SW of Okmok, that may be associated with hot springs seen in the area. The other two clusters are in the caldera: underneath Cone A, and to the NE of the caldera center.

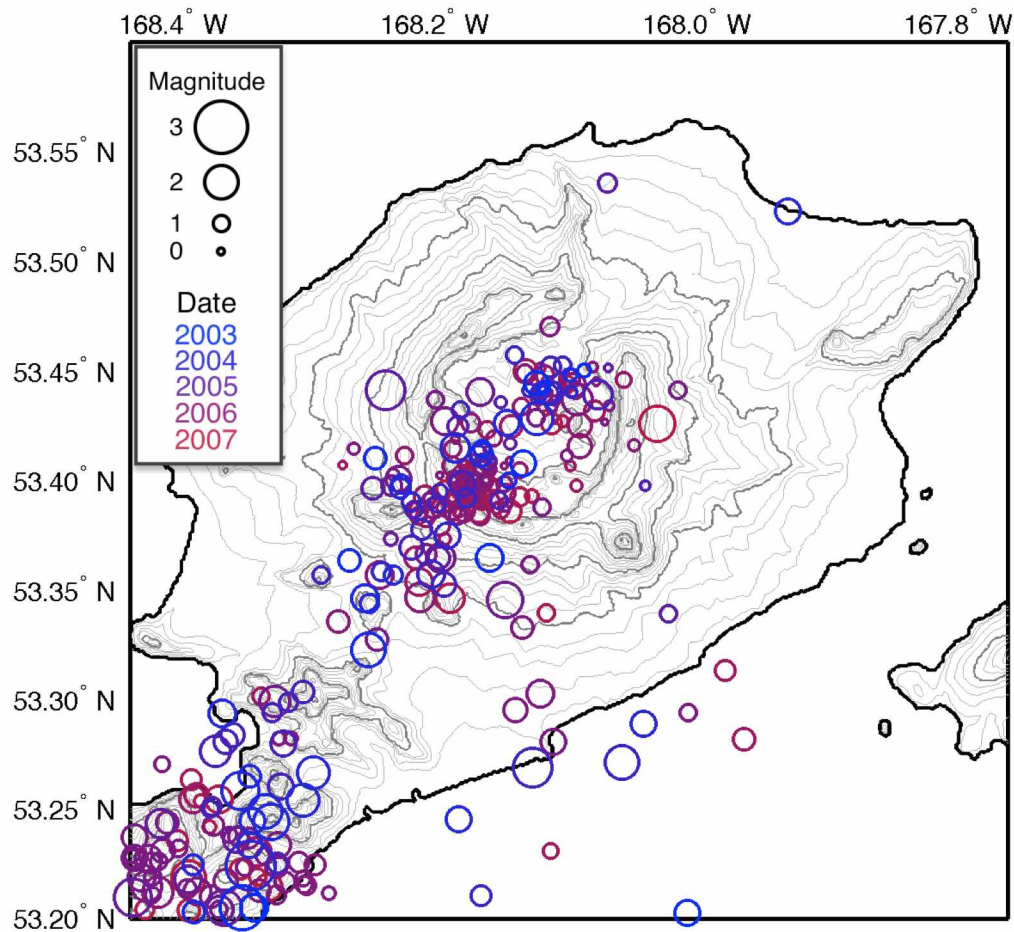


Figure 4.6 Locally recorded earthquakes through 2006. Circle size reflects the earthquake magnitude, while circle color indicates the relative timing of the earthquakes.

Additional observations were retrieved from the internal AVO logs, where field observations, thermal anomalies, and interesting features of the seismic signal were frequently noted.

4.3 Methods

4.3.1 Measuring amplitudes

There are several strategies for assigning a numerical value to the strength of seismic tremor. Two of the most common methods are Real-time Seismic Amplitude Measurement (RSAM) (Endo and Murray, 1991) and Reduced Displacement (Aki and Koyanagi, 1981; Fehler, 1983). RSAM is the 1-minute average of the absolute amplitude of a seismic signal. Reduced displacement (D_R) is a normalized amplitude measurement that takes into account the frequency of the seismic signal, the calibration of the instrument, and the assumed location of the source. This normalized measurement is useful for comparing tremor amplitudes across different stations and different volcanoes. However, the assumption of a known location makes D_R unsuitable for this study, where tremor may emanate from a number of locations.

I opted instead to use root-mean-square (RMS) measurements. Like RSAM, RMS measurements require no assumptions about the source location. Since the energy of a seismic signal scales with the square of the amplitude, RMS values are a more accurate reflection than the mean or median. This direct relationship to energy made the RMS a more attractive tremor metric than the venerable RSAM.

The RMS for each data segment was calculated using

$$A_{rms} = \sqrt{\frac{\sum_{i=1}^N x_i^2}{(N-1)}} \quad (4.1)$$

where N is the number of samples, x_i is the amplitude of the i^{th} sample in nm s^{-1} . These filtered RMS values, A_{rms} , provide a simple metric for assessing the strength of seismic tremor over long time scales. These tremor strengths are the basis for much of the following study.

I decided to use RMS values, gathered in 10-second samples, as my yardstick for tracking the seismic activity. The 10-second time window provided reasonable resolution for tremor start-stop times and still protected against some of the observed short-scale variations in tremor strength. I first scaled the data from each station by each instrument's calibration to get velocity (nm s^{-1}). I then filtered the data with a 0.8 to 6.0 Hz bandpass Butterworth filter. The filter was applied both forward and backward in time, which canceled out any time-shift in the data resulting from the filtering operation. Figure 4.7 illustrates how the RMS values and the filtered signal relate.

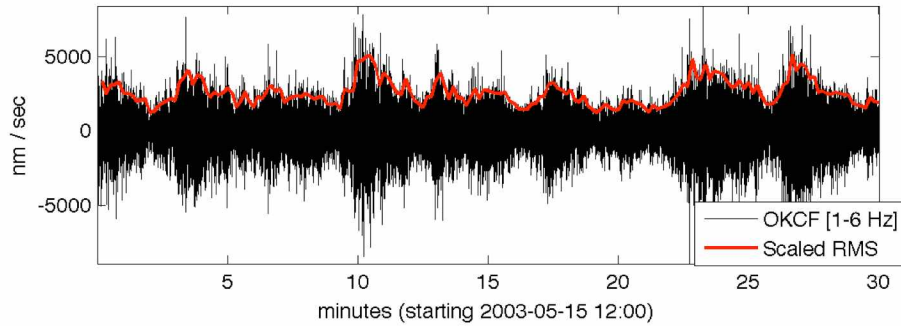


Figure 4.7 Comparison of calculated 10-second RMS values to filtered raw data, demonstrated with the vertical short-period station OKCF.

4.3.2 A Catalog of tremor start and end times

4.3.2.1 Automating tremor detection

In order to automatically pick tremor, I needed to establish appropriate guidelines. The simplest solution would have been to choose a single RMS amplitude threshold value with which to define tremor. Values above the threshold could be considered active tremor. Unfortunately I could not define a single threshold because both the tremor strength and background noise levels fluctuate greatly over time. For example, on a particular day the strongest tremor might be below the background noise-levels for another day. Even if background levels remained constant, I still could not use this technique alone because I would include many non-tremor signals, such as earthquakes, calibration pulses, and seismic “noise” from stormy days. A manual review would solve the latter issue, but the former remained a challenge.

Furthermore, I couldn’t simply use the short-term-average divided by the long-term-average (STA/LTA) approach, common in earthquake detections (Vanderkulk *et al.*, 1965). The wildly variable durations of tremor (~3–60 min), similarly variable repose, and the typically emergent onset of seismic tremor made this solution unfeasible.

A further challenge was to compensate for both the variable availability of data at stations and the fluctuating ability of each station to detect and record tremor. I decided to compare the signal across all the local stations using cross-correlation. I used the “correlation” class in the GISMO MATLAB toolbox (Buurman and West, 2010; Reyes and West, 2011) to perform these operations. In cross-correlation the envelopes recorded at each station are compared to those at other stations. When signals align perfectly, such as when a station is cross-correlated with itself, the normalized cross-correlation value approaches 1. Correlation values degrade toward zero as the signals become less similar. If the highest correlation can

be achieved by shifting the alignment of the signals in time, then this “lag” value is used to indicate this optimal offset.

Before I could cross-correlate the signals, I first removed data spikes. Data spikes were uncharacteristically high RMS values caused by hardware, noise, or artifacts of filtering. Because they had high values, they affected the ability to compare data across stations. I removed these by replacing them with the mean of adjacent values.

I then cross-correlated the RMS time series across stations in 1.5-hour segments. These windows were chosen because they were long enough to encompass at least one complete tremor episode, should one exist. To avoid catching completely unrelated signals, correlations with large lag times (>150 seconds) were ignored. If, for a given time period, two or more stations had signals with correlation values > 0.7 , then that time period became a candidate for containing tremor.

Determining the start and stop time of each tremor episode required that I define some critical amplitude threshold, which would vary in time at each station. Ideally, background noise should be below this threshold, while active tremor should stay above it. Background levels could vary greatly over the course of hours to days, providing an additional challenge to establishing a simple signal threshold. Noise levels are affected by wind, rain, a herd of grazing cows, etc.

I calculated a threshold for each 1.5-hour time segment that might hold tremor. I first normalized each segment by dividing it by its median value, A_{med} . Signals were grouped according to amplitude in order to see what the most common amplitude was. I operated under the assumption, gained through examining the spread of the signal values, that the background level accounted for approximately half the total signal and that the mode typically represented the high-end of the background noise. Therefore, the mode became my normalized minimum threshold level. The final threshold at each station was determined by multiplying A_{med} by 1.1, an empirically determined scaling value that resulted in a relatively good split between tremor and background. This was confirmed through visual inspection.

At this stage of the process, I could treat each 90-minute block of time individually. For each of these time segments, I knew which stations recorded similar signals. I term these qualifying stations. For each qualifying station, I had a minimum amplitude threshold for tremor, which depended upon the station and varied through time.

I then searched these qualifying stations and times for high-amplitude periods, using a three-hour window. This duration was long enough to encompass multiple tremor cycles, but not so long as to be

strongly affected by the changing background amplitudes. After I determined when the RMS values were above the threshold value at multiple stations, I considered it to be tremor and added it to the catalog of tremor observations. Then, I stepped forward 1.5 hours in time and repeated the process.

I refined this catalog by combining closely spaced tremor and removing tremor periods that were too brief. If adjacent detections were separated by 20 seconds or less, I treated the entire time as an individual tremor episode. I further curated the list by removing detections with durations <150 s, because tremor at Okmok was generally observed to last longer than that. More often than not, these short detections represented other types of seismic events, such as teleseisms. These detections became the first iteration of a master tremor catalog.

4.3.2.2 Manually reviewing tremor picks

I manually reviewed the entire tremor catalog using an approach that displayed the tremor catalog atop the filtered seismic records for each day (Figure 4.8). I added and removed tremor detections based on visual inspection of the seismic record, omitting stray signals such as teleseisms, regional earthquakes and noise spikes. I also adjusted the start and stop times of tremor periods when they appeared to be egregiously incorrect.

The final catalog contained 16,956 episodes of tremor from February 25 2003 to September 4 2005 (Figure 4.9). In general, both the duration and the number of episodes are under-reported, so this catalog should be considered a minimum baseline. The durations may be underreported at times when the tremor slowly emerged or merged into the background noise. Tremor was not reported on noisy days, such as when storms buffeted the island. I did not manually catalog tremor on days where only one station detected tremor, even if the tremor was obvious, because it failed to meet the multi-station criteria.

4.3.3 Determining tremor strength

I represent the amplitude of each tremor pulse with the median RMS value for the event at each station. I chose to use these values, rather than using maximum amplitudes, because episodes were often observed to have brief, strong onsets during the first 3–5 minutes, followed by extended periods of lower amplitudes lasting 20 minutes or longer. I only plot the median values for OKTU when the values for OKWE are either nonexistent, or when the values appear to be incorrect. For example, I use OKTU values when the RMS at OKWE < 10 nm s⁻¹, because that is well within the noise level, and when OKWE > 10000 nm s⁻¹, which would result only from data spikes and other non-signal noise. Median values typically ranged from 50 to 400 nm s⁻¹ (Figure 4.10).

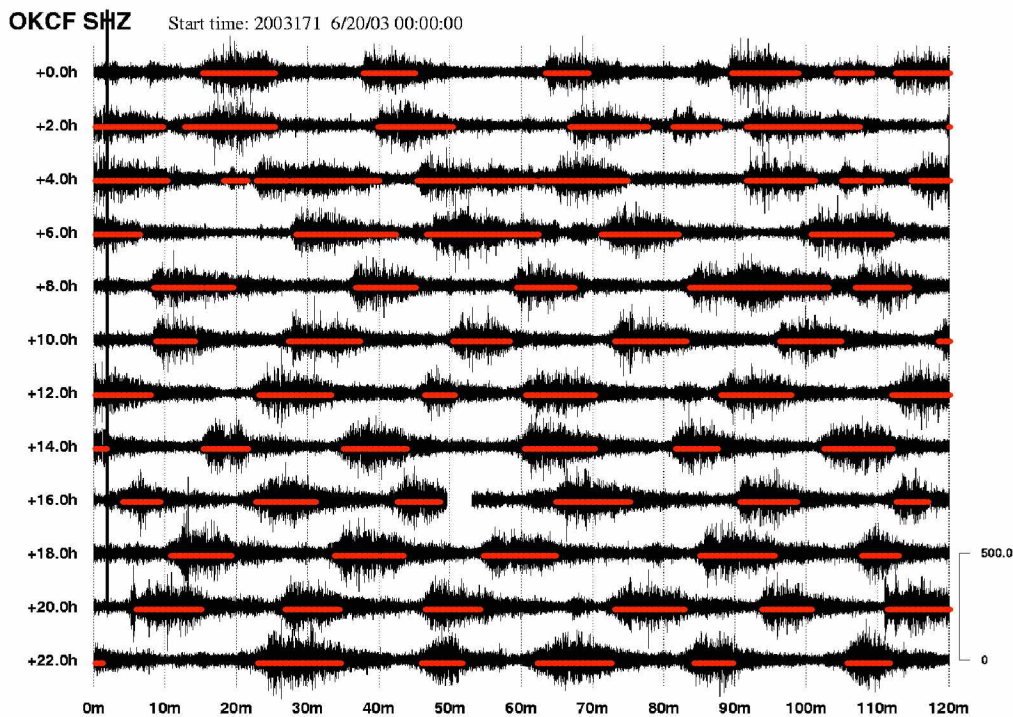


Figure 4.8 Manual picking program. Each day's seismicity data are stored as images of filtered seismograms, such as this. The periods marked as tremor are overlain as red bars. This program allowed me to traverse each day of tremor and to look at signals recorded at each station. I was able to add, delete, or modify each segment of marked tremor. As this sample shows, the tremor amplitude slowly diminishes to a background level, which may or may not still be tremor.

4.3.4 Determining frequency content

I wanted to assess whether the frequency content remained consistent or evolved over time. A change in frequency content could indicate a change in the underlying tremor source, possibly pointing toward an evolution of the magmatic system. I computed the power spectral density for the first two minutes of each tremor episode using Welch's method with 20.48-second windows (2048 samples), in 10-second steps. Because episodes did not occur evenly spaced in time, I plotted them on a timescale at their respective temporal positions.

Stations OKTU and OKWE were located at similar distances from the likely tremor sources, a fact that was reflected in the similarity of both their amplitudes and spectra. The final spectral plot comes from station OKWE, with the exception of September 2004 through mid-October 2004, when data were not accurately received from OKWE.

One of AVO's systematic methods of reviewing volcano seismicity is to examine daily spectrograms. Whenever an interesting signal is discovered, a note is made in the logs. These logs contain several mentions of gliding tremor, which are also shown on Figure 4.10.

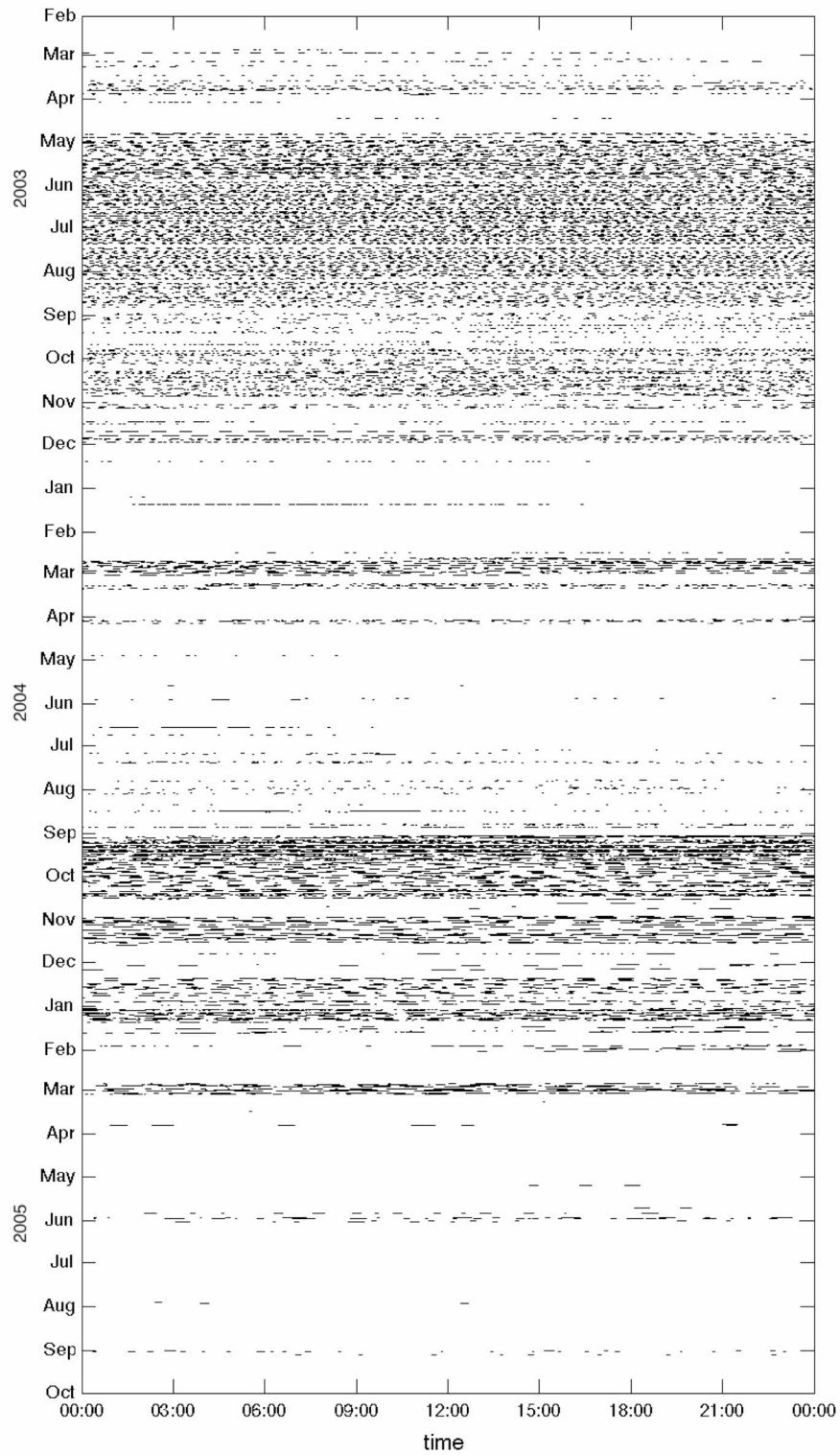


Figure 4.9 Catalog of active tremor at Okmok. Each row represents one day, and each line segment represents an episode of elevated tremor.

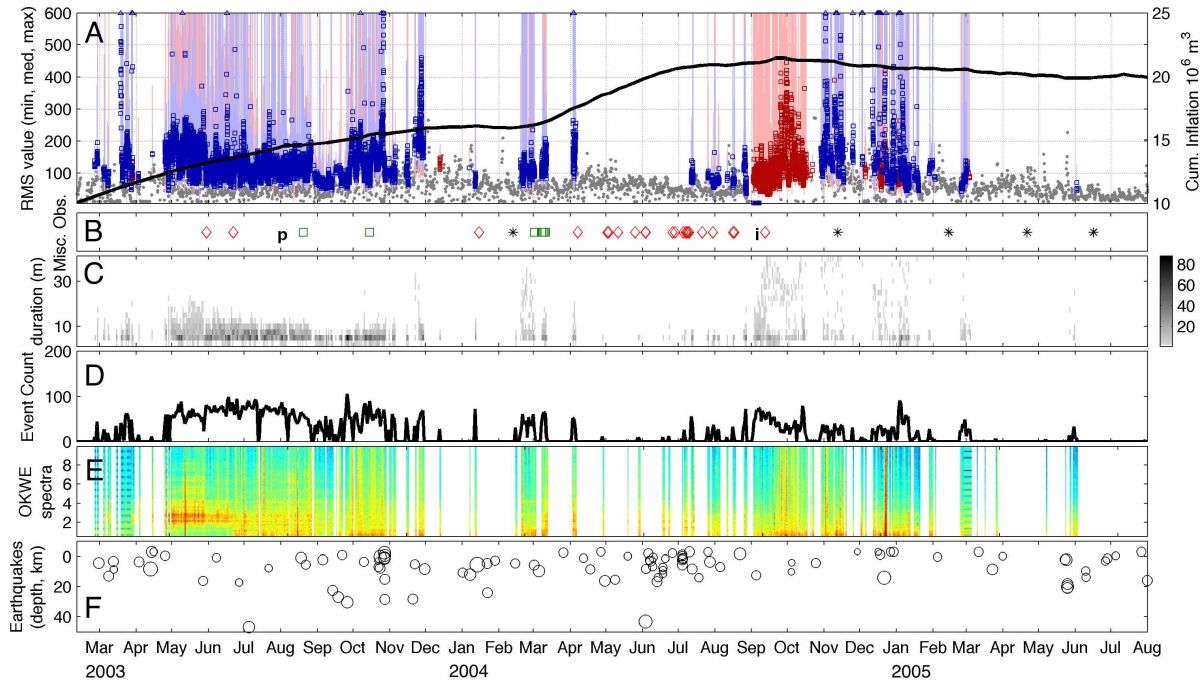


Figure 4.10 Overview of Okmok unrest: 2003–2005. Multiple observations are plotted along the same time scale to bring the overall changes at Okmok into perspective.

Panel A shows the RMS amplitudes of all cataloged tremor episodes at stations OKWE (blue) and OKTU (red). Boxes show the median amplitude for each episode. Off-scale values are shown by triangles. The lighter bars show the full range of tremor amplitudes. Grey dots represent the background “noise” level, defined by the minimum RMS value for each six-hour period of continuous data.

The black line, also shown in panel A, represents the cumulative influx of magma, modeled from geodetic data. (10^6 m^3)

Panel B shows miscellaneous point observations. These include:

- Satellite based thermal anomaly reports: red diamonds
- Tremor that exhibited “gliding” behavior: green squares
- Multiplet earthquakes (Johnson *et al.*, 2010): asterisks
- Report of a blue plume: “p”
- Report of incandescence: “I”

Panel C shows the tremor durations, which are plotted as a histogram. Each bin is 2.5 minutes long.

The event count (panel D) shows the number of cataloged tremor events occurred each day.

Panel E shows the spectra for the first 2-minutes of the onset of each tremor, as recorded at station OKWE from 0.5 to 10 Hz. Warmer colors represent a stronger signal. When OKWE data is unavailable (i.e., when panel A displays red data instead of blue), spectra from station OKWR is shown instead.

Panel F shows earthquakes from the earthquake catalog that occurred within 20 km of Cone A. The depth is plotted on the vertical axis, while the magnitude of the earthquake is shown by the size of the circle. Locations of these events are shown in Figure 4.6.

4.4 Two years of unrest at Okmok: 2003–2005

4.4.1 Evolution and occurrence of tremor

4.4.1.1 Tremor amplitude

At first glimpse, tremor amplitudes waxed and waned in a pseudo-sinusoidal fashion with a period of approximately 4–7 days. This is particularly evident in the top panel of Figure 4.11. This pattern is seen concurrently at multiple stations and is often set against a much lower amplitude background, which suggests that this is a true volcanic pattern and not merely the effect of storms. Even the brief glimpse of tremor in mid-March 2003 showed this pattern. Amplitudes were generally highest in May 2003, when

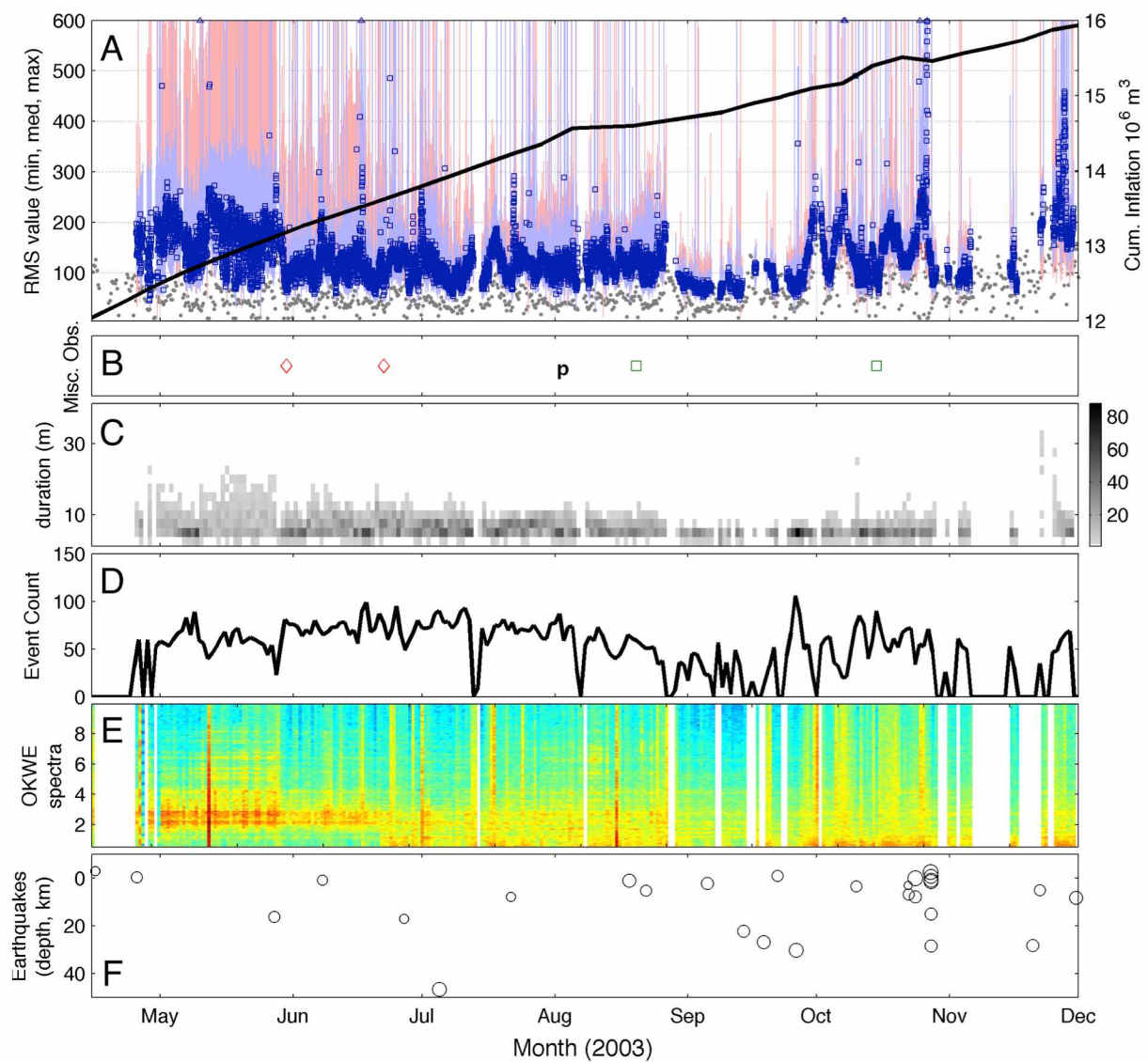


Figure 4.11 Inflation during 2003. For a description, see Figure 4.10.

OKWE had many tremor episodes with $RMS > 200 \text{ nm s}^{-1}$. In June through the end of August, amplitudes were typically lower, but peaked once a week or so. In September, the signal remained notably weak until the last week, when it once again oscillated strongly to $>200 \text{ nm s}^{-1}$ for the month. From December through mid-February 2004 little tremor occurred. Tremor reappeared and remained until mid-March (Figure 4.12), at which point it displayed harmonics that varied in time. Another strong series of tremor occurred at the beginning of April 2004. Then tremor appeared only sporadically until late August, at which point it hovered around 100 nm s^{-1} until spiking three times at the end of September and into October (Figure 4.13). Data were unavailable for brief periods in October and November. In the first half of November, tremor was as strong as in October, with peaks to over 400 nm s^{-1} (Figure 4.14).

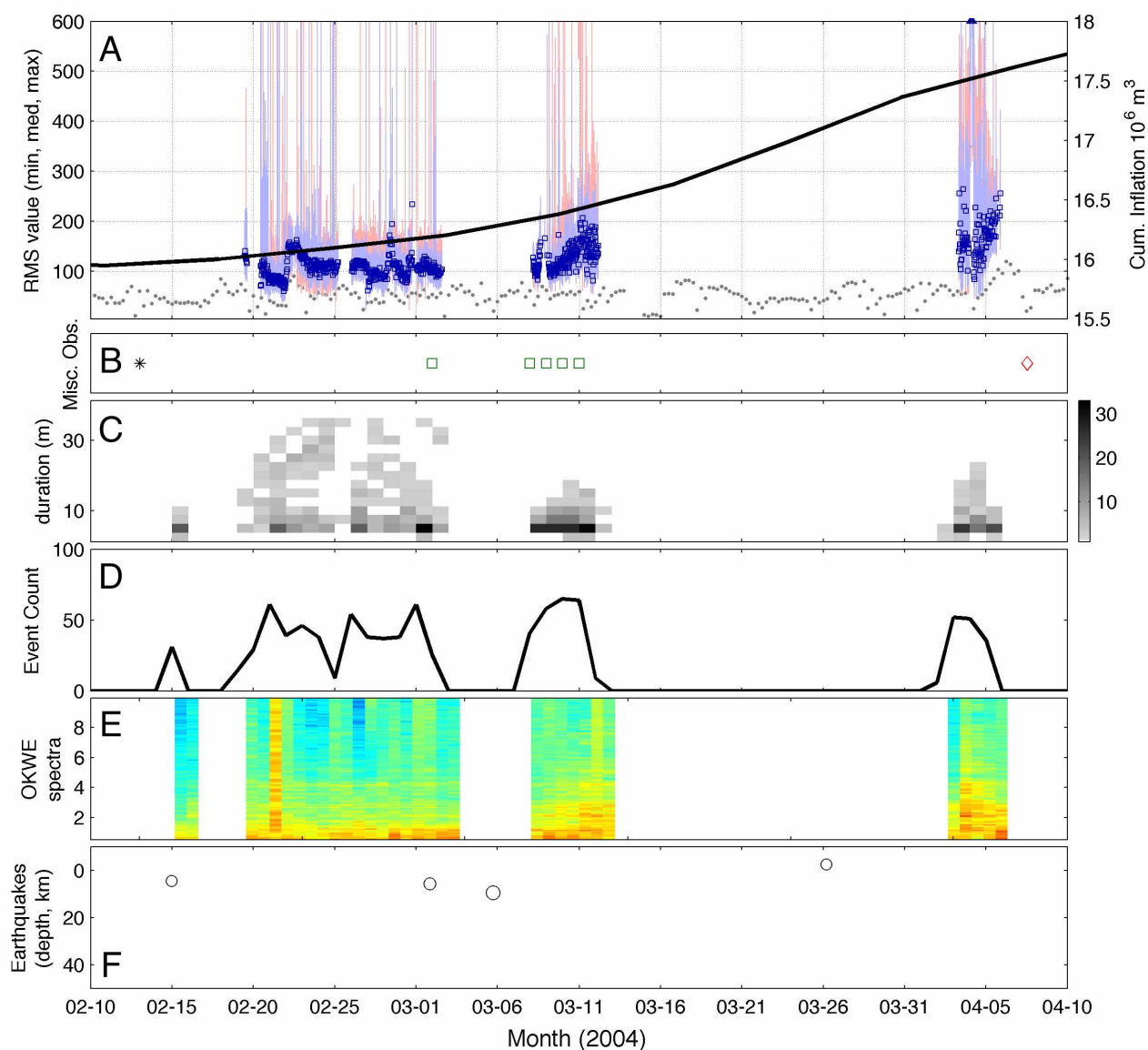


Figure 4.12 Start of 2004 inflation. See Figure 4.10 for explanation.

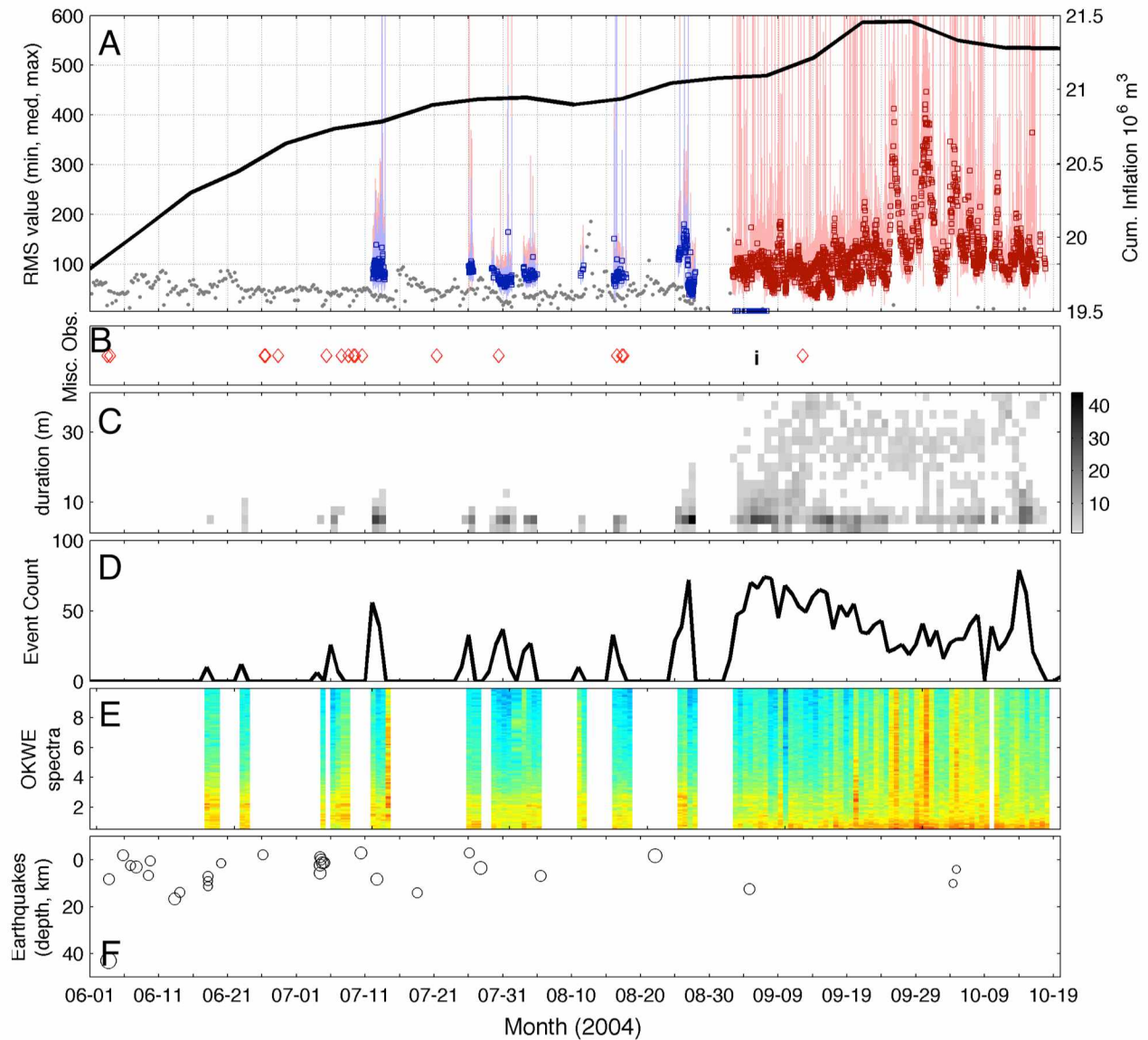


Figure 4.13 Inflation during 2004. See Figure 4.10 for explanation.

4.4.1.2 Distribution

The first appearance of tremor was on the sole-functioning station OKTU on February 15 2003 as barely discernible changes in seismic intensity that continued to appear regularly throughout 2003. As 2004 began, tremor was not observed for approximately 1.5 months. This period of time coincided with station outages and high noise, though no tremor appeared on the occasional day with lower background noise. Tremor reemerged from February 14 2004 through March 5 2004 (Figure 4.12), displaying a marked bimodal behavior in duration (Figures 4.15 and 4.16). Thereafter, the tremor occurred only occasionally (1–2 days at a time) until August 2004, when a relatively stable period of tremor began. Day

after day similar patterns of tremor continued; the general shape, amplitudes, and durations changed slowly until October. Activity occurred until June 2 2005, after which tremor was rarely seen until shortly before the July 2008 eruption.

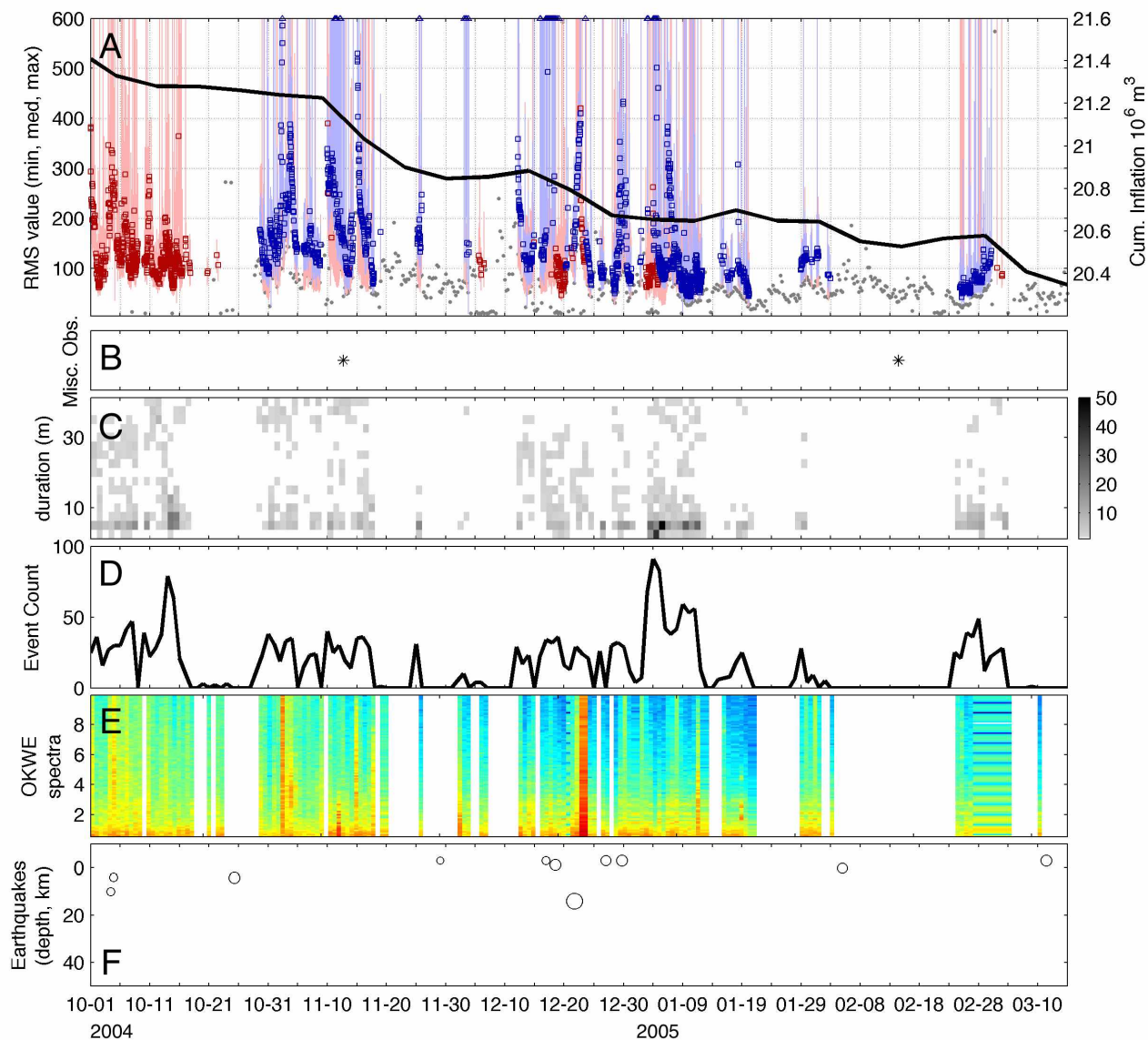


Figure 4.14 Deflationary period, 2004–2005. See Figure 4.10 for explanation.

Between station power and telemetry issues and high background noise levels, it was difficult to make definitive statements about tremor until the network became fully operational in May 2003. When conditions were favorable however, tremor appeared as 5–10 minutes bursts occurring approximately twice per hour with many possible smaller amplitude events in between, sometimes suggesting

continuous tremor (Fig 4.17 A). Occasionally, such as the latter half of March 15 2003, the style temporarily shifted into many short, discrete events. While interesting, this style of tremor didn't persist for more than a half day at a time, after which it reverted back to longer bursts.

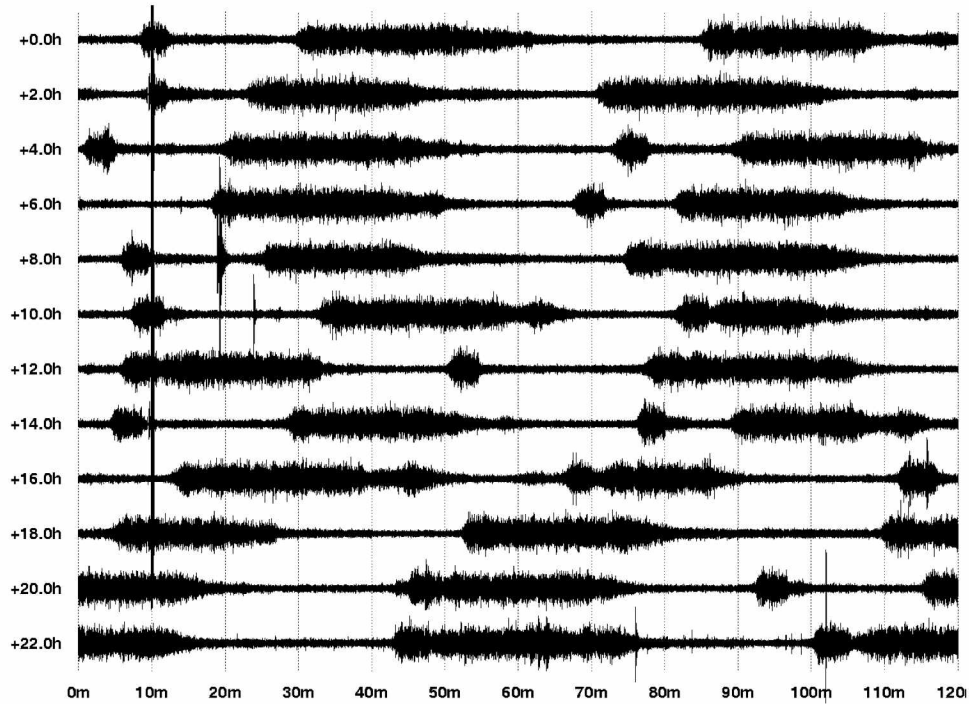


Figure 4.15 Example of bimodal tremor. Seismogram traces for February 24 2004 at station OKCF.

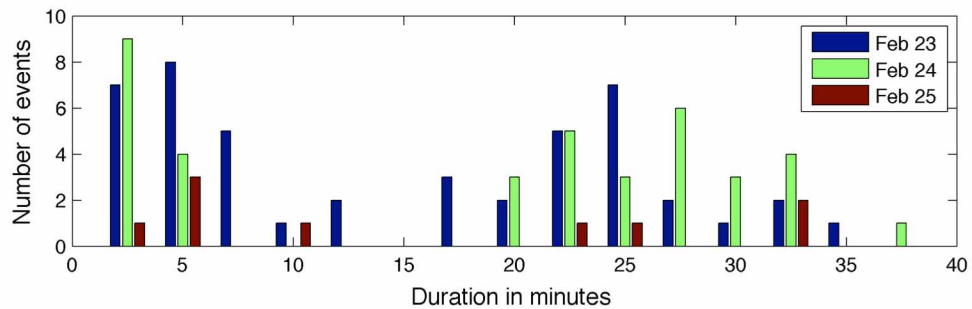


Figure 4.16 Tremor durations for February 23–25 2004.

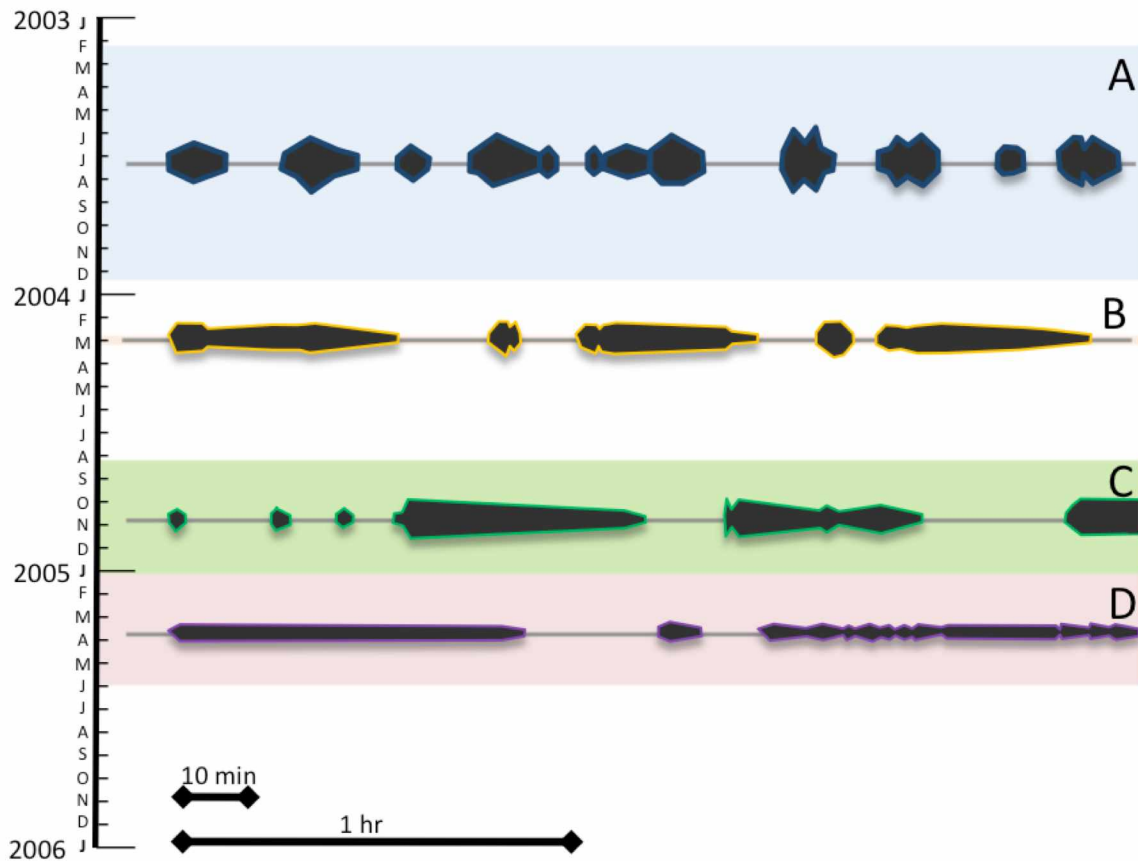


Figure 4.17 Generalized tremor styles, as recorded at OKCF. Tremor at Okmok Volcano exhibits relatively stable behaviors for periods of weeks to months. Shown here are generalized examples of how the tremor appears on filtered plots. Each colored block outlines the time period that a tremor style is dominant. Each line of dark shapes depicts approximately two hours of stylized seismicity. Tremor does not necessarily appear at all times for the station and may be unrecognized due to noise, station malfunction, or small amplitudes. Very short periods (< 3 days) where tremor temporarily appears are not shown here. A) Tremor occurring frequently, with durations between 5 and 20 minutes, sometimes continuous. B) Approximately nine days of bimodal tremor, with longer sequences (20–30 minute) interspersed with shorter (~3–5 min) sequences. C) Strong sequences of relatively consistent length (25–40 min) tremor, along with small bursts (<5 min) of tremor activity. D) Long episodes of tremor, showing only weakly above background.

By May 1 2003 clear signals are seen at OKTU, OKWE, and even OKRE. At this time other stations such as OKCF, OKSP, and OKWR were not functioning. Mean tremor durations for May 2003 were approximately 7 minutes with occasional episodes exceeding half an hour. These signals persisted through August 26, but were occasionally masked by increasing background noise.

From September 26 to December 23 2003 tremor was clear on all stations within about 16 km of Cone A. The shape of the tremor envelopes could be described as “stubby screws” (Figure 4.18). These

were not monotonic “tornillo” events, first described at Galeras Volcano, Colombia, by Narváez *et al.* (1997). These tremor events at Okmok began with brief high amplitudes, which then decreased into a sustained lower-amplitude tremor before ending gradually. In addition, from June through September, durations shortened to just a couple of minutes, lengthening again in October to an average duration of about 5 minutes. Throughout December 2003, tremor was generally only visible at OKCF before it disappeared into the background in late December.

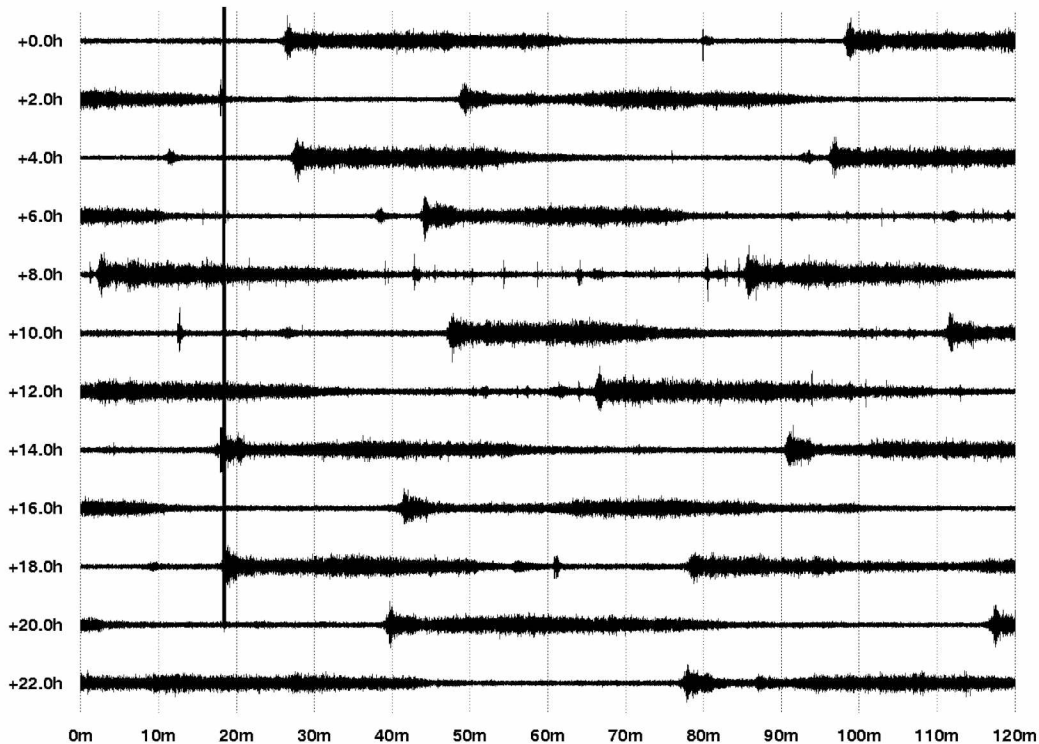


Figure 4.18 Example of tremor initiated by a strong signal. This seismogram shows filtered data from station OKCF on October 30 2004.

Tremor reemerged on February 19 2004, and continued until March 5 2004. Unfortunately, the seismic network was experiencing problems. Much of this time the tremor durations appeared to be bimodal, with 3–5 minute bursts interspersed with bursts of 15–25 minutes. These were strongest at station OKCF (Figures 4.15, 4.17 B). In early March, tremor began to fade, except for the occasional recurrence lasting from a few hours to a couple of days.

There was an intense flurry of short tremor bursts on August 25 2004, followed by a period of data outage lasting through September 1. The next day, when data were available once more, the tremor activity continued to be evident. This signal, which generally appeared as 20–40 minute periods of relatively stable amplitude with the overall appearance reminiscent of caterpillars, occurred once or twice

per hour, intensified, and then fluctuated in intensity (Figures 4.17 C, 4.19). By October 26 2004, the tremor events appeared somewhat like 20-minute-long screws, with sharp, higher amplitude onsets followed by a period of sustained, albeit weaker, tremor signals (Figures 4.17 D, 4.18). These were strongest at OKCF, and were also visible on OKWR. The other stations were too noisy to record these. Some days, such as November 24 2004, these tremor episodes appeared to disassociate into many individual events. This is evidence that the continuous seismic signal was comprised of numerous short-lived tremor events. These grew weaker and faded among small low-frequency events on November 27.

Both types of events, "screw" style and "caterpillar" style, dominated the remainder of 2004 and were visible into March 2005. Occasionally, these episodes were broken into many discrete events (e.g., January 5 2005) or occurred in families of both short- and long-events (e.g., December 28 2004). However, as was typically the case in winter, there were several extended periods of time where data from stations both within and nearest-to the caldera were not received.

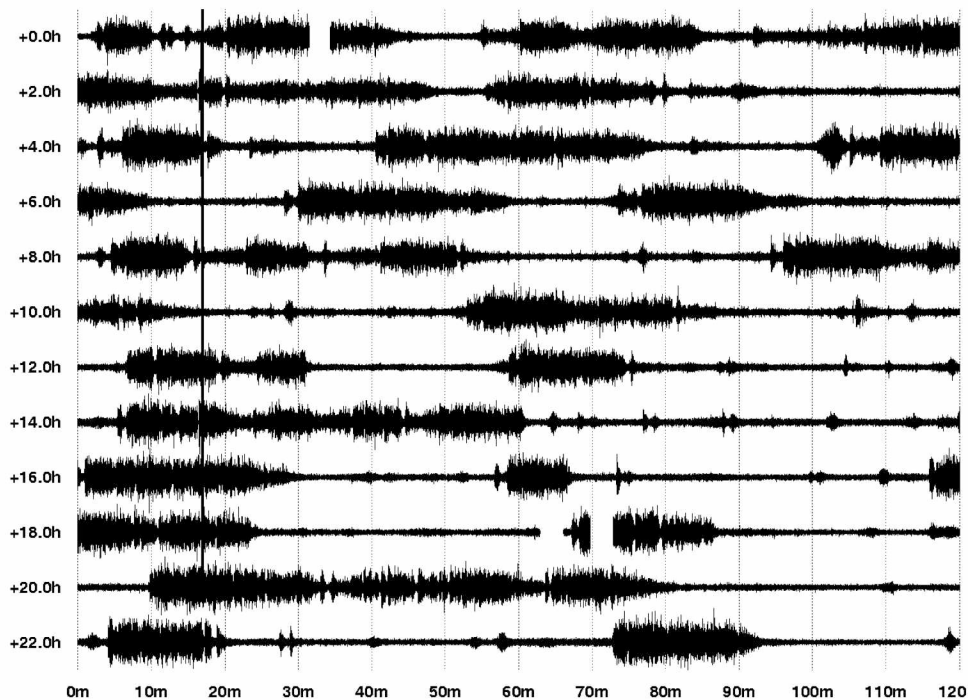


Figure 4.19 Example of tremor from September 15 2004 at station OKCF. Tremor has caterpillar appearance, along with numerous small events that resemble beads.

Tremor was apparent once again from May 26 to June 2 2005 after emerging from decreasing background noise levels at stations OKTU and OKWE (data were not being received from the closer stations, OKCF and OKWR). This style of tremor started abruptly and faded over the course of a half-

hour or so and was repeated approximately every two hours. After this brief period, tremor patterns were no longer readily apparent until June 2008.

4.4.2 Spectrograms

Frequencies of the tremor remained relatively consistent throughout the time period (Figure 4.10, spectra). Occasionally the tremor displayed gliding harmonics. Dates of gliding harmonics can be seen in Figure 4.10 (bottom axis) and a sample is detailed in Figure 4.20, as evidenced in a series of tremor starting October 15 2003, at 14:00. Harmonics reached to ~20 Hz as measured at station OKCF. The lowest frequency signal climbed from 2.2 Hz to 3.8 Hz in approximately ten minutes. This is the first of seven visible harmonics, where the highest clearly visible harmonic climbed from 11.8 Hz to 18.5 Hz during the same time period. Additionally, it appears that many events from June 20 through June 29 had a gliding component that started at ~2.5 Hz and glided up towards 5 Hz during each period of active tremor.

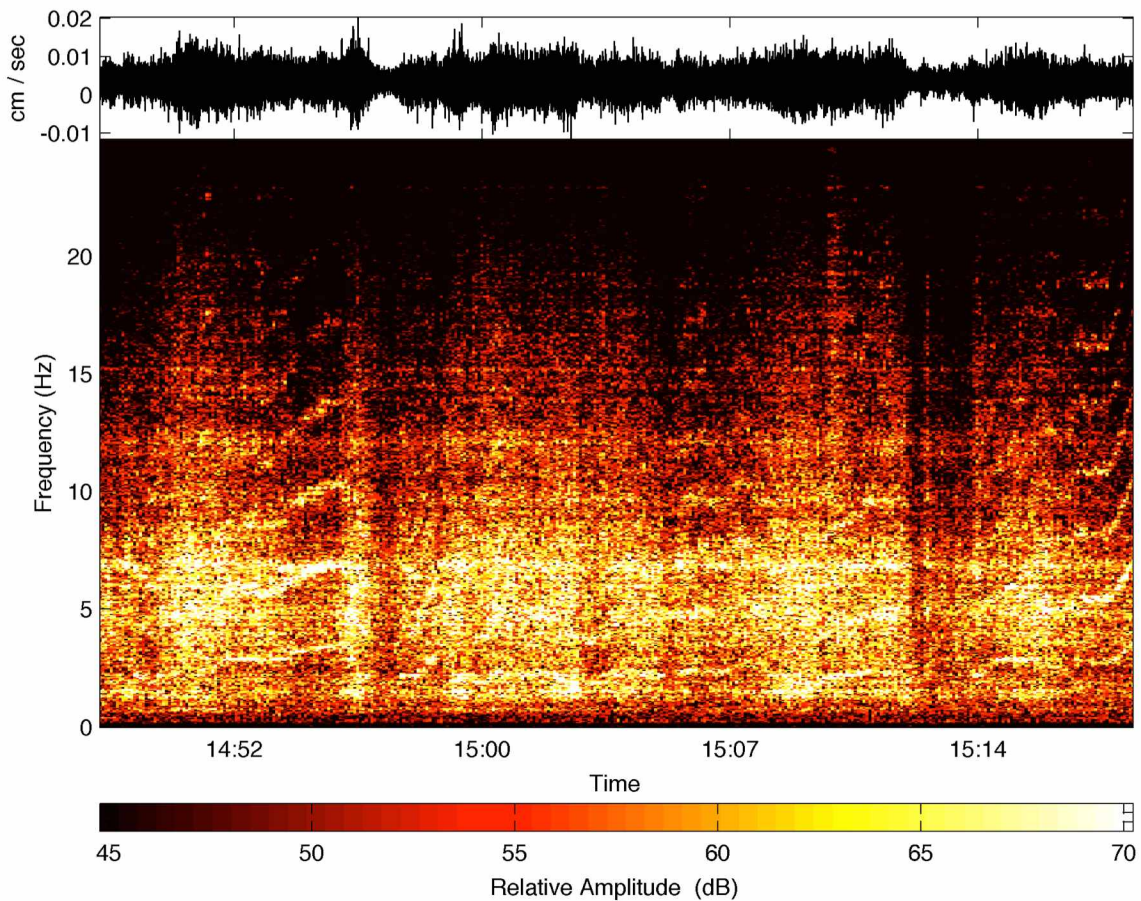


Figure 4.20 Gliding tremor at OKCF. This spectrogram, starting October 15 2003 at 14:45, shows several episodes of gliding tremor.

4.4.3 Earthquakes

The tremor appears to be resilient and is rarely affected by earthquakes in the region. However, an earthquake did disrupt tremor at least once. A magnitude 4.2 earthquake on February 29 2004 that occurred approximately 100 km south of Okmok was able to disrupt tremor for seven hours before the tremor pattern firmly reestablished itself (Figure 4.21). The earthquake's peak velocity, as recorded at OKCF, was approximately $7.4 \times 10^4 \text{ nm s}^{-1}$. During the recovery period, strong upward gliding was observed in the spectrograms.

Johnson *et al.* (2010) searched the existing catalog looking for earthquakes that repeated. They recognized that earthquakes with high correlations (> 0.95) occurred under Cone A. These events were found to have occurred in the same volume spanning 300 m vertically and 150 m horizontally. The first of these occurred February 13 2004, with events continuing until May 2008. A subset of these earthquakes, listed in Table 4.2, appears in Figure 4.10 in the bottom axis. It is possible that these are not the only repeating events, since the seismic network may not have been robust enough for similar earthquakes to

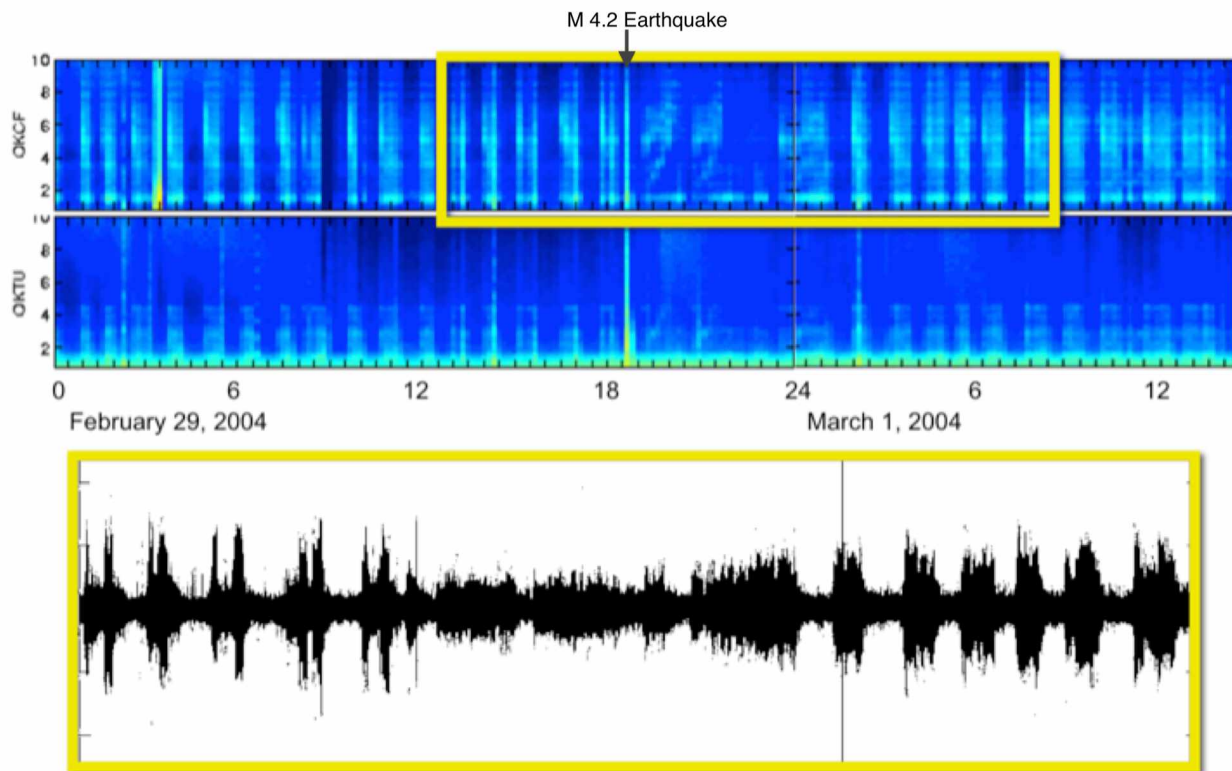


Figure 4.21 Example of tremor being disrupted by an earthquake. On February 29 2004 at 18:37:44, a magnitude 4.2 earthquake, located approximately 100 miles south Okmok, disrupted the tremor sequences for approximately 7 hours. The top panels show the frequency content of seismic signals. Tremor appears as the quasi-regular streaks of energy. After the earthquake, tremor is reestablished, but only after a period of frequency gliding. The lower panel shows the velocity trace for station OKCF during this time

be recognized and cataloged. The presence of these very similar, repeating earthquakes suggests that a consistent process was ongoing under Cone A at least as far back as February 2004.

4.4.4 Remote sensing

Thermal anomalies were reported at Okmok volcano multiple times during the study period (Figure 4.10, bottom axis). The first pair of thermal anomalies occurred in June 2003. Then one appeared in mid January 2004, followed by a series of anomalies between June and October 2004. These coincided with the second inflationary event. Observations were limited by weather, so it is not known with certainty whether the thermal anomaly persisted or was intermittent. The strongest clustering of observations occurred between June 25 and July 11 2004.

4.5 Interpretations

Masterlark *et al.* (2010) suggest that at the time of the 1997 eruption, a crack might have propagated upward from the edge of the magma reservoir in the direction of Cone A. If cracks exist with similar orientation, then the activation of a crack that extends from a shallow magmatic source up to Cone A provides a reasonably good resonator for the tremor. Heat from the magmatic body could provide energy to activate boiling an overlying hydrologic system. Additionally, degassing from the equilibrating magma could provide both an efficient way to transfer heat and additional fluid to generate tremor.

The tremor source demonstrated the ability to go through a full cycle from initiation to sustained tremor to quiescence on scales of a few minutes to an hour, which suggests a relatively rapid recharge of whatever pressures are required to create the tremor energy. Fujita (2008) recognized similar tremor patterns, “banded tremor”, at Miyakejima Volcano, located in Japan. The intervals, frequency content, and amplitude behavior closely match the tremor at Okmok, although Miyakejima only exhibited this behavior for 1–2 days at a time. Fujita modeled this as the interaction between two phases of a steam-water mixture in a shallow hydrothermal system.

The eruption of 2008 was phreatomagmatic, and Masterlark *et al.* (2010) suggest that the top 2 km of the caldera consist of wet fill. The influx of water from the magma, flashing of water to steam, and upward migration of volatiles, spurred by heat entering the system could provide the necessary energy.

In 2003, Cone A continued to exhibit features of an open volcanic system. The volcano had also been in the process of inflating, as noted by geodetic surveys. Although the fine-scale evolution of inflation isn't known before mid-2002, interpretations of InSAR data suggest that Okmok was inflating at roughly

the same rate as during the 2001 seismic survey, when Caplan-Auerbach *et al.* recorded tremor possibly coming from Cone A (Fournier *et al.*, 2009; Caplan-Auerbach *et al.*, 2004).

In early 2003, magma continued to enter the system, albeit at a slowing rate. The nearly constant high-amplitude tremor likely reflected the system attempting to shed the volatiles that were exsolving. This excess heat was affecting the wet subsurface and providing additional water, causing boiling and visible steam generation from Cone A. With enough heat entering the system, the water was unable to carry it away nearly as efficiently, and the excess gas, now dryer, worked its way out through cracks to the surface of Cone A. Surficial observations included a bluish steam plume emanating from the cone (Freymueller, pers. comm.; AVO logs), likely indicating that SO₂ was present in the gases. Meanwhile the extra heat appeared on satellite images as increased ground temperatures.

One explanation for the intermittent nature of the tremor is based on the tendency for pathways to become choked with fluids when the throughput is insufficient. In this model, during times of strong gas and volatile input, the plumbing and cracks remain open. Depending upon how chaotic the fluid flow is, the seismic signal may appear as ragged, continuous tremor. Other times it appears as a great many short events, suggesting that tremor could be composed of the overlapping of many short bursts. After periods of sustained venting, the pressure and/or volatile flux begins to drop. This pressure is no longer sufficient to hold open the pathways, and they collapse, with the interstitial spaces filling with water. This chokes off the flow of volatiles. Pressure begins to build in the system as gas and heat increase behind the choked vent. Eventually this pressure builds to a level sufficient to breach the choke. At this point, gas escapes and perhaps the decreasing pressure allows the subsurface waters to continue boiling off. Though we do not have volatile flux data to confirm this theory, the concept of intermittently plugged pathways fits many observations in the Okmok data (Julian, 1994; Fujita, 2008). There appears to be a delay between inflation rates and seismicity, with peak seismicity lagging approximately 5.5 months behind peak inflation rates (Figure 4.10).

In August 2003, inflation began to taper (Figure 4.11). The reduced flux of volatiles may have decreased the pressure available in the gas pathways. I speculate that a small influx of magma, or the continued exsolution of gas appeared as a small bump in inflation rates, as seen in August and October 2003 (Figure 4.11). However, the input was rather weak, and the volcano almost immediately started to subside again. During this time period there were several occasions when gliding tremor can be observed. The gliding tremor is fairly rare and likely indicates a unique set of conditions. The ephemeral nature of the gliding tremor indicates a transient set of conditions that presumably reflect changes in pressure, gas flux or the nature of the conduit system. Perhaps the frequency changes represent the pressure

overcoming some critical level that allowed it to open a constriction. As degassing increased, there was a corresponding drop in pressure, allowing more water to flash to steam. This positive feedback would further accelerate the gas, creating higher frequencies. Figure 4.20, from October 15 2003 shows such gliding behavior.

Eventually, the input of new magma into the shallow crust was unable to keep up with the volume decrease through degassing, and the volcano started to relax once more. In mid-February 2004, for the first time in years, the volcano started to deflate. As pressure within Cone A started to decline, minor cracks and faults relaxed and readjusted slightly, allowing the repeating earthquakes observed by Johnson *et al.* (2010) to happen.

However, this pressure decline was short-lived, and another pulse of magma soon entered the system. Between late February 2004 and August the volcano inflated rapidly. At the start, tremor appeared to occur with two modes, the short-lived (3–5 minute) tremor was interspersed with longer (20–35 minute) episodes. Short pulses might reflect minor degassing events or the shallow hydrothermal boiling that didn't activate the entire system.

Some of the longer episodes appeared to be triggered by the short-lived ones, as might be the case when near-surface boiling opens the system, relieving just enough pressure to allow flash boiling deeper in the system. Some days nearly every longer tremor event was initiated by a brief, but strong signal (Figure 4.18). This had the appearance of nails marched across the seismograph. Another mark of the sensitivity of the tremor can be seen in Figure 4.21, when an earthquake was able to disrupt tremor activity for 7 hours.

As the heat and pressure input crossed some threshold, the tremor started to exhibit gliding once more. Eventually, the tremor gave way to strong background noise.

The inflation in early 2004 was accompanied in June 2004 by an uptick in the number of earthquakes. These earthquakes were presumably a response to the stresses created by injecting new magmas into the shallow crust. Around this time, a series of thermal anomalies were spotted in the satellite images of Okmok. These anomalies were likely the surface manifestation of the heat associated with the new magmas. Since there was no eruptive activity at this time, the only way for the new heat in the magma reservoir to transit to the surface was to be carried through massive amounts of steam. This steam is precisely the mechanism suspected of being responsible for the seismic tremor. On September 6, a field crew reported seeing incandescence within the summit crater (Neal, pers. comm). It was around this time that tremor resumed with the strongest amplitudes since 2003. Both the incandescence and the timing of

the tremor suggest that the tremor was manifesting the transfer of heat from the shallow crust to the surface.

The volcano reached peak inflation in mid-September 2004, roughly coincident with the last thermal anomaly. After a week's pause, it started to deflate once more. Tremor remained strong as the edifice continued to deal with the heat, volatiles, and fluids from the previous slug of magma. The related tremor was unusually consistent in appearance, suggesting that the volcano experienced a type of equilibrium. Eventually, the system started to deflate, at which point the equilibrium was lost. The tremor patterns changed. Repeating earthquakes occurred around this time, too. The deflation wasn't uniform, and this fact was expressed in the varied appearance of tremor as well as the reappearance of repeating earthquakes.

These observations agree with the conclusions of Lu *et al.* (2010), who speculated that the preferred pathway in a given eruption

[...] might be determined by the reservoir pressure and the relative strengths of potential pathways, i.e., portions of the ring fracture. If so, repeated eruptions from the same vent might be expected until its feeder becomes blocked during a long repose or by some other change that favors an alternative magma migration path. (Lu *et al.*, 2010)

The idea of a feeder becoming blocked during a long repose, offered above, is supported by the ability of a dike to solidify in the time between observed activity in 2004 and renewed inflation in 2007. To test the feasibility of Cone A shutting off on this timescale, I modeled a cooling dike using the equations from Turcotte and Schubert (2002). I used September 1 2004 as the start time, since this roughly coincides with the cessation of

Table 4.4 Dike model parameters

Description	Symbol	Value
Magma Temp	T	1200 C
Wall Rock Temp	T	630 C
Thermal diffusivity	κ	$5.0e-7 \text{ m}^2 \text{ s}^{-1}$
Latent heat of fusion	L	320 kJ kg^{-1}
Specific heat	c	$1.200 \text{ kJ kg}^{-1} \text{ K}^{-1}$
density	ρ	2900 kg m^{-3}

inflation and the end of satellite thermal anomaly reports. At this time, the visual incandescence suggests the wall rock may have been roughly 630 °C. I set January 1 2006 as the end time, since that roughly marks the onset of renewed inflation. Other values were set according to values used in Turcotte and Schubert (Table 4.4). I then varied the width of the dike to determine the maximum width of a dike that could solidify under these conditions in the given amount of time. According to the model, a dike up to approximately 10 m width is able to solidify in this time.

It is possible that the extended period of deflation that followed could reflect the draining back of magma deeper into the system. If this were so, then it could provide an additional mechanism for breaking contact with the dike. The repeating earthquakes might be a reflection of the change in stress in the area above the magma pod.

Perhaps as the dike solidified, the next injection of magma forced new cracks that were oriented in line with the overall stress regime, which runs NNE through the system in a line that crosses from Cone A roughly through the caldera center. It is plausible that this new feature intersected water saturated ground, resulting in the eruption from the new vent NW of cone D.

4.6 Conclusion

I propose that heat and pressure (degassing) from repeated injections of magma were responsible for maintaining an open system at Cone A until about June 2005. The observed tremor resulted from the boiling of a shallow hydrothermal system in the vicinity of Cone A, which was heated by contact with fluids coming off the magma. This tremor may be delayed ~5.5 months in relation to the inflation, suggesting a characteristic time period for degassing. Such behavior has also been seen at Long Valley (Hill *et al.*, 2003). The ability to continuously degas may have helped keep pressure from building up to an eruption at Okmok.

The deflation between 2004 and 2007 created conditions that allowed the existing pathways to close. When new magma entered the system in 2006, tremor did not occur, since volatiles needed to seek a new pathway and therefore did not come into contact with the same hydrothermal system. In 2008, this path intersected an older pod of differentiated magma (Johnson *et al.*, 2010; Larsen *et al.*, 2013). That, combined with the increased pressure, triggered the eruption from new vents.

Chapter 5 Conclusions

I created a software framework to make working with seismic data easier. Using it, I investigated a persistently present quasi-periodic tremor signal that appeared to be emanating from the area around Cone A, starting as late as 2002, and ending in 2005 (Figure 5.1). Because the network was sparse and the tremor signals were emergent, I couldn't locate them with conventional techniques. I opted to use the amplitude ratios between pairs of stations to attempt to say where the tremor originated. Although I couldn't offer a precise location, observations support the idea that the tremor originates from a region that spread from shallow depths within Cone A, deeper toward a either a shallow pod of magma at 2–3 km or toward a magma chamber that lay to the NE at depths of 4–6 km.

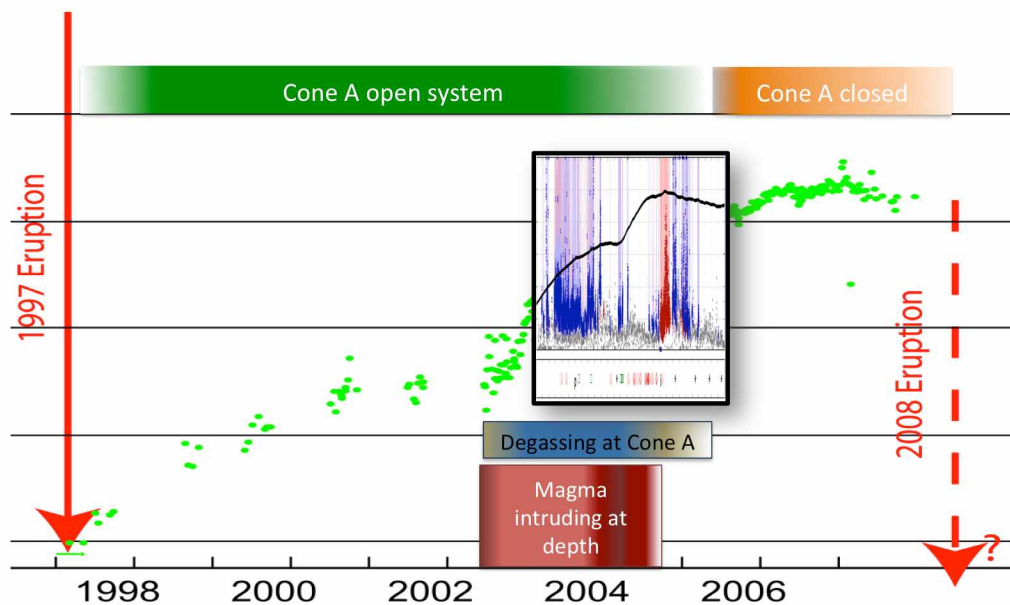


Figure 5.1 Summary of Okmok activity from 1997 to 2008. The green circles represent cumulative inflation at Okmok (from Biggs *et al.*, 2010). The red arrows represent the 1997 and 2008 eruptions. The inset figure is a scaled version of Figure 4.10. See that figure's caption for details.

When I analyzed the tremor patterns and combined my observations with a variety of existing observations, the story of Okmok seemed to unfold of its own accord. Between 2003 and mid 2004, repeated injections of magma into the central reservoir caused the volcano to inflate. Volatiles and fluids carried heat away from this magma out through the already-open system at Cone A. These fluids heated the surrounding hydrological system, causing boiling and tremor. Although inflation stopped in 2004, heat continued to enter the system and fluids continued to exsolve, with the result that tremor continued to

be seen until mid 2005. This five-and-a-half month delay can be applied to the entire sequence. At this point, the pressure reduction and lack of heat input allowed the existing pathways toward Cone A to seal tight.

In 2006, as seen by GPS, inflation started once more. New magma had entered the system but was unable to degas. Tremor did not occur at this point, because heat was no longer being transferred to the shallow hydrothermal system. Pressure likely built up as the exsolved volatiles searched for a new exit. In 2008, they found their way into an older pod of differentiated magma (Johnson *et al.*, 2010; Larsen *et al.*, 2013), resulting in the June 12 Eruption of Okmok from a new vent, northwest of Cone D.

Results of this study have implications, not only for describing what happened as activity transferred away from Cone A, but for elucidating how and why activity remains at or migrates away from vents in general. Perhaps this could be applied to understanding how monogenetic cones migrate across a volcanic landscape.

Although Okmok represents one of the better-instrumented volcanoes in the Aleutians, it would have been immensely helpful to have multiple functioning three-component broadband stations within the caldera. These likely would have provided enough information to quickly settle where the tremor source was located. In addition, a network with less symmetry would have provided additional constraints upon the tremor locations.

References

- Ahern, T.K., Buland, R., Halbert, S., 2009. SEED Format Version 2.4 Reference Manual, IRIS. http://www.iris.washington.edu/manuals/SEEDManual_V2.4.pdf [referenced October 31 2010].
- Aki, K., Koyanagi, R.Y., 1981. Deep volcanic tremor and magma ascent mechanism under Kilauea, Hawaii. *Journal of Geophysical Research*, 86(B8), p. 7095–7109, DOI:10.1029/JB086iB08p07095.
- Aki, K., Fehler, M., Das, S., 1977. Source mechanism of volcanic tremor: fluid-driven crack models and their application to the 1963 Kilauea eruption, *Journal of Volcanological and Geothermal Research*, 2(3), p. 259–287, DOI:10.1016/0377-0273(77)90003-8.
- Aki, K., Richards, P.G., 2002. *Quantitative Seismology*, 2nd Ed. University Science Books, Sausalito, CA, ISBN 0-935702-96-2, 704 p., 2002. Vol. 1.
- Barry, K.M., Carvers, D.A., Kneale, C.W., 1975. Report on recommended standards for digital tape formats. *Geophysics* 40(2), p. 344–352. DOI:10.1190/1.1440530
- Battaglia, J., Aki, K., 2003. Location of seismic events and eruptive fissures on the Piton de la Fournaise volcano using seismic amplitudes. *Journal of Geophysical Research*, 108(B8), p. 2364, DOI:10.1029/2002JB002193.
- Begét, J.E., Larsen, J.F., Neal, C.A., Nye, C.J., Schaefer, J.R., 2005. Preliminary Volcano-Hazard Assessment for Okmok Volcano, Umnak Island Alaska. Report of Investigations 2004-3: Division of Geological and Geophysical Surveys, Alaska Department of Natural Resources, 32 p., DOI:10.14509/7042
- Benoit, J.P., McNutt, S.R., 1997. New constraints on source processes of volcanic tremor at Arenal Volcano, Costa Rica, using broadband seismic data. *Geophysical Research Letters*, 24(4), p. 449–452.
- Biggs, J., Lu, Z., Fournier, T., Freymueller, J.T., 2010. Magma flux at Okmok Volcano, Alaska, from a joint inversion of continuous GPS, campaign GPS, and Interferometric Synthetic Aperture Radar. *Journal of Geophysical Research*, 115(B12401), DOI:10.1029/2010JB007577.
- BRTT, 2010. Boulder Real Time Technologies. <http://www.brtt.com>. [referenced April 13 2010].
- Buurman, H., West, M.E., 2010. Seismic precursors to volcanic explosions during the 2006 eruption of Augustine Volcano, chapter 2 of Power, J.A., Coombs, M.L., Freymueller, J.T. (Eds.), *The 2006 eruption of Augustine Volcano, Alaska*: U.S. Geological Survey Professional Paper 1769, p. 41–57.
- Byers, F.M., 1959. Geology of Umnak and Bogoslof Islands, Aleutian Islands, Alaska. U.S. Geological Survey Bulletin 1028-L, p. 107–367.
- Caplan-Auerbach, J., Moran, S.C., Tytgat, G., Plucinski, T.A., McNutt, S.R., Paskievitch, J.F., 2004. Seismic Explorations in the Eastern Aleutians, Alaska. *Seismological Research Letters*, 75(1), p. 8–21, DOI:10.1785/gssrl.75.1.8.
- Cervelli, D.P., Cervelli, P.F., Murray, T.L., 2004. New Software for Long-Term Storage and Analysis of Seismic Wave Data. *Eos, Transactions, American Geophysical Union* 85(47), Fall meeting Supplement, abstract SF13A-0705.

- Chouet, B.A., 1981. Ground motion in the near field of a fluid-driven crack and its interpretation in the study of shallow volcanic tremor. *Journal of Geophysical Research*, 86(B7), p. 5985–6016.
- Chouet, B.A., 1983. Ground motion near an expanding preexisting crack. *Journal of Volcanology and Geothermal Research*, 19(3), p. 367–379.
- Chouet, B.A., 1985. Excitation of a buried magmatic pipe: A seismic source model for volcanic tremor. *Journal of Geophysical Research*, 90(B2), p. 1881–1893, DOI:10.1029/JB090iB02p01881.
- Chouet, B.A., 1988. Resonance of a fluid-driven crack: Radiation properties and implications for the source of long-period events and harmonic tremor. *Journal of Geophysical Research*, 93(B5), p. 4375–4400, DOI:10.1029/JB093iB05p04375.
- Chouet, B.A., 1996. Long-period volcano seismicity: Its source and use in eruption forecasting. *Nature*, 380 (6572), p. 309–316.
- Chouet, B.A., 2003. Volcano seismology. *Pure and Applied Geophysics*, 160(3–4), p. 739–788.
- Chouet, B.A., Koyanagi, R.Y., Aki, K., 1987. Origin of volcanic tremor in Hawaii: Part II, theory and discussion. *Volcanism in Hawaii*, 2, p. 1259–1280.
- Crosson, R.S., Bame, D.A., 1985. A spherical source model for low frequency volcanic earthquakes. *Journal of Geophysical Research*, 90(B12), p. 10237–10247.
- Creager, K., 1997. Coral. *Seismological Research Letters*, 68 (2), p. 267–269.
- Dean, K., Dehn, J., McNutt, S.R., Neal, C.A., Moore, R.B., Schneider, D.J., 2002. Satellite imagery proves essential for monitoring erupting Aleutian volcano. *Eos, Transactions, American Geophysical Union*, 83, 241, p. 246–247.
- Dehn, J., Dean, K., Engle, K., 2000. Thermal monitoring of North Pacific volcanoes from space. *Geology*, 28(8), p. 755–758.
- Del Pezzo, E., Lombardo, G., Spampinato, S., 1989. Attenuation of volcanic tremor at Mt. Etna, Sicily. *Bulletin of the Seismological Society of America*, 79(6), p. 1989–1994.
- Dixon, J.P., Stihler, S.D., Power, J.A., Tytgat, G., Moran, S.C., Sanchez, J.J., McNutt, S.R., Estes, S., Paskievitch, J., 2004. Catalog of earthquake hypocenters at Alaskan volcanoes: January 1 through December 31, 2003: U.S. Geological Survey Open-File Report OF 2004–1234, 69 p.
- Dixon, J.P., Stihler, S.D., Power, J.A., Tytgat, G., Estes, S., Prejean, S., Sanchez, J.J., Sanches, R., McNutt, S.R., Paskievitch, J., 2005. Catalog of earthquake hypocenters at Alaskan volcanoes: January 1 through December 31, 2004: U.S. Geological Survey Open-File Report 2005-1312, 74 p., available at <http://pubs.usgs.gov/of/2005/1312/>.
- Dixon, J.P., Stihler, S.D., Power, J.A., Tytgat, G., Estes, S., McNutt, S.R., 2006. Catalog of earthquake hypocenters at Alaskan volcanoes: January 1 through December 31, 2005: U.S. Geological Survey Open-File Report 2006-1264, 78 p., available at <http://pubs.usgs.gov/of/2006/1264/>.

- Endo, E.T., Murray, T.L., 1991. Real-time Seismic Amplitude Measurement (RSAM): a volcano monitoring and prediction tool. *Bulletin of Volcanology*, 53(7), p. 533–545, DOI:10.1007/BF00298154.
- Fehler, M., 1983. Observations of volcanic tremor at Mount St. Helens volcano. *Journal of Geophysical Research*, 88(B4), p. 3476–3484, DOI:10.1029/JB088iB04p03476.
- Fournier, T., Freymueller, J.T., Cervelli, P., 2009. Tracking magma volume recovery at Okmok Volcano using GPS and an unscented Kalman filter. *Journal of Geophysical Research*, 114(B02405), DOI:10.1029/2008JB005837.
- Freymueller, J.T., Kaufman, A.M., 2010. Changes in the magma system during the 2008 eruption of Okmok volcano, Alaska, based on GPS measurements. *Journal of Geophysical Research*, 115(B12415), DOI:10.1029/2010JB007716.
- Fujita, E., 2008. Banded tremor at Miyakejima volcano, Japan: Implication for two-phase flow instability. *Journal of Geophysical Research*, 113(B04207), DOI:10.1029/2006JB004829.
- Haney, M., 2010. Location and mechanism of very long period tremor during the 2008 eruption of Okmok Volcano from interstation arrival times. *Journal of Geophysical Research*, 115(B00B05), DOI:10.1029/2010JB007440.
- Haney, M., 2014. Backprojection of volcanic tremor. *Geophysical Research Letters*, 41(6), p.1923–1928, DOI:10.1002/2013GL058836.
- Havskov, J., Ottemöller, L., 1999. SeisAn Earthquake Analysis Software. *Seismological Research Letters*, 70(5), p. 532-534.
- Hill, D., Langbein, J.O., Prejean, S., 2003. Relations between seismicity and deformation during unrest in Long Valley Caldera, California, from 1995 through 1999. *Journal of Volcanological and Geothermal Research*, 127(3–4), p. 175–193, DOI:10.1016/S0377-0273(03)00169-0.
- Johnson, J.H., Prejean, S., Savage, M.K., Townend, J., 2010. Anisotropy, repeating earthquakes, and seismicity associated with the 2008 eruption of Okmok Volcano, Alaska. *Journal of Geophysical Research*, 115, B00B04, DOI:10.1029/2009JB006991.
- Julian, B.R., 1994. Volcanic tremor: Nonlinear excitation by fluid flow. *Journal of Geophysical Research*, 99(B6), p. 11859–11877, DOI:10.1029/93JB03129.
- Kedar, S., Kanamori, H., Sturtevant, B., 1998. Bubble collapse as the source of tremor at Old Faithful Geyser. *Journal of Geophysical Research*, 103(B10), p. 24283–24299, DOI:10.1029/98JB01824.
- Kienle, J., Nye, C.J., 1990. Volcano tectonics of Alaska. In: Wood, C.A., Kienle, J., *Volcanoes of North America: United States and Canada*. The Press Syndicate of the University of Cambridge, New York, NY, p. 9–16.
- Koyanagi, R.Y., Chouet, B., Aki, K., 1987. Origin of volcanic tremor in Hawaii, Part 1: Data from the Hawaiian Volcano Observatory, 1969–1985. In: Decker, R.W., Wright, T.L., Stauffer P.H. (Eds.), *Volcanism in Hawaii*, U.S. Geological Survey Professional Paper 1350, Volume 2, p. 1221–1258.

- Larsen, J.F., Neal, C., Schaefer, J., Begét, J., Nye, C., 2007. Late Pleistocene and Holocene caldera-forming eruptions of Okmok Caldera, Aleutian Islands, Alaska. *Volcanism and subduction: The Kamchatka region*, p. 343–364.
- Larsen, J., Neal, C., Webley, P., Freymueller, J., Haney, M., McNutt, S., Schneider, D., Prejean, S., Schaefer, J., Wessels R., 2009. Eruption of Alaska volcano breaks historic pattern, *Eos, Transactions, American Geophysical Union*, 90(20), p. 173–174, DOI:10.1029/2009EO200001.
- Larsen, J.F., Śliwiński, M.G., Nye, C.J., Cameron, C., Schaefer, J.R., 2013. The 2008 eruption of Okmok Volcano, Alaska: Petrological and geochemical constraints on the subsurface magma plumbing system. *Journal of Volcanological and Geothermal Research*. 264, p. 85–106, DOI:10.1016/j.jvolgeores.2013.07.003.
- Leet, R.C., 1988. Saturated and subcooled hydrothermal boiling in groundwater flow channels as a source of harmonic tremor. *Journal of Geophysical Research*, 93(B5), p. 4835–4849.
- Lindquist, K.G., 2009. Antelope Toolbox for Matlab: Version 1.1, User's Manual and Tutorial, updated Aug. 21, 2009. Lindquist Consulting, Inc; http://github.com/antelopeusersgroup/antelope_contrib/blob/master/data/matlab/antelope/doc/Antelope_Toolbox_for_Matlab.pdf [referenced March 17 2010].
- Lu, Z., Dzurisin, D., 2010. Ground surface deformation patterns, magma supply, and magma storage at Okmok volcano, Alaska, from InSAR analysis: 2. Coeruptive deflation, July–August 2008. *Journal of Geophysical Research*, 115(B5), DOI:10.1029/2009JB006970.
- Lu, Z., Fielding, E., Patrick, M.R., Trautwein, C.M., 2003. Estimating lava volume by precision combination of multiple baseline spaceborne and airborne Interferometric Synthetic Aperture Radar: the 1997 eruption of Okmok Volcano, Alaska. *IEEE Transactions on Geoscience and Remote Sensing*, 41(6), p. 1428-1436, DOI:10.1109/TGRS.2003.811553.
- Lu, Z., Masterlark, T., Dzurisin, D., 2005. Interferometric synthetic aperture radar study of Okmok volcano, Alaska, 1992–2003: Magma supply dynamics and postemplacement lava flow deformation. *Journal of Geophysical Research*, 110(B2), DOI:10.1029/2004JB003148.
- Lu, Z., Dzurisin, D., Biggs, J., Wicks, C., McNutt, S.R., 2010. Ground surface deformation patterns, magma supply, and magma storage at Okmok volcano, Alaska, from InSAR analysis: 1. Intereruption deformation, 1997–2008. *Journal of Geophysical Research*, 115(B00B02), DOI:10.1029/2009JB006969.
- Mann, D., Freymueller J., Lu, Z., 2002. Deformation associated with the 1997 eruption of Okmok Volcano, Alaska. *Journal of Geophysical Research*, 115(B00B03), p. ETG 7-1–7-12, DOI:10.1029/2001JB000163.
- Masterlark, T., Haney, M., Dickinson, H., Fournier, T., Searcy, C., 2010. Rheologic and structural controls on the deformation of Okmok Volcano, Alaska: FEMs, InSAR, and ambient noise tomography. *Journal of Geophysical Research*, 115(B02409), DOI:10.1029/2009JB006324.
- McConnell, S., 2004. *Code Complete, Second Edition*, Microsoft Press, Redmond, WA.

- McGimsey, R.G., Wallace, K.L., 1999., 1997 Volcanic Activity in Alaska and Kamchatka: Summary of events and response of the Alaska Volcano Observatory. U.S. Geological Survey Open-File Report 99-448, p. 18-23.
- McNutt, S.R., 1986. Observations and analysis of B-Type Earthquakes, Explosions, and Volcanic Tremor at Pavlof Volcano, Alaska. *Bulletin of the Seismological Society of America*, 76 (1), p. 153-175.
- McNutt, S.R., 1989. Volcanic tremor from around the world. In: *Continental Magmatism, Abstracts. Bulletin 131*, New Mexico Bureau of Mines and Mineral Resources, Socorro, New Mexico, p. 183.
- McNutt, S.R., 1992. Volcanic tremor. *Encyclopedia of Earth System Science*, 4. Academic Press, Inc., San Diego, CA, p. 417-425.
- McNutt, S.R., 1996. Seismic monitoring of volcanoes: A review of the state-of-the-art and recent trends. In R. Scarpa and R. Tilling (Eds.), *Monitoring and Mitigation of Volcano Hazards*, Berlin: Springer-Verlag, p. 99-146.
- McNutt, S.R., Nishimura, T., 2008. Volcanic tremor during eruptions: Temporal characteristics, scaling and constraints on conduit size and processes. *Journal of Volcanological and Geothermal Research*, 178, p. 10-18.
- Miller, T.P., McGimsey, R.G., Richter, D.H., Riehle, J.R., Nye, C.J., Yount, M.E., Domoulin, J.A., 1998. Catalog of the historically active volcanoes of Alaska. U.S. Geological Survey Open File Report 98-582, 104 p.
- Miyagi, Y., Freymueller, J.T., Kimata, F, Sato, T., Mann, D., 2004. Surface deformation caused by shallow magmatic activity at Okmok volcano, Alaska, detected by GPS campaigns 2000-2002. *Earth Planets Space*, 56(12), p. E29-E32.
- Mogi, K., 1958. Relations between the eruptions of various volcanoes and the deformations of the ground surfaces around them. *Bulletin of the Earthquake Research Institute*, 25, p. 99-134.
- Narváez, L., Cepeda, H., Stix, J., 1997. 'Tornillo'-type seismic signals at Galeras volcano, Colomba, 1992-1993. *Journal of Volcanology and Geothermal Research*, 77(1), p. 159-171.
- Neal, C.A., Larsen, J.F., Schaefer, J., 2009. The July-August 2008 hydrovolcanic eruption of Okmok Volcano, Umnak Island, Alaska. *Alaska Geological Society Newsletter*, 39(5), p. 1-3.
- Ohlendorf, S.J., Thurber, C.H., Pesicek, J.D., Prejean, S.G., 2014. Seismicity and seismic structure at Okmok Volcano, Alaska. *Journal of Volcanology and Geothermal Research*, 278-279, p. 103-119, DOI:10.1016/j.jvolgeores.2014.04.002.
- Patrick, M.R., Dehn, J., Dean, K., 2004. Numerical modeling of lava flow cooling applied to the 1997 Okmok eruption: Approach and analysis, *Journal of Geophysical Research*, 109(B03202), DOI:10.1029/2003JB002537.
- Patrick, M.R., Dehn, J., Dean, K., 2005. Numerical modeling of lava flow cooling applied to the 1997 Okmok eruption: Comparison with Advanced Very High Resolution Radiometer thermal imagery: *Journal of Geophysical Research*, 110(B02210), 9 p., DOI:10.1029/2003JB002538.

- Reyes, C.G., West, M.E., 2011. The Waveform Suite: A Robust Platform for Manipulating Waveforms in MATLAB, *Seismological Research Letters* 82(1), p. 104–110, DOI:10.1785/gssrl.82.1.104.
- Saccorotti, G., Chouet, B., Dawson, P., 2003. Shallow-velocity models at the Kilauea Volcano, Hawaii, determined from array analyses of tremor wavefields. *Geophysical Journal International*, 152(3), p. 633–648, DOI:10.1046/j.1365-246X.2003.01867.x.
- Schaefer, J.R., Larsen, J.F., Unema, J.A., 2011. Digital elevation model (DEM) and shaded relief image of Okmok Caldera, 2010. Alaska Division of Geological & Geophysical Surveys Raw Data File 2011-6, available at <http://www.dggs.dnr.state.ak.us/pubs/id/23223>.
- Sostman, H.E., Metz, P.D., 1995. Fundamentals of thermometry part VIII Radiation thermometry and calibration. *Isotech Journal of Thermometry*, 6(2), p. 74–86.
- Takagi, N., Kaneshima, S., Kawakatsu, H., Yamamoto, M., Sudo, Y., Ohkura, T., Yoshikawa, S., Mori, T., 2006. Apparent migration of tremor source synchronized with the change in the tremor amplitude observed at Aso volcano, Japan, *Journal of Volcanological and Geothermal Research*, 154(3–4), p. 181–200, DOI:10.1016/j.jvolgeores.2006.02.001.
- Tapley, W.C., Tull, J.E., 1992. SAC-Seismic Analysis Code: User's manual, Lawrence Livermore National Laboratory, Regents of the University of California, CA.
- Thompson, G., McNutt, S.R., Tytgat, G., 2002. Three distinct regimes of volcanic tremor associated with the eruption of Shishaldin Volcano, Alaska 1999. *Bulletin of Volcanology*, 64(8), p. 535–547, DOI:10.1007/s00445-002-0228-z.
- Turcotte, D.L., Schubert, G.J., 2002. *Geodynamics: Applications of Continuum Physics to Geological Problems*, 2nd ed., 456 p., Cambridge Univ. Press, New York, NY.
- Vanderkulk, W., Rosen, F., Lorenz, S., 1965. Large Aperture Seismic Array Signal Processing Study, IBM Final Report, ARPA Contract SD-296, International Business Machines, Rockville, MD.